NASA TECHNICAL MEMORANDUM

NASA TM X-1266

NASA TM X-1266

EXPERIMENTAL EVALUATION OF THROAT INSERTS IN A STORABLE-PROPELLANT ROCKET ENGINE

by Jerry M. Winter, Larry D. Plews, and James R. Johnston

Lewis Research Center

Cleveland, Ohio

NATIONAL AERONAUTICS AND SPACE ADMINISTRATION • WASHINGTON, D. C. • OCTOBER 1966

DISCLAIMER NOTICE

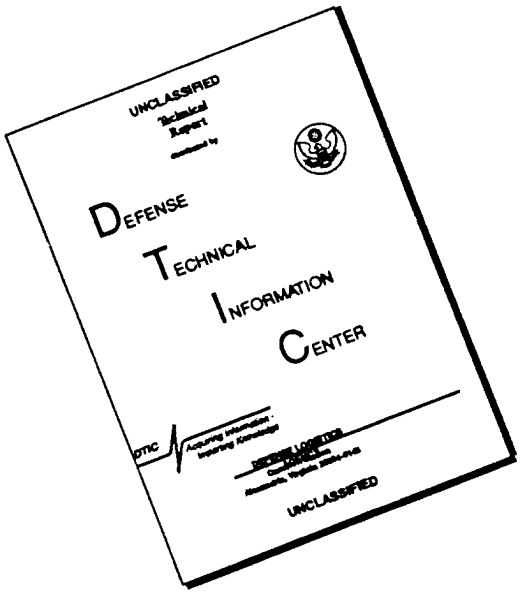

THIS DOCUMENT IS BEST QUALITY AVAILABLE. THE COPY FURNISHED TO DTIC CONTAINED A SIGNIFICANT NUMBER OF PAGES WHICH DO NOT REPRODUCE LEGIBLY.

NASA TM X-1266

EXPERIMENTAL EVALUATION OF THROAT INSERTS IN A STORABLE-PROPELLANT ROCKET ENGINE

By Jerry M. Winter, Larry D. Plews, and James R. Johnston

Lewis Research Center
Cleveland, Ohio

NATIONAL AERONAUTICS AND SPACE ADMINISTRATION

For sale by the Clearinghouse for Federal Scientific and Technical Information
Springfield, Virginia 22151 – Price $2.50

EXPERIMENTAL EVALUATION OF THROAT INSERTS IN A STORABLE-PROPELLANT ROCKET ENGINE

by Jerry M. Winter, Larry D. Plews, and James R. Johnston

Lewis Research Center

SUMMARY

A total of 57 throat inserts for ablative-material nozzle sections were tested at a nominal throat diameter of 1.20 inches. The two propellants used were nitrogen tetroxide and a blend of 50 percent hydrazine and 50 percent unsymmetrical dimethyl hydrazine. Nominal engine conditions included a chamber pressure of 100 pounds per square inch absolute and an oxidant-fuel ratio of 2.0. The materials tested ranged from ablative-reinforced plastics to refractory alloys. No throat erosion, low outer envelope temperature, and structural integrity were the criteria for an acceptable insert. Hypereutectic zirconium carbide met these criteria after two 60-second firing cycles. Refractory metals such as tungsten and molybdenum were found to oxidize rapidly in the test environment. The refractory oxides provided good erosion resistance but suffered thermal shock failures. Pyrolytic graphite gave encouraging results but requires further design work. The best insert was a 0.040-inch-thick pyrolytic silicon carbide coating on graphite, which underwent four test cycles totalling 722 seconds before failure.

INTRODUCTION

Uncooled ablative thrust chambers are being used in many important applications ranging from small control rockets (ref. 1) to primary propulsion engines. Many of these applications use storable propellants. Ablative thrust chambers have often required a compromise between characteristic exhaust velocity C* efficiency level (T_{gas}) and acceptable throat erosion. An increase in throat area results in a decrease in performance because of a decrease in nozzle expansion ratio. Excessive erosion could also lead to structural or thermal failure of the thrust chamber. One approach to improving ablative thrust chambers is to use a throat material that minimizes erosion; such a throat insert could provide greater engine capability through higher performance and/or longer engine life.

General problems in achieving the successful application of throat inserts to ablative thrust chambers include the following: (1) compatibility of the throat insert material with the products of ablation as well as the combustion products, (2) loss of insert material due to melting, sublimation, oxidation, or mechanical removal due to stream shear forces, and (3) structural failure such as cracking or spalling. The term "erosion" will be used herein to denote loss of material by any of the preceding means. A more detailed discussion of failure mechanisms may be found in reference 2. The high-temperature materials under consideration suffer from one or more of the preceding problems in the test environment. Materials combining good structural properties with erosion resistance (such as metal-ceramic composites, ref. 3) or protective coatings on good high-temperature structural materials (such as graphite) seem the most likely for satisfactory throat inserts.

The investigation reported herein was conducted to evaluate a large number of throat insert materials in a small, relatively high performance rocket engine. With one exception, all throat inserts were enclosed in an ablative-reinforced plastic material (silica phenolic). The results obtained provided information for more detailed design and screened the most promising materials for further testing in nozzles with throat diameters of both 1.20 and 7.82 inches. For the present investigation, the throat diameter was 1.20 inches, and the outside diameter of the ablative envelope was arbitrarily 4.0 inches. The two propellants were nitrogen tetroxide and a blend of 50 percent hydrazine and 50 percent unsymmetrical dimethyl hydrazine. Nominal combustion conditions were a chamber pressure of 100 pounds per square inch absolute at an oxidant-fuel ratio of 2.0. A nozzle with a low expansion area ratio was used since all firings were made at sea-level conditions. A total of 57 throat inserts was tested. Classes of materials included the following: (1) ablative-reinforced plastics, (2) composites, (3) refractory compounds, (4) refractory metals and alloys, (5) infiltrated refractory metals, (6) graphites, and (7) high-temperature coatings. Criteria for an acceptable insert included no erosion at steady-state temperature, an external temperature of the ablative envelope below the charring temperature, good structural integrity, and the ability to withstand repeated firings. The results should then be applicable to both control rockets (cyclic firing) and propulsion rockets (steady-state firing).

The results are presented by category in the order given in the preceding paragraph. Each category is discussed separately, and comparisons are made of the various categories.

APPARATUS

Facility

Figure 1 shows the test cell with the engine in place. The flow system schematic

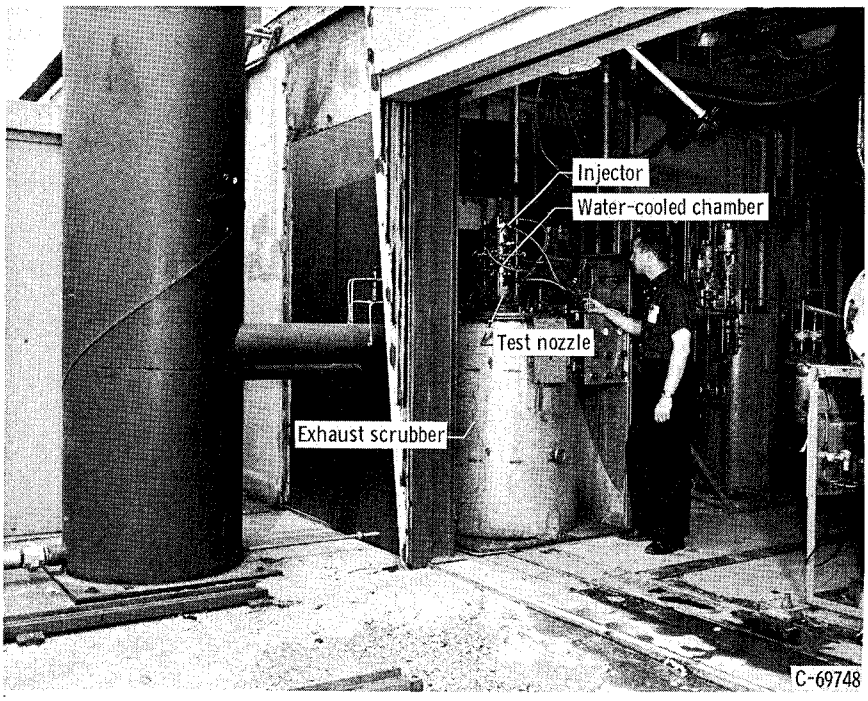

Figure 1. - Sea-level test facility.

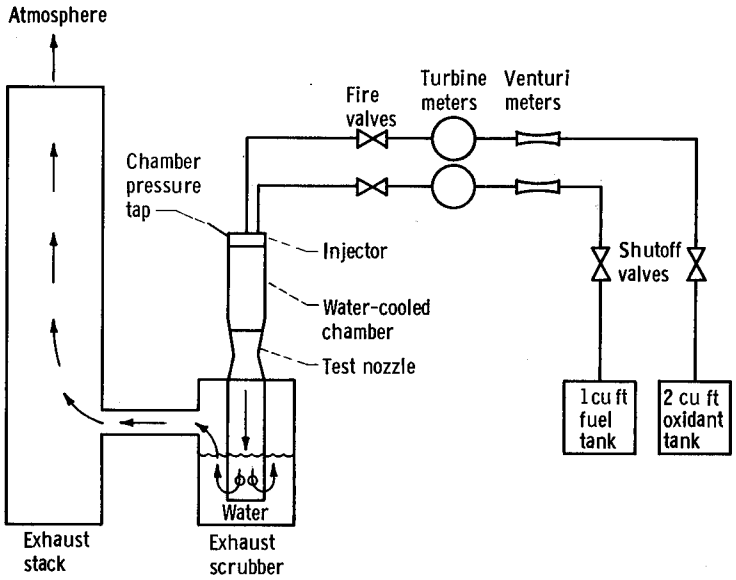

Figure 2. - Schematic of oxidant-fuel flow.

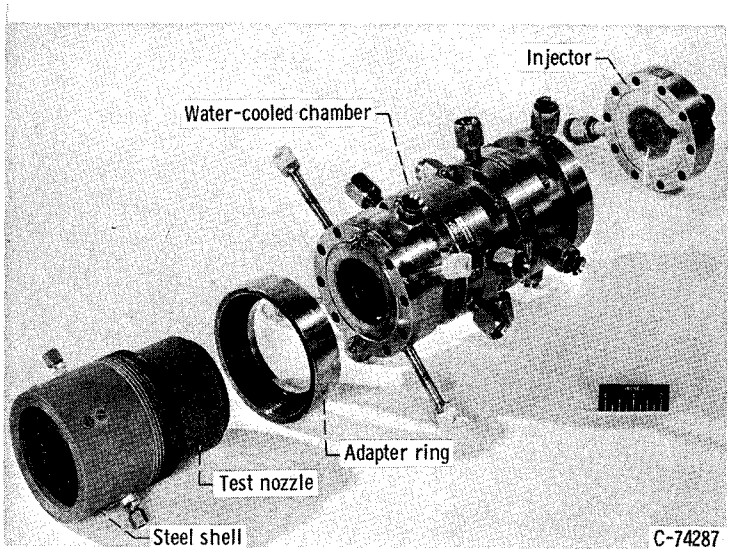

Figure 3. - Engine assembly.

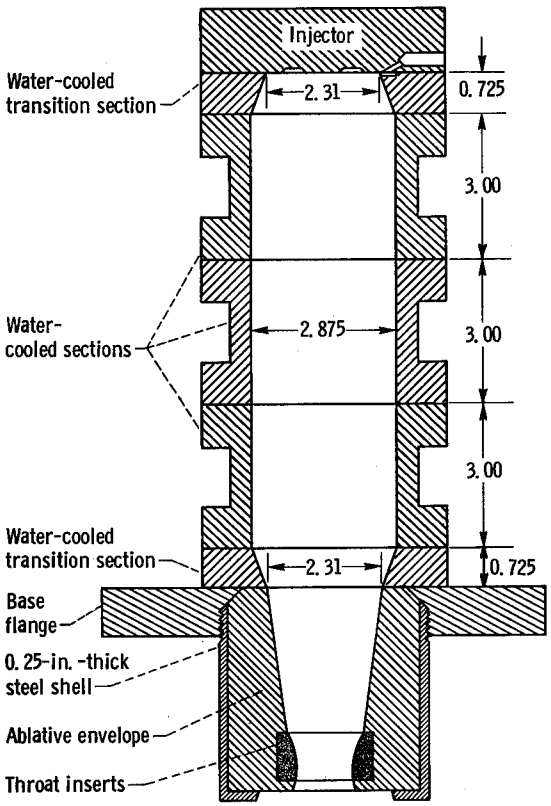

Figure 4. - Water-cooled engine assembly. (All dimensions are in inches.)

(fig. 2) includes instrumentation locations. The storable-propellant exhaust products were water scrubbed before being exhausted to atmosphere. In order to assure proper temperatures, propellants were stored in a controlled environment until shortly before firing.

Chambers and Injectors

Figure 3 shows the components of a typical engine, which included the injector, a chamber of three water-cooled sections, and the nozzle section. A dimensioned sketch of the engine assembly is shown in figure 4. For the tests conducted in this investigation, engines consisting of either two or three water-cooled chamber sections were used, which gave lengths from injector to throat of 11.3 and 14.4 inches, respectively. The nominal characteristic length L^* values for these lengths were 50 and 65 inches, respectively, based on a 1.20-inch-diameter throat size. Characteristic length L^* values for each

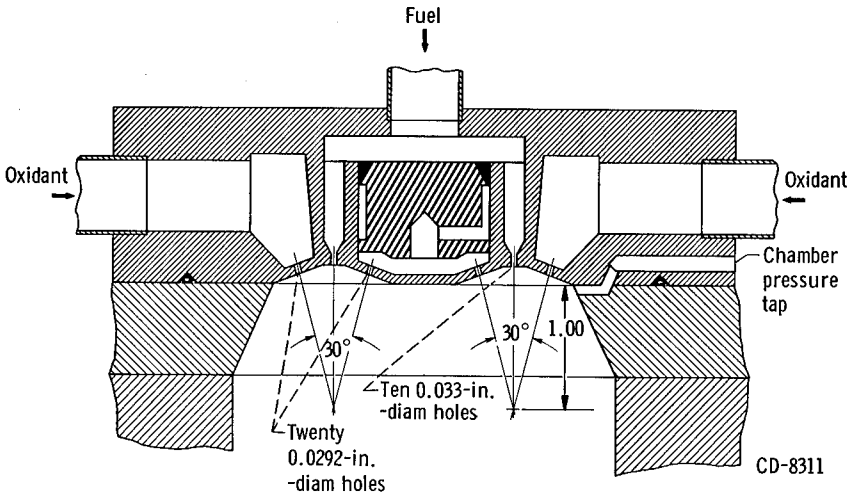

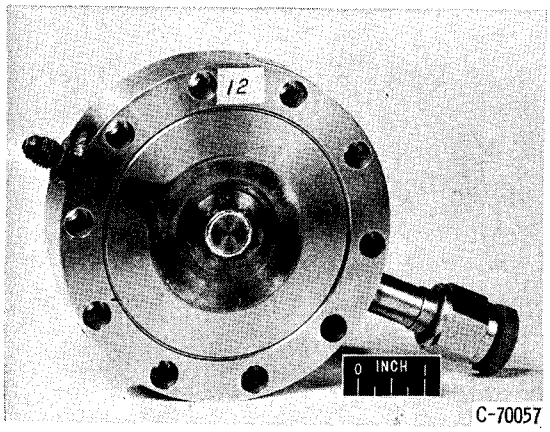

Figure 5. - Injector configuration.

insert firing are given in table I.

The test nozzle was held in place by a steel cylinder clamped to the water-cooled chamber. The seal between the ablative material and the water-cooled sections was made by a steel O-ring or by asbestos gaskets. The injector (fig. 5) was a circular pattern oxidant-on-fuel triplet with 10 triplet elements. Three injectors of identical construction were used for this test series. The injectors were designed to give relatively high performance (above 95 percent theoretical equilibrium C*) with a uniform circumferential temperature distribution.

Instrumentation

Table II gives all the measured variables and an estimate of the standard deviation s involved in each measurement. The locations of the primary measured variables are shown in the flow schematic (fig. 2). A light-beam oscillograph recording system was

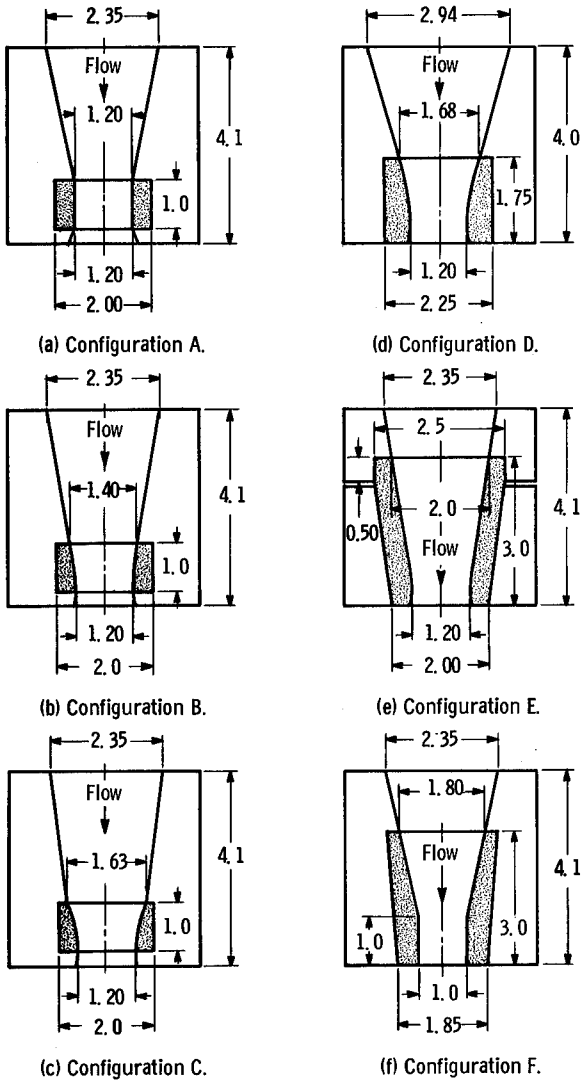

Figure 6. - Nozzle configurations. Outside diameter for all configurations, 4.0 inches. (All dimensions are in inches.)

used to monitor engine performance continuously during each firing.

Ablative-Material Nozzles with Throat Inserts

The six nozzle configurations used are shown in figure 6. The throat insert for configuration A was a cylinder, which was relatively simple to manufacture and was used in three nozzles. The change to configuration B was made to locate the throat plane, to reduce heat transfer at the insert leading edge, and to avoid possible shock-wave networks in the throat. Configuration B was used to test 27 inserts. Configuration C reduced the flow Mach number at the insert leading edge from 0.52 (configuration B) to 0.31 and was used to test 20 inserts. This configuration was used to decrease erosion of the ablative material at the insert-ablative interface and to reduce insert failure at the leading edge. Configurations D and F were designed by their manufacturers. Configuration E, used to test one insert, was intended to provide for shrinkage and to prevent delamination of a stack of pyrolytic graphite washers by allowing translation of the ablative envelopes. The inlet diameter was also sized to lower the flow Mach number in order to minimize erosion of the ablative material at the insert leading edge.

The ablative envelope for all configurations was Fiberite MX 2641 material (70 percent silica - 30 percent phenolic), usually with the reinforcement oriented 90° to the nozzle centerline. Some chopped square moldings were also used and these are listed in table I.

Each insert material tested and its specific configuration are given in table III. The materials are divided into seven different classes: ablative-reinforced plastics, composites, refractory compounds, refractory metals and alloys, infiltrated refractory metals, graphites, and coatings. The table also gives total firing time and number of

test firings for each insert. The inserts are described fully in table I (see p. 29) and are cross referenced in table III.

PROCEDURE

For each test firing, the propellant tanks were pressurized to a value calculated to produce a chamber pressure of 100 pounds per square inch absolute and an oxidant-fuel ratio of 2.0. The fire valves were then opened fully to start the run. Run termination was arbitrarily timed (60 sec normally) or was automatic when the chamber pressure dropped below 90 pounds per square inch absolute or when either of the propellants was exhausted. A chamber pressure decrease to 90 pounds per square inch absolute normally signified throat erosion. When this took place, the propellant tank pressures were adjusted so that subsequent firings of the same nozzle each started at a chamber pressure of 100 pounds per square inch absolute.

A visual inspection of each insert was made after firing. The throat profile was traced from an X10 shadowgraph image. The image was measured with a planimeter to determine the throat area, and this area was then converted to an effective radius. The initial radius was subtracted from the effective radius, and the result divided by the total run time gave the overall erosion rate. Where planimeter measurements were not possible, the propellant weight flow, chamber pressure, and calibration C* values were used to calculate the throat radius near the end of the firing. Most of the nozzles were bisected, and all were photographed when the test was completed. These results are given in table I. Metallographic examinations of the inserts were made in some cases to assist in the failure analysis.

The combustion performance of the system was measured periodically by using a fixed-diameter heat-sink nozzle and short-duration firings. The nozzle contour in figure 6(b) was used for the heat-sink nozzle. The method for calculation of C* efficiency is given in table IV.

The continuously recorded oscillograph data were used to calculate chamber pressure and propellant flow rates. These calculations were made at discrete time intervals starting at 5 seconds after start and ending 1 second before shutdown. The run time was measured by a clock timer, which was automatically started and stopped by the operation of the fire valve. Table IV gives all the calculations made and gives an estimate of the standard deviation s associated with the results.

RESULTS AND DISCUSSION

Each class of material tested will be discussed separately. Detailed nozzle descrip-

tions, post-test photographs, and complete firing data for each nozzle are presented in table I.

Combustion Performance Evaluation

Combustion performance was determined during 10-second firings with a fixed-diameter heat-sink nozzle. The average performance level for the three injectors was 96.0 percent of theoretical equilibrium C*. The calculations were based on chamber pressure measured at the injector face. The calculated momentum pressure loss of 0.8 percent was ignored. As indicated in table IV, the standard deviation s for C* efficiency on calibration firings was estimated at ±2.2 percent. The data spread indicates the difficulty of basing C* calculations on measured chamber pressure. The characteristic velocity efficiency was also determined during insert test firings. The average performance level for 93 data points was 96.3 percent theoretical equilibrium C*. The calculation was made 5 seconds after the start of firing before erosion could change the throat area significantly. The standard deviation for these data was estimated at ±2.7 percent.

Insert Behavior

Ablative-reinforced plastic materials. - Ablative-reinforced plastic materials were tested as throat inserts in an ablative envelope (Fiberite MX 2641) to lower the cost of the insert. All of these materials contained graphite reinforcement or precharred epoxy - silica reinforcement. Detailed insert descriptions and test results are listed in table V(a). All inserts suffered relatively high erosion. Since the inserts contained a large proportion of graphite, oxidation is believed to be a major failure mechanism. The effective throat radius change as a function of time is given in figure 7(a). Insert 1 (pyrolized graphite phenolic with silicon carbide - silicon additive) showed superior performance during the initial firing. This performance was probably due to pyrolysis products protecting the graphite fiber structure until a porous char was established, which allowed oxidation to begin. The erosion rates following the initial firing were similar for most of these materials. None of the erosion rates were significantly better than those for standard ablative materials (ref. 4).

Composite materials. - Composite materials are those which contain a mixture of two or more substances. A description of the composite materials and a summary of the test results are given in table V(b). Loss of structural integrity and erosion due to oxidation were the usual failure mechanisms. Throat erosion as a function of run time is

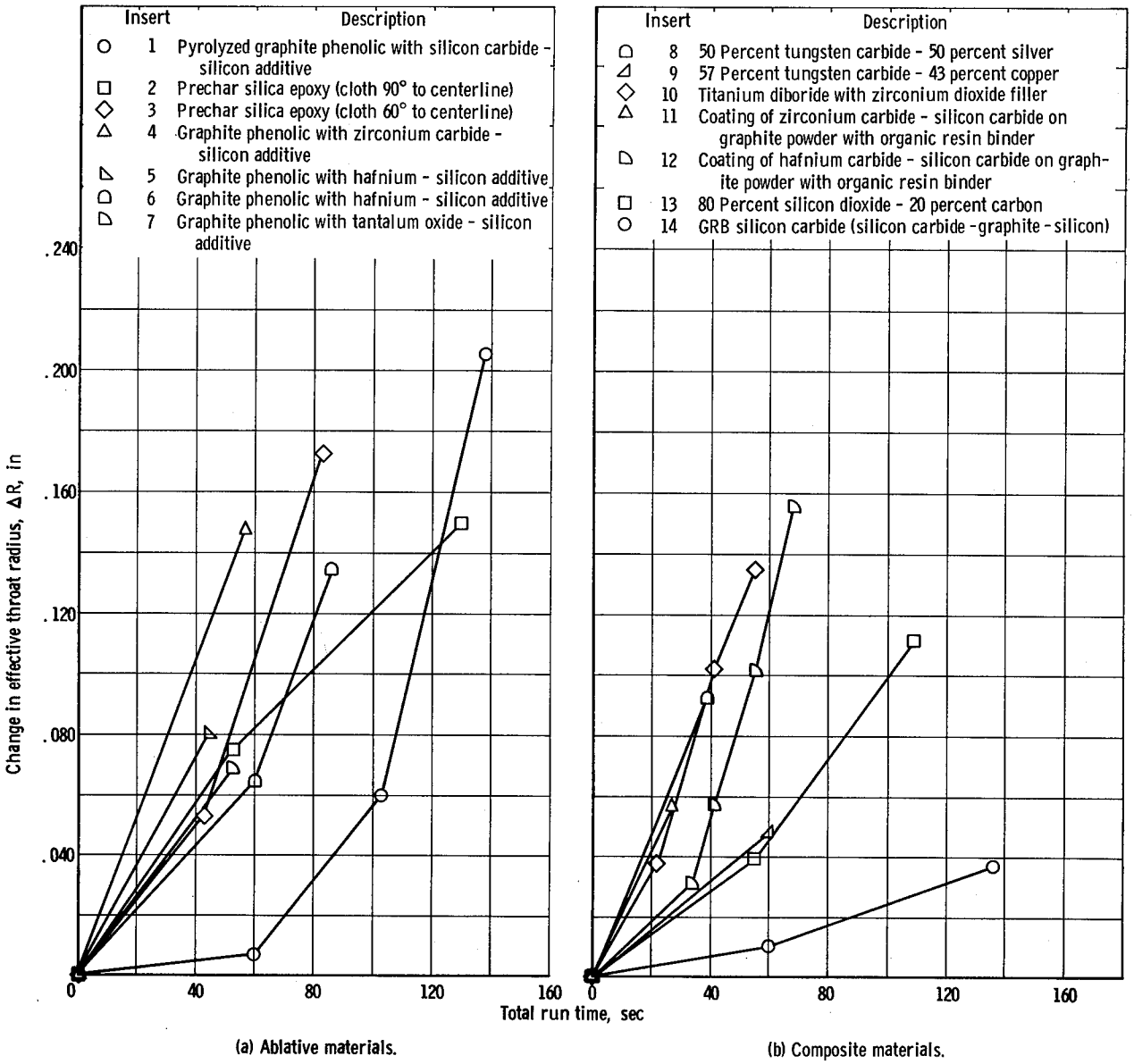

(a) Ablative materials.

(b) Composite materials.

Figure 7. - Erosion of nozzle inserts.

shown on figure 7(b). With the exception of the GRB material (insert 14), these erosion curves do not show a significant improvement over the ablative-material erosion shown in figure 7(a).

The apparent high degree of erosion of the tungsten carbide - silver insert (insert 8) compared with that of the tungsten carbide - copper insert (insert 9) was evidently caused by an inward radial distortion of the throat for the tungsten carbide - copper material caused by delamination and/or melting of the insert. Delaminations of the tungsten carbide - copper are shown in figure 8(a). The dark areas are voids running parallel to the nozzle axis. The gray areas are tungsten carbide particles in a copper matrix.

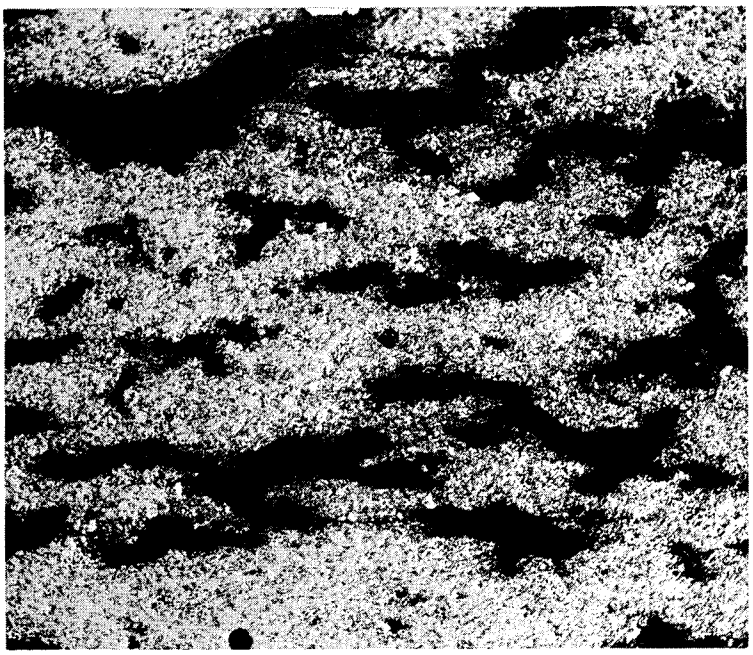

X100

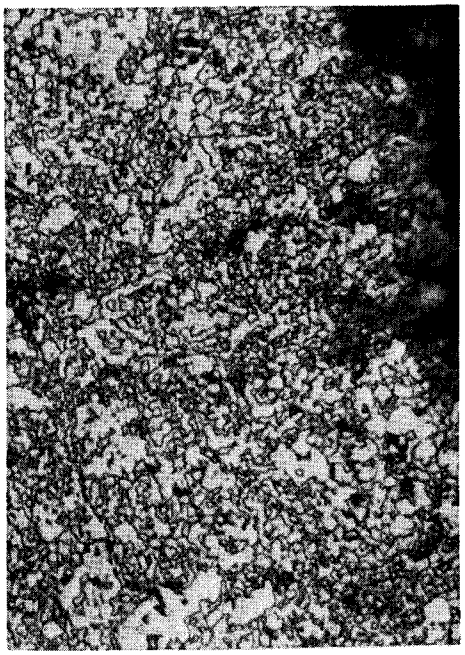

X750

(a) Insert 9 (57 percent tungsten carbide - 43 percent copper).

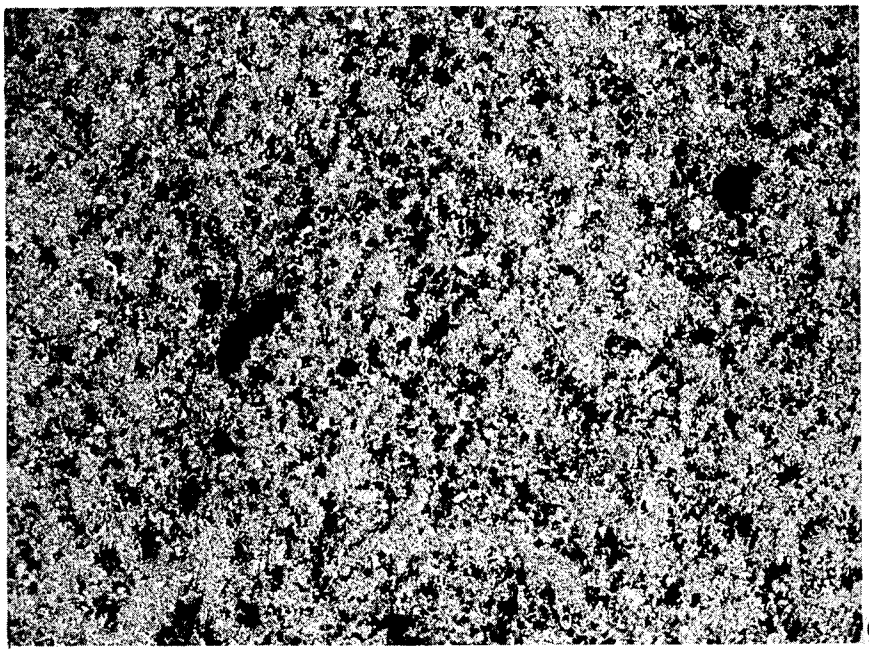

C-66-1211

X100

(b) Insert 8 (50 percent tungsten carbide - 50 percent silver). X100.

Figure 8. - Photomicrographs of nozzle inserts 8 and 9 after firing. Unetched.

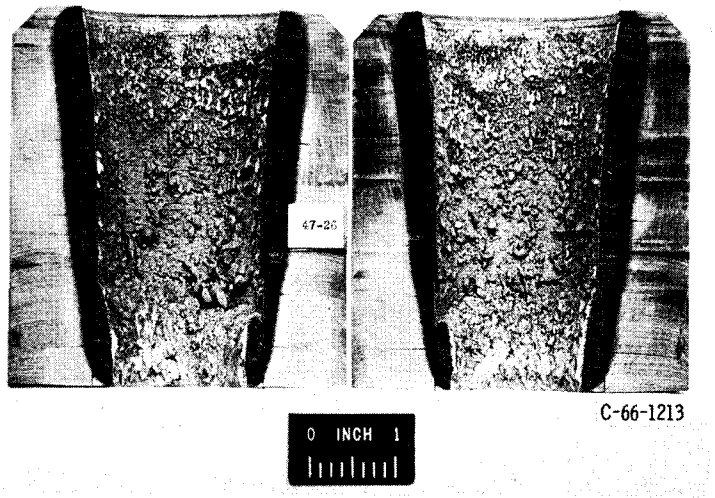

Figure 9. - Silica coating on nozzle insert 13 (80 percent silicon dioxide - 20 percent carbon) after firing.

Figure 8(b) shows the microstructure of tungsten carbide - silver (insert 8). The voids are smaller and no cracklike alinement exists. The poor erosion resistance of both inserts 8 and 9 was due to rapid oxidation, melting, and mechanical removal of the weak metal matrix.

The titanium diboride with zirconium dioxide filler (insert 10) failed by oxidation of the titanium diboride, as shown by X-ray analysis of the reaction products. The two carbide-powder - organic-resin-bonded materials (inserts 11 and 12) failed by cracking in spite of a molybdenum reinforcing band. The primary mode of failure, however, was erosion due to loss of particles as the organic binder was removed during firing. The structure remaining after loss of the binder was not strong enough to withstand the shear forces in the rocket nozzle environment.

The 80 percent silicon dioxide - 20 percent carbon composite (insert 13) gave an overall erosion rate comparable to the better ablative inserts. The silica was believed to melt from the ablative envelope upstream of the insert and to form a foamed layer of silica over the insert surface, which protected it from oxidation and erosion. Figure 9 illustrates the protective layer of silica.

The GRB silicon carbide (silicon carbide - graphite - silicon) composite (insert 14) consisted of graphite and silicon particles in a silicon carbide matrix, as shown in figure 10. The purpose of the graphite particles was to prevent thermal shock cracking of the insert. In spite of the graphite, the insert failed by cracking during its second firing. Visual inspection of the insert following its initial 60-second firing indicated no cracking. While the erosion of the GRB insert was the lowest in its class, the structural failure prohibits its use in this configuration.

Refractory compounds. - The refractory compounds included oxides, carbides, borides, nitrides, and combinations of these. The materials tested and the test results

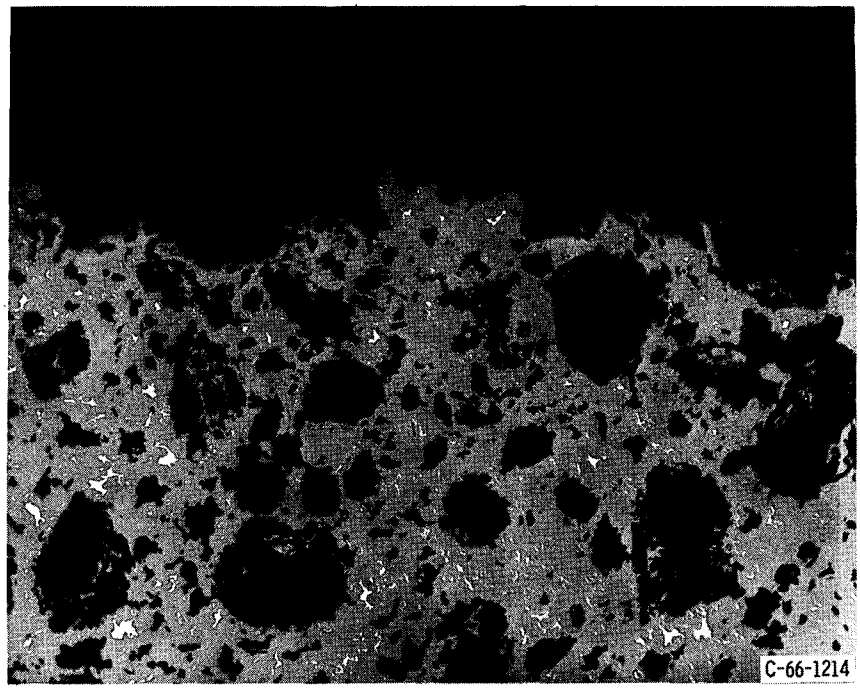

Figure 10. - Photomicrograph of nozzle insert 14 (GRB silicon carbide (64 percent silicon carbide - 33 percent carbon - 3 percent silicon)) after firing. Black particles are graphite; white particles are silicon; gray matrix is silicon carbide. Unetched. X75.

are summarized in table V(c). Reinforcing metal sleeves applied with an interference fit of 0.003 to 0.005 inch on the outside diameter were used on seven of these inserts. Even with reinforcing sleeves, the most prevalent mode of failure, as revealed by examination of tables I and V(c), was thermal stress or thermal shock cracking. Only the hypereutectic zirconium carbide (insert 28) was crack free following testing. This was the most promising insert of the group although it was fired for a relatively short duration. The zirconium diboride - stainless-steel sleeve combination (insert 20) was lost during testing and could not be checked for cracks. A drop in chamber pressure during firing indicated that the zirconium diboride material (insert 20), along with other borides and nitrides, suffered high erosion, probably due to rapid oxidation in the test environment.

Aluminum oxide (insert 18) and zirconium dioxide - silicon dioxide (insert 15) inserts experienced local erosion upstream of the throat in addition to cracking. The local erosion was caused by melting and fluxing of the inserts by molten silica from the ablative envelope upstream. The molten silica combined with both the aluminum oxide and the zirconium dioxide - silicon dioxide to lower their melting point.

The promising materials from an erosion standpoint included beryllium oxide, 85 percent beryllium oxide - 15 percent silicon carbide, silicon carbide, zirconium carbide, and niobium carbide, but all of these failed by cracking. Perhaps an added reinforcement or modified material combinations and processing techniques could be used

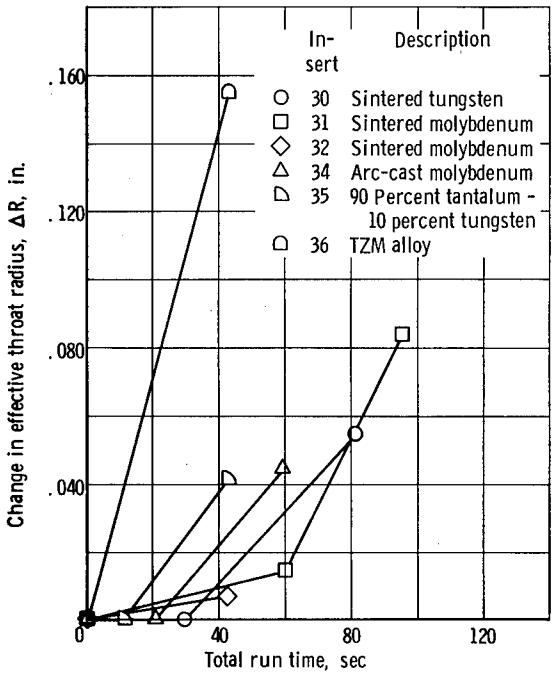

Figure 11. - Nozzle insert erosion of refractory metals and alloys.

to eliminate or control cracking of these refractory compounds.

An effort to apply controlled cracking was made by axially segmenting (six pieces) a silicon carbide insert (insert 24). The insert was lost due to downstream ablative failure; thus redesign of the mounting for this type of insert is required.

Refractory metals and alloys. - Three refractory metals (tungsten, molybdenum, and niobium) and two refractory metal alloys (90 percent tantalum - 10 percent tungsten and TZM (99 percent molybdenum, 1/2 percent titanium, and 1/2 percent zirconium)) were tested as inserts. The inserts and test results are listed in table V(d). All the inserts failed by oxidation or reaction with the combustion products, while the 90 percent tantalum - 10 percent tungsten also cracked. Erosion data are plotted in figure 11 for these inserts. Erosion due to oxidation was severe, particularly during the second test firing. The oxidation was frequently accompanied by severe gouging and the formation of a glassy deposit on the surface of the insert (see table I). Even in cases where throat erosion was relatively low, such as for the sintered molybdenum (insert 32), the severe oxidation at the upstream end of the insert indicated the need for redesign of the ablative-insert interface. No melting of the refractory metals was expected and none occurred. Figure 12(a), a photomicrograph of the sintered tungsten insert (insert 30), shows a recrystallized sintered tungsten with a dark glassy layer (believed to be amorphous silica) on the inside surface of the insert. Figure 12(b) shows the microstructure of TZM alloy (insert 36) after firing. A layer believed to be a nitride was found on the metal-gas interface of this insert.

The refractory metals and alloys generally were not suitable for the test environment. The niobium insert (insert 33) oxidized most severely of the 57 inserts tested and was almost completely consumed during the 17 seconds of testing.

Infiltrated refractory metals. - Tungsten specimens with three different infiltrants were evaluated as throat inserts. The results of these tests are summarized in table V(e). All three inserts failed by oxidation although only the tungsten-silver (insert 37) was badly oxidized over its entire surface. Erosion of the ablative material at the leading edge of the insert contributed to the failure of the 75 percent tungsten - 25 percent silver-copper eutectic (insert 38) and the 80 percent tungsten - 20 percent copper

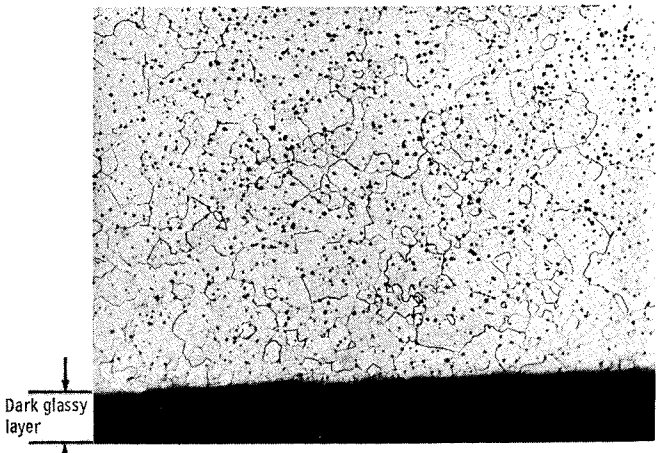

(a) Insert 30 (sintered tungsten). Etchant, 3-percent hydrogen peroxide solution. X250.

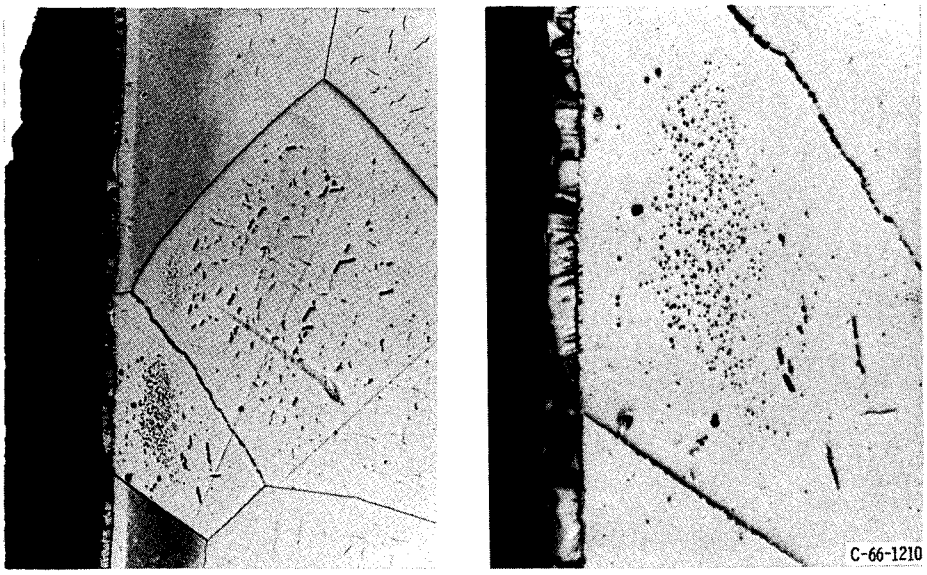

X250 X750

(b) Insert 36 (TZM alloy). Etchant, 5-percent potassium hydroxide - 5-percent potassium ferricynide solution. X750.

Figure 12. - Photomicrographs of nozzle inserts 30 and 36 after firing.

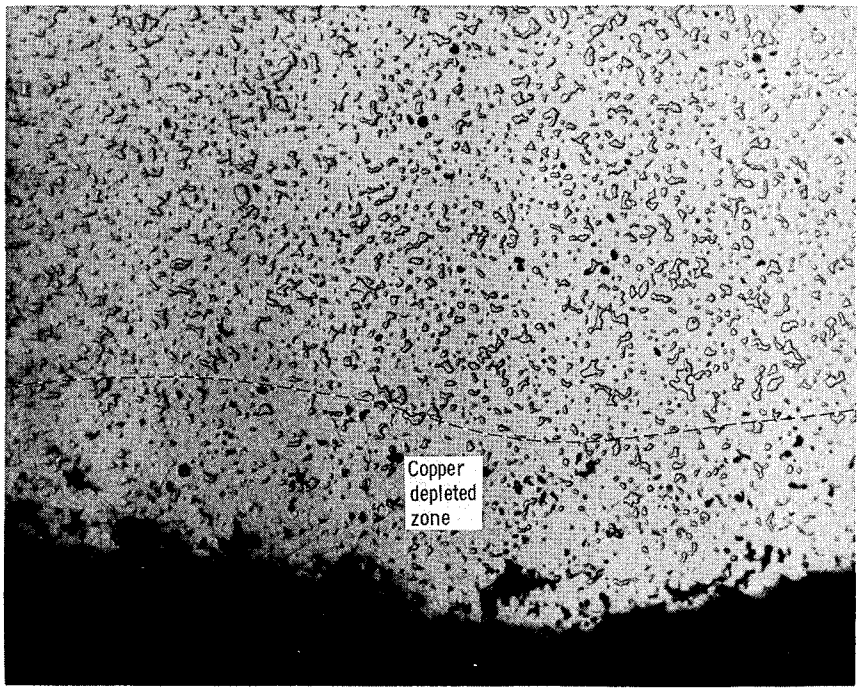

X250

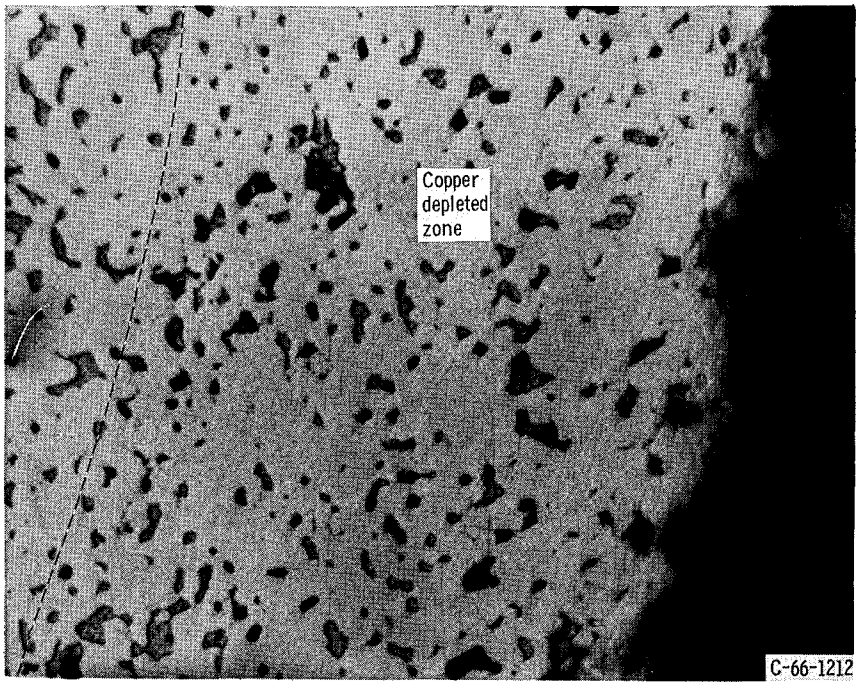

X750

Figure 13. - Photomicrographs of nozzle insert 39 (80 percent tungsten - 20 percent copper) after firing. Unetched.

(insert 39) inserts. The effect of the ablative-material erosion on the insert could include increased temperature because the insert leading edge was exposed to total stream temperature, increased mechanical erosion due to higher shear forces at the insert leading edge, or possible fluxing action of the molten silica on the insert material.

Figure 13 shows a photomicrograph of the throat section of the 80 percent tungsten - 20 percent copper insert (insert 39) after firing. The continuous matrix of tungsten is infiltrated with copper. On the hot-gas side is a region approximately 0.004 inch thick that has been depleted of copper. The dark islands are voids where copper has been removed. The gray islands are intruded copper. There was no evidence of melting or other structural change in the tungsten itself.

The manufacturer of the 75 percent tungsten - 25 percent silver-copper eutectic insert (insert 38) made a postfiring analysis, which is presented in the appendix. There was no throat erosion during the 60-second firing, but other tests indicate erosion failure might occur soon after 60 seconds.

While addition of infiltrants to the refractory metals was not sufficient to prevent oxidation in the test environment, the tungsten - silver-copper eutectic insert (insert 38) gave the best results of the three infiltrated refractory metal combinations tested and was a definite improvement over the pure refractory alloys listed in table V(d).

Graphite materials. - The materials tested included two high-density graphite inserts, four pyrolytic graphite inserts, and four graphites with additives intended to improve the oxidation resistance. Three of these inserts (inserts 45, 48, and 49) were used with a configuration (figs. 6(d) and (e)) designed to decrease erosion of the ablative material at the leading edge of the insert. The results are summarized in table V(f). Measurable erosion due to oxidation occurred with all of these inserts except the pyrolytic graphite insert, which had the ab plane axially oriented (insert 44) and failed primarily by delamination. The erosion rates of the graphite inserts are shown in figure 14. The most erosion-resistant graphite insert was pyrolytic graphite in the configuration of figure 6(e) (insert 45), which had relatively low erosion (ΔR = 0.036 in.) after 307 seconds total firing time. The ablative envelope used with insert 45 was completely charred through (see table I) because of the high radial heat transfer through the insert. Loss of insert retention resulted from overheating and melting of the ablative envelope.

The graphites with additives were more erosion resistant than ablative materials and ATJ graphite, but they had more erosion than desired for an insert (fig. 14). The additives were expected to oxidize and to form a protective coating on the hot-gas surface of the insert during engine operation. Figure 15 shows the protective layer formed on the surface of the JTA graphite insert (insert 46) during firing. The dark area is graphite, the bright spots are zirconium diboride, and the wavy band is the protective layer formed by the reaction of zirconium diboride and silicon carbide with the combustion gas products. The coating was evidently not sufficient to prevent oxidation. A protective coating

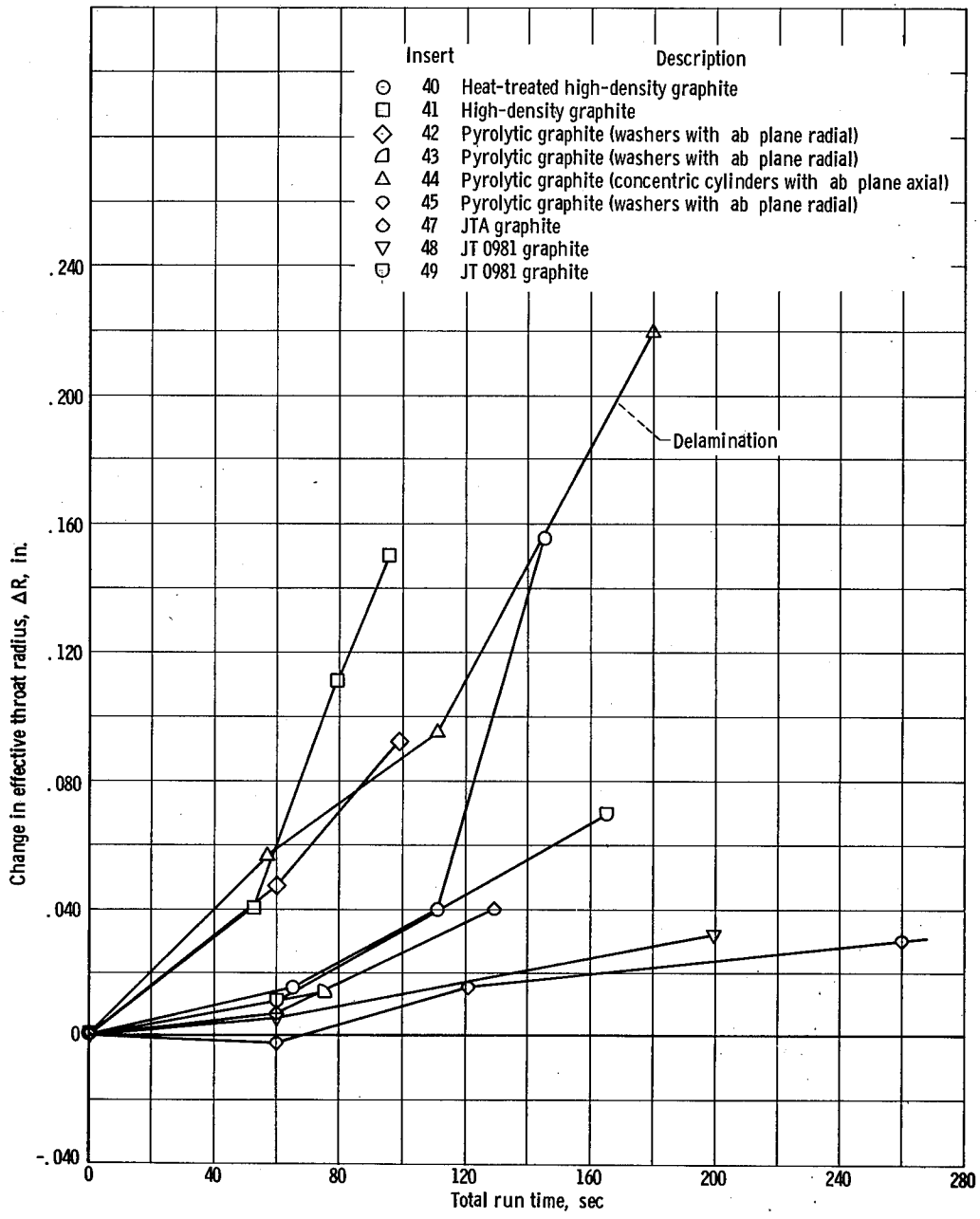

Figure 14. - Nozzle insert erosion of graphite materials.

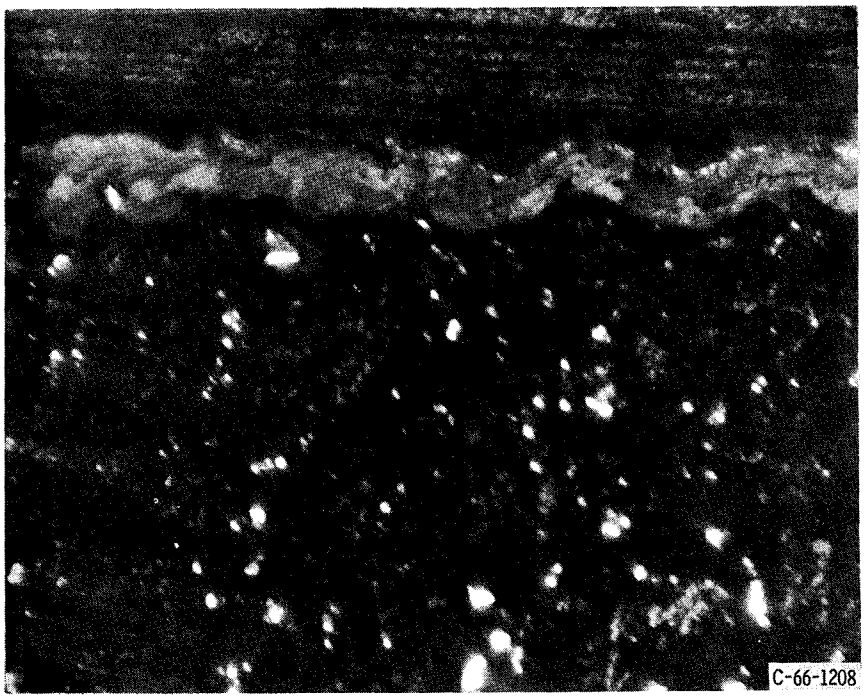

Figure 15. - Photomicrographs of nozzle insert 46 (JTA graphite) after firing. Unetched. X100.

was also formed on the JT 0981 graphite inserts (inserts 48 and 49), but this coating was nonadherent under repeated firing conditions. Examination of the photographs in tables I (48) and (49) shows that erosion of the ablative material at the insert leading edge caused excessive erosion of the JTO 981 graphite inserts at this point. The results indicate the need for a larger insert inlet diameter or the use of a nonablative material in the converging section of the nozzle.

Coated materials. - Six coatings and three substrates were evaluated. The materials and test results are listed in table V(g). The most successful coating was pyrolytic silicon carbide on a graphite substrate with an increased insert inlet diameter (fig. 6(f)) to alleviate erosion of the ablative material at the insert-ablative material interface. The silicon-carbide coated insert (insert 50) was tested in a configuration providing a large graphite heat sink (see table I(50)). In this configuration the coating was practically indestructible; however, some local spalling was observed, and the outside diameter of the envelope reached a temperature of approximately 1000° F during steady-state firing. This configuration was not applicable directly to an actual ablative engine. When a thinner graphite substrate was used in an ablative envelope (insert 51), the silicon carbide coating experienced no failure until 230 seconds of the fourth firing at 722 seconds of total run time. The failure at that time was associated with complete charring of the ablative envelope (see table I(51)) causing an increase in coating temperature. The pyrolytic-silicon-carbide-coated insert (insert 51) was the best of all the inserts tested.

Both of the pyrolytic graphite coatings (inserts 52 and 53) failed and permitted

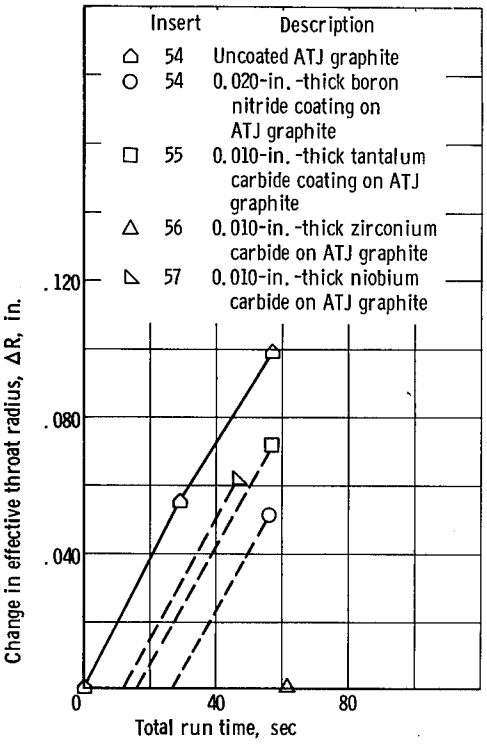

Figure 16. - Nozzle insert erosion of coated materials.

severe erosion of the graphite cloth substrate. Whether these coatings failed by erosion or cracking was not established. Cracking is the most likely cause since no evidence of erosion was found on the undisturbed coating remaining. Three of the coatings, boron nitride (insert 54), tantalum carbide (insert 55), and niobium carbide (insert 57), were completely eroded from their graphite substrates at the end of the 60-second firings. The zirconium carbide coating (insert 56) was oxidized to zirconium dioxide during firing and in this form offered protection to the graphite substrate. There were, however, pin holes in the zirconium dioxide coating as well as some indications of a reaction with the molten silica from the ablative block; moreover, the leading edge of the coating at the ablative-insert interface was completely removed. Leading edge failure may also have resulted in coating loss for inserts 54, 55, and 57.

The erosion of coated ATJ graphite inserts was compared with that of ATJ graphite alone (fig. 16) as an indication of specific coating advantages. Insert 54 was tested after the coating was completely removed to determine uncoated ATJ graphite erosion. The unprotected ATJ graphite was found to have an erosion rate of 1.75 mils per second in the test environment. If no graphite erosion occurred until the coating was removed, it is assumed that the coatings protected the ATJ graphite for relatively short times, on the order of 10 to 30 seconds, for those coatings removed completely during firing.

Theoretical Calculations

Thermal-shock index. - An arbitrary indicator of thermal-shock sensitivity was used to correlate insert crack failures. The parameter used for this correlation is as follows (ref. 2):

$$R' = \frac{kS}{\alpha E}$$

where

R' thermal-shock index

k thermal conductivity, Btu/(ft)(hr)(^{o}F)

S tensile strength, lb/in.^{2}

α Linear coefficient of thermal expansion, in./(in.)(^{o}F)

E Young's modulus, lb/in.^{2}

The values calculated for the materials tested are listed in table VI along with the degree of cracking found for the configuration tested. The cracking fell into four general classifications: none, minor, moderate, and severe. The relative magnitude of the parameter R' gives a fair indication of the degree of thermal cracking to be expected. The R' values for the 100-percent-dense beryllium oxide and the JTA graphite indicate that the cracking results are reversed. The inconsistency may be due to incorrect material properties being used to calculate either of the parameters. The R' value was calculated by using ambient temperature property values since these properties were most readily available and since the thermal shock was normally applied to an insert at relatively low temperature. Note that the degree of cracking observed experimentally and associated with the R' values applied only to the particular test geometry used.

Temperature and stress analyses. - As an aid in evaluating the problem of thermal stress failure of the more erosion-resistant insert materials, a program using the methods of reference 5 was developed for use on a IBM 7094 computer. The purpose of the program was to compute radial temperature gradients required for computing the associated thermal stresses. A solution of the Bartz simple heat-transfer equation (ref. 6) was incorporated into the program to solve for front-face boundary conditions. The program was set up so that transport properties could be evaluated at a mean boundary layer temperature equal to the average of the wall temperature and effective driving temperature. It was programmed so that at each time a wall temperature was computed a new convective heat-transfer coefficient h_c was calculated. Material properties (conductivity and specific heat) as functions of temperature were also used in the program because these change quite rapidly for many materials. The temperature analysis was normally run until the maximum temperature difference across the insert was obtained. At this point of maximum ΔT, the insert stresses were computed by using the method outlined in reference 7 and were programmed for use on an IBM 7094 computer using FORTRAN IV language. The program makes the following assumptions:

(1) The materials are layerwise elastic, homogeneous, and isotropic.

(2) The elastic properties and the coefficient of thermal expansion are layerwise temperature independent, but are different from one layer to the next.

(3) The temperature is independent of the axial position (z-axis).

(4) The assembly under consideration is sufficiently long so that end effects are negligible in accordance with Saint Venant's principle.

The results of these analyses are presented in table VII. The test results for the refractory metals tungsten (insert 30) and molybdenum (insert 34) verified the analytical calculation that showed no stress failure. The zirconium dioxide - silicon dioxide insert (insert 15) failed in all modes during the test, as was predicted analytically. The reinforced aluminum oxide insert (insert 18) also failed in all modes as predicted. The results of this type of failure for both inserts are shown in tables I(15) and (18). For the reinforced aluminum oxide, it was not possible to find a restraint that would prevent both internal compression failure and external tension failure. The solution to the stress problem with aluminum oxide must involve a decreased insert thickness, some other means of reinforcement, or both. The insert analyses for the reinforced silicon carbide predicted success for both materials. The KT silicon carbide, however, was not tested, and the Avco silicon carbide (insert 25) failed as indicated in table V(c). The tantalum sleeve could not be applied to this insert with the required 0.005-inch interference fit because of a temperature limitation for the tantalum ring. The actual assembly, therefore, utilized a 0.003-inch interference fit, which was not sufficient to prevent cracking.

Design Considerations

Successful application of throat inserts to ablative-material rocket chambers requires considerable knowledge of the operating environment, properties of the materials involved, and compatibility of the various components.

The use of reinforcing sleeves requires precise interference values to be effective. Reinforcing rings must also be applied in an area where they will survive the rocket environment. Tables I(17), (22), (25) and (27) illustrate sleeves which failed because of melting and/or oxidation. Even when the sleeves were not damaged (the first run with insert 25), circumferential cracking occurred. This cracking may have been due to differential expansion between the sleeve and the insert in the longitudinal dimension, or to anisotropy of the insert material. Other methods of reinforcement, such as honeycomb structures or dispersed wires, may prove more practical than the use of sleeves with an interference fit.

Pyrolytic graphite presents special design problems because of its unique properties. As was shown in an earlier section, pyrolytic graphite with the high-conductivity plane oriented radially provided good erosion resistance but caused the ablative envelope to melt (table I(45)). On the other hand, pyrolytic graphite with the high-conductivity plane oriented axially failed by delamination but kept the ablative char to a minimum (see

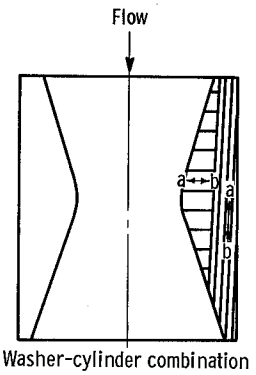

Washer-cylinder combination

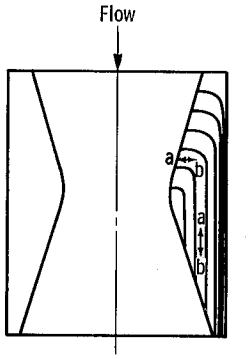

Curved-plane orientation

Figure 17. - Pyrolytic graphite nozzle inserts.

table I(44)). Two methods for combining these concepts are shown in figure 17. These designs would both be compromises between low erosion (oxidation), because they would keep the inside surface relatively cool, and protection of the ablative envelope, because they would insulate the outside diameter.

Many of the more promising insert materials, such as the oxides and carbides, are subject to attack by molten silica from the ablative material upstream of the insert. The test results suggest that the flow of molten silica could be eliminated if the silica is replaced by a nonreactive material or removed to an area where molten flow will not occur. Evidence of ablative-material erosion at the insert leading edge was found in all inserts of this test series. The most effective method for solving this problem would be to replace the ablative with a noneroding material in all areas where the flow conditions are severe enough to melt and erode the ablative. Placing the insert-ablative interface at as low a flow velocity location as possible helped to minimize this problem. The most successful design in this respect was that of figure 6(f), which was used for inserts 50 and 51. Erosion at the insert leading edge was slowed considerably as shown by the photographs in tables I(50) and (51) taken after the relatively long run times experienced by these inserts.

The final design consideration should be the thickness relation between the insert and the ablative envelope required by the firing time and duty cycle of a particular engine. Failure of inserts 45 and 51, for instance, was associated with complete char-through of the ablative envelope. Each insert design requires knowledge of the precise firing requirements if a realistic approach is to be made. Some insert materials may be applicable only to single long-duration, firings while others may be more applicable to cyclic operation.

SUMMARY OF RESULTS

A total of 57 throat inserts for ablative nozzles with nominal 1.20-inch throat diameters were tested at an oxidant-fuel ratio of approximately 2.0 and a chamber pressure of 100 pounds per square inch absolute with nitrogen tetroxide and a blend of 50-percent hydrazine and 50-percent unsymmetrical dimethyl hydrazine as propellants. The following results were obtained:

1. A pyrolytic-silicon-carbide-coated graphite insert showed the best results totaling 722 seconds in four test firings before failure.

2. Special ablative-reinforced plastic materials tested as inserts did not perform significantly better than standard ablative materials.

3. The composite materials failed structurally and by erosion because of oxidation. While the GRB silicon carbide - graphite insert gave the best erosion resistance of the composites tested, it failed structurally after the second test firing.

4. The major problem with refractory compounds was structural failure. The only material that did not fail was a hypereutectic zirconium carbide. The remainder of these materials required some type of reinforcement to prevent cracking. Material properties at high temperature and precise temperature and stress analyses are required to design inserts of refractory compounds. Initial theoretical analyses indicated that this tool will be only a design guide until more precise definitions of engine environment and material properties are available.

5. Rapid oxidation was experienced by the refractory metals and alloys in the test environment.

6. The cooling effect or blocking of oxidizing gases from the surface by infiltrants in tungsten was not sufficient to prevent oxidation in the test environment but did provide an improvement over pure tungsten.

7. Pyrolytic graphite was a promising material but required a compromise design to keep both the throat and the ablative envelope as cool as possible. Other graphites were generally subject to erosion because of rapid oxidation in the test environment. Protective oxides that were formed on the surface of graphite composites before and during firing did not prevent erosion.

8. The causes of coating failures were not completely defined. The coating must resist attack by the exhaust environment as well as maintain structural integrity with its substrate. Attention must be given to protection of the leading edge of the coating at the ablative-insert interface since failure at any point of the coating leads to rapid substrate erosion.

9. The possibility of reactions between the throat insert and reaction products, such as molten silica from the upstream ablative material, must be considered in designing throat inserts for ablative engines.

10. Test experience indicated that the interface between the ablative material and the insert should be placed at as low a flow velocity point as possible to minimize erosion of the ablative material.

Lewis Research Center,
National Aeronautics and Space Administration,
Cleveland, Ohio, March 14, 1966.

APPENDIX - ANALYSIS BY UNION CARBIDE LINDE DIVISION OF INSERT 38 (75 W - 25 Ag-Cu EUTECTIC) TEST FIRED BY LEWIS RESEARCH CENTER

Introduction

A rocket nozzle fabricated by Union Carbide (Linde Division) was test fired by the Lewis Research Center as part of their materials evaluation program for the development of an uncooled liquid engine. The nozzle material was LW-6 (tungsten) infiltrated with silver-copper eutectic. This appendix contains a summary of the evaluation results obtained by Union Carbide on the fired nozzle.

Nozzle Evaluation

In order to simplify the evaluation, the nozzle was divided into five zones, as shown in figure 18.

Zone 1 was exposed to the flame throughout the test and, as a result, suffered material loss from erosion and oxidation of the tungsten. This loss was concentrated in the entrance section of the nozzle and had a maximum depth of penetration of approximately 0.054 inch. The erosion was nonuniform and decreased in severity toward the exit section.

Zone 2 is the area adjacent to the eroded surface of the nozzle. This zone is quite thin (from 0.003 to 0.007 in.) and represents the area weakened by oxidation. Again, the depth of the zone decreased toward the exit section of the nozzle. It is interesting to note that even though loss of the infiltrant had occurred, a substantial volume was still present.

In Zone 3 the laminar tungsten had been recrystallized into an equiaxed structure.

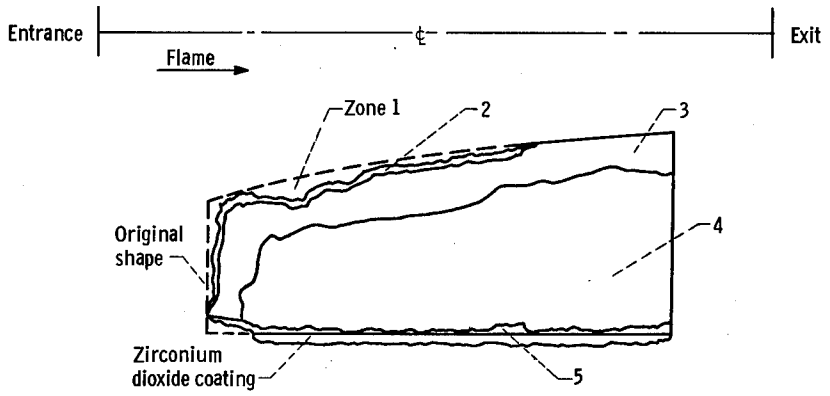

Figure 18. - Cross section of nozzle insert.

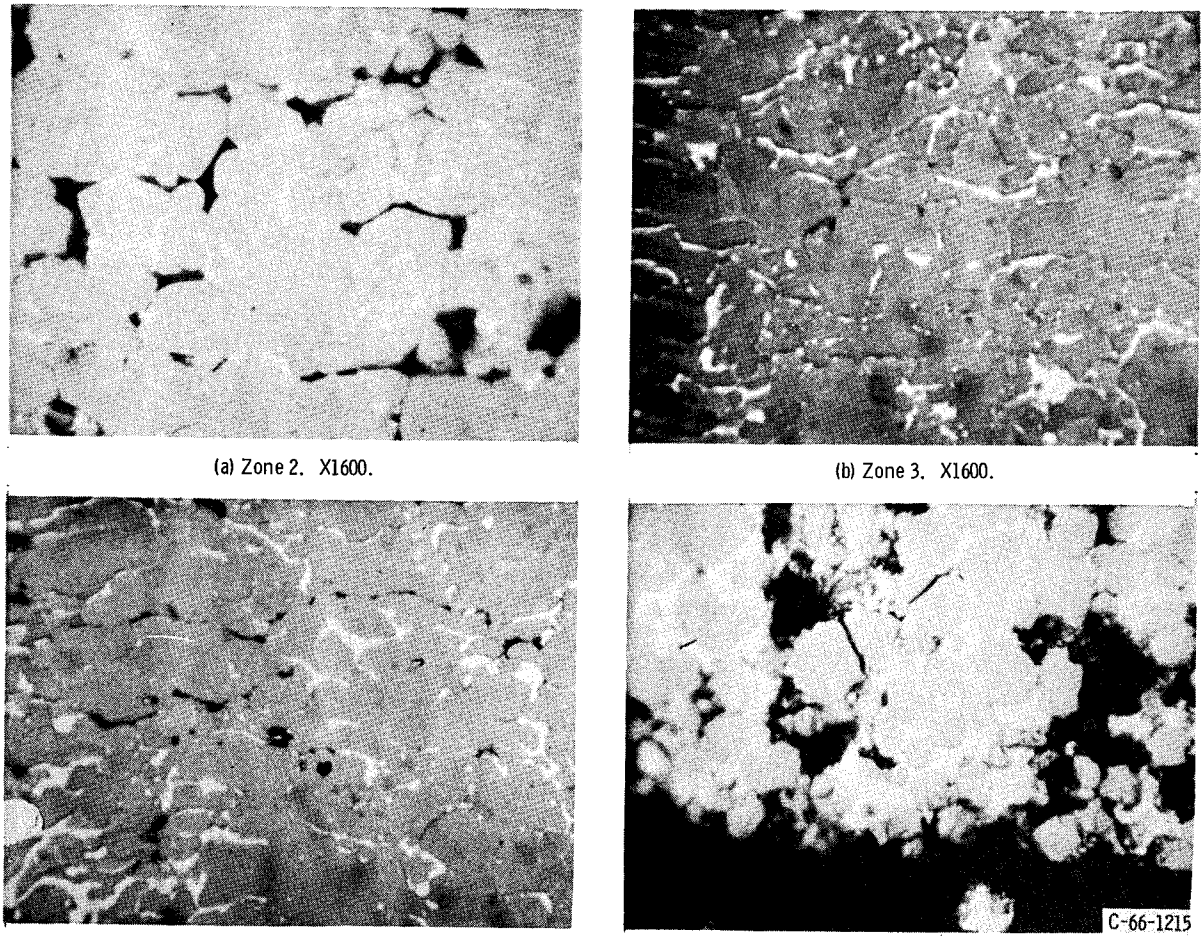

(a) Zone 2. X1600.

(b) Zone 3. X1600.

(c) Zone 4. X1600.

(d) Zone 5. X1200.

Figure 19. - Photomicrographs of test nozzle zones.

No loss of infiltrant was found.

Zone 4 had areas of porosity produced from migration of the infiltrant into surrounding areas around the zone; however, these areas were small and did not constitute the major volume of the infiltrant.

Zone 5 includes the outside surface of the nozzle, which was coated by NASA with zirconia dioxide prior to firing. This zone was evidently exposed to the flame because of leakage around the nozzle since the entrance was eroded and since massive recrystallization of the tungsten had occurred. In addition, oxidation attack and loss of infiltrant, similar to that found in zone 2, was present.

Photomicrographs of the different zones are shown in figure 19. The photomicrographs in figure 20 show the structure of the nozzle before firing. This structure is uniform and, therefore, represents the entire nozzle.

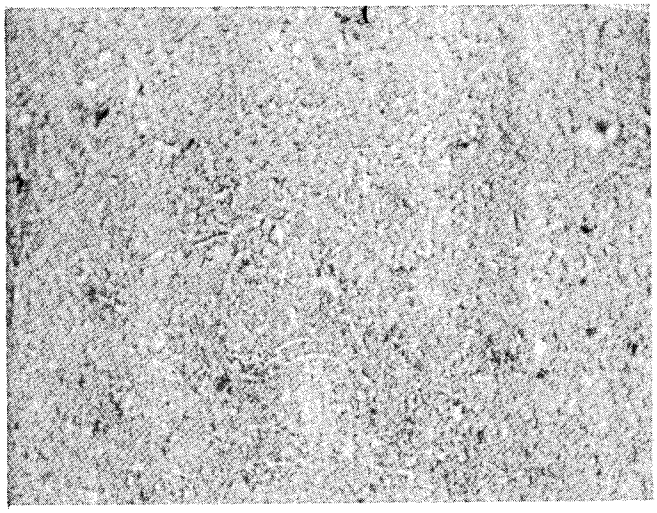

X500

X1000

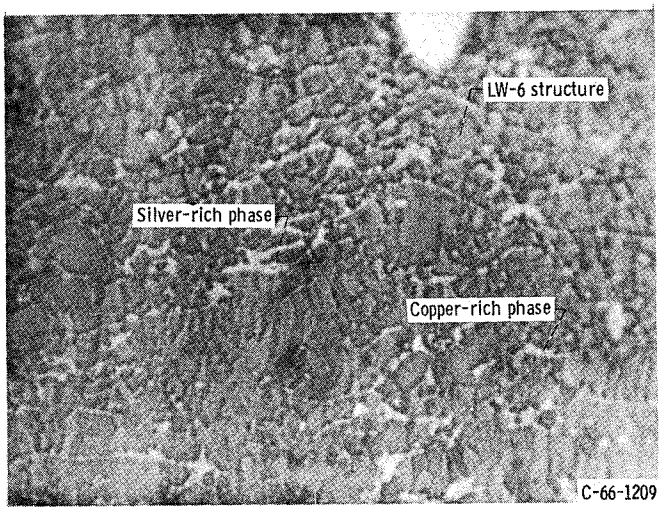

X1600

Figure 20. - Photomicrographs of test nozzle before firing.

Conclusions

Surface erosion caused by oxidation of the tungsten had occurred in the entrance and throat sections of the nozzle. Because of the high temperatures, the laminar tungsten structure had been recrystallized. The temperature was at least 779^{o} C since the infiltrant had melted and migrated to the hot surfaces of the nozzle.

REFERENCES

1. Anon: Reaction Control Engines and Positive Expulsion Tankage for Space Vehicles. Rept. No. 8500-945006, Bell Aerosystems Co., Jan. 1964.

2. Anon: On the Evaluation of Nozzle Materials. Rept. No. 19-65 (DDC No. AD 461305), Thiokol Chemical Corp., 1965.

3. Vogan, J.W.; and Trumbull, J.L.: Metal-Ceramic Structural Composite Materials. (AF ML-TDR-64-83, DDC No. AD604685), Boeing Company, June 1964.

4. Peterson, Donald A.; and Meyer, Carl L.: Experimental Evaluation of Several Ablative Materials as Nozzle Sections of a Storable Propellant Rocket Engine, NASA TM X-1223, 1966.

5. Hatch, James E.; Schacht, Ralph L.; Albers, Lynn U.; and Saper, Paul G.: Graphical Presentation of Difference Solutions for Transient Radial Heat Conduction in Hollow Cylinders with Heat Transfer at the Inner Radius and Finite Slabs with Heat Transfer at One Boundary, NASA TR R-56, 1960.

6. Bartz, D.R.: A Simple Equation for Rapid Estimation of Rocket Nozzle Convective Heat Transfer Coefficients. Jet Propulsion, vol. 27, no. 1, Jan. 1957, pp. 49-51.

7. Au, Norman N.: Stresses and Strains in Multi-Layer Disks, Cylinders, and Spheres Under Pressure Loading and an Arbitrary Radial Temperature Gradient. Rept. No. TDR-269(4304)-2(SSD-TDR-63-227), Aerospace Corp., Oct. 1963.

TABLE I. - INSERT DESCRIPTION

(1) Insert 1; configuration A; injector 11; characteristic length, 65; no coating

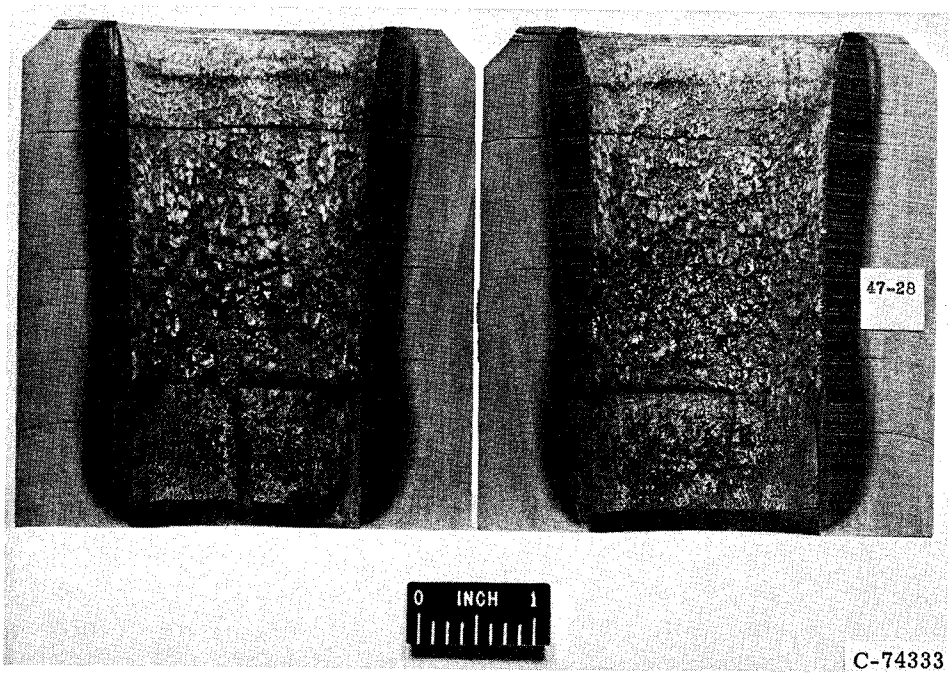

	Material	Form	Manufacturer	Additional layer
Insert	Pyrolyzed graphite phenolic with SiC-Si additive	Cloth (90^{o} to centerline)	Chance-Vought	None
Envelope	Silica phenolic (MX 2641)	Cloth (90^{o} to centerline)	Fiberite	0.25-in.-thick stainless-steel shell

Run	Chamber pressure, P_c, psia	Oxidant-fuel ratio, O/F	Run time, sec	Total change in effective throat radius, ΔR, in.	Remarks
22	106.6 to 101.6	1.92	60.2	0.0065	Timed shutdown
28	101.8 to 86.9	2.04	43.3	.060	Low chamber pressure shutdown
37	105.7 to 85.7	2.16	34.1	.206	Low chamber pressure shutdown
			137.6		

TABLE I. - Continued. INSERT DESCRIPTION

(2) Insert 2; configuration B; injector 11; characteristic length, 67; no coating

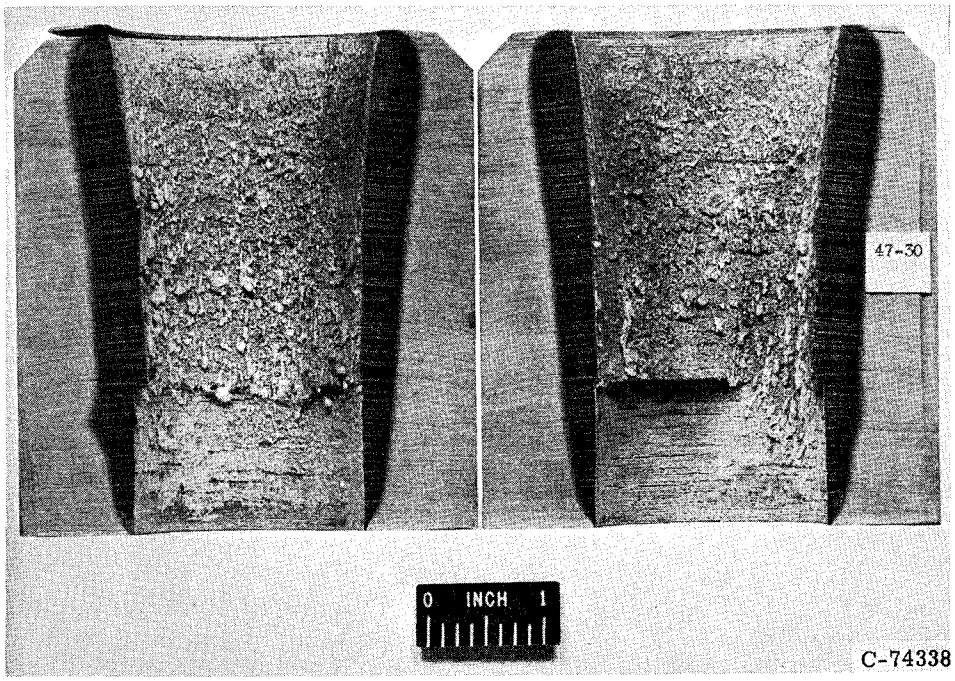

	Material	Form	Manufacturer	Additional layer
Insert	Precharred silica epoxy	C1554-48 cloth (90^{o} to centerline)	Avco Corp	None
Envelope	Silica phenolic MX 2641	Cloth (90^{o} to centerline)	Haveg	0.250-in.-thick stainless-steel shell

Run	Chamber pressure, P_c, psia	Oxidant-fuel ratio, O/F	Run time, sec	Total change in effective throat radius, ΔR, in.	Remarks
32	106.9 to 87.6	1.97	49.7	0.0755	Low chamber pressure shutdown
44	101.0 to 90.0	2.38	79.8	.1505 (calc)	Low chamber pressure shutdown
			129.5		

TABLE I. - Continued. INSERT DESCRIPTION

(3) Insert 3; configuration B; injector 11; characteristic length, 67; no coating

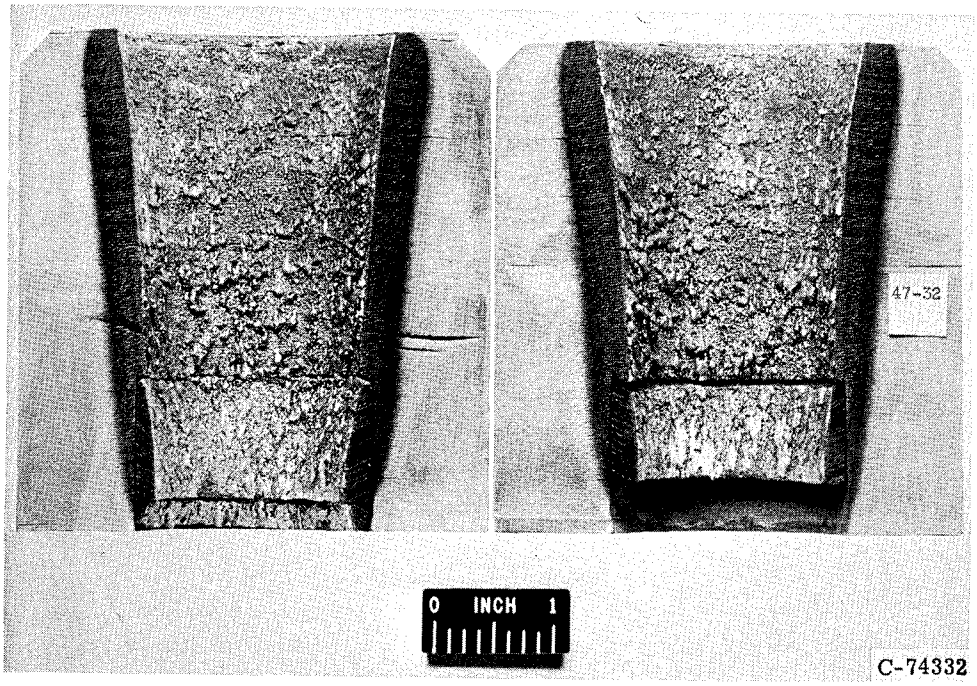

	Material	Form	Manufacturer	Additional layer
Insert	Precharred silica epoxy	C1554-48 cloth (60^{o} to centerline)	Avco Corp	None
Envelope	Silica phenolic MX 2641	Cloth (90^{o} to centerline)	Haveg	0.25-in.-thick stainless-steel shell

Run	Chamber pressure, P_c, psia	Oxidant-fuel ratio, O/F	Run time, sec	Total change in effective throat radius, ΔR, in.	Remarks
33	106.2 to 86.8	1.97	43.7	0.0535	Low chamber pressure shutdown
49	103.0 to 83.3	1.93	39.5	.173 (calc)	Low chamber pressure shutdown
			83.2		

TABLE I. - Continued. INSERT DESCRIPTION

(4) Insert 4; configuration B; injector 11; characteristic length, 67; no coating

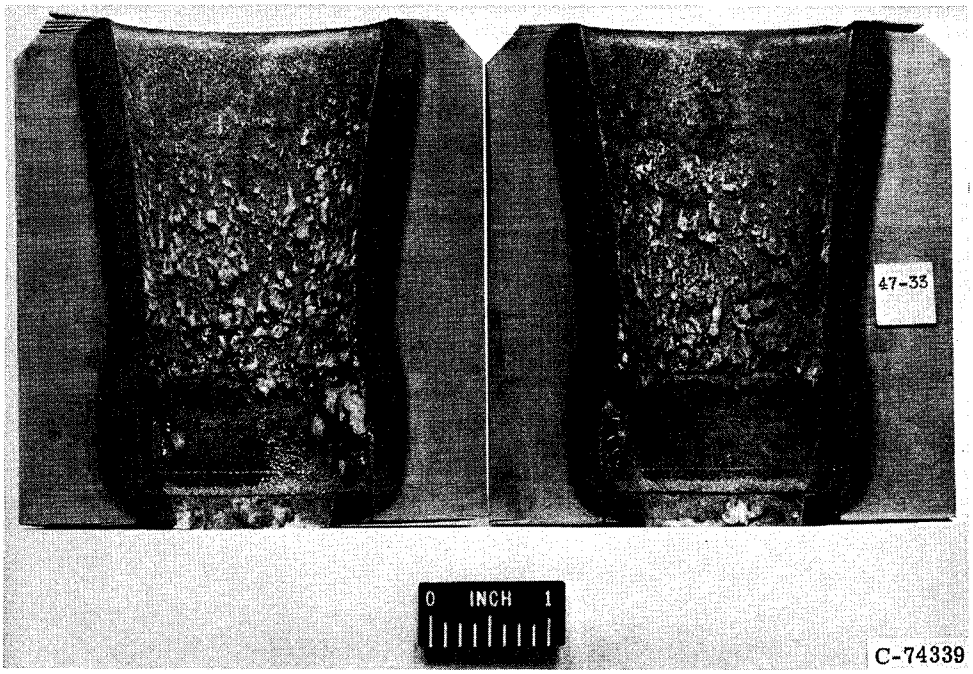

	Material	Form	Manufacturer	Additional layer
Insert	Graphite phenolic with ZrC-SiC powder additive	Cloth (90^{o} to centerline)	Chance-Vought	None
Envelope	Silica phenolic (MX 2641)	Cloth (90^{o} to centerline)	Fiberite	0.250-in.-thick stainless-steel shell

Run	Chamber pressure, P_c, psia	Oxidant-fuel ratio, O/F	Run time, sec	Total change in effective throat radius, ΔR, in.	Remarks
38	119.0 to 85.6	2.24	57.0	0.1465 (calc)	Low chamber pressure shutdown

TABLE I. - Continued. INSERT DESCRIPTION

(5) Insert 5; configuration B; injector 11; characteristic length, 67; no coating

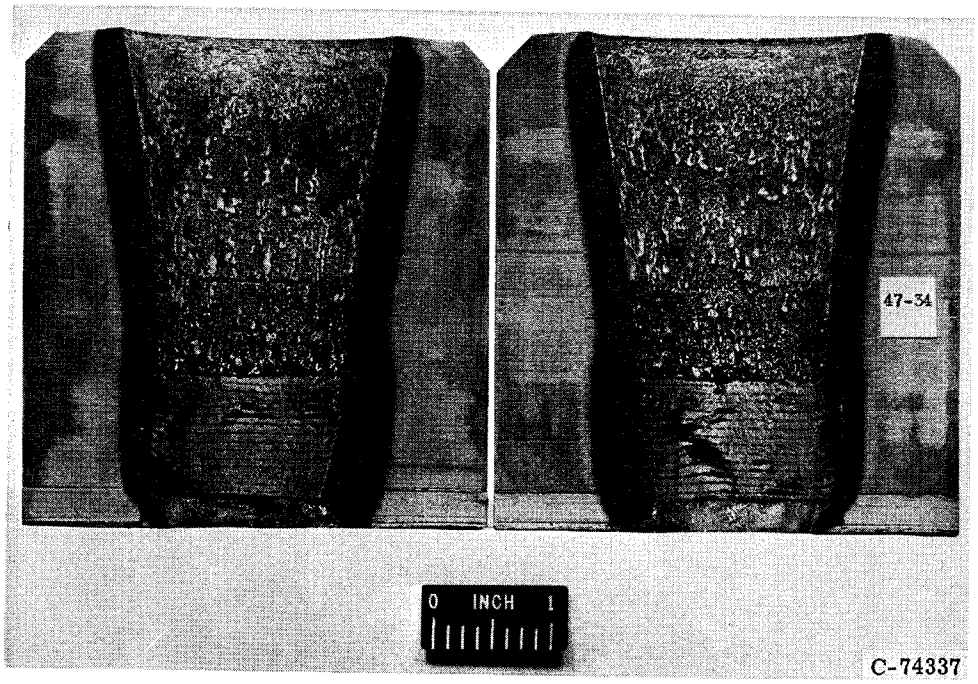

	Material	Form	Manufacturer	Additional layer
Insert	Graphite phenolic with Hf-Si powder additive	Cloth (90^{o} to centerline)	Chance-Vought	None
Envelope	Silica phenolic (MX 2641)	Cloth (90^{o} to centerline)	Fiberite	0.25-in.-thick stainless-steel shell

Run	Chamber pressure, P_c, psia	Oxidant-fuel ratio, O/F	Run time, sec	Total change in effective throat radius, ΔR, in.	Remarks
46	103.5 to 102.6	1.54	5.5	-----	Timer shutdown for facility check
47	106.6 to 85.1	1.71	39.8	0.080	Low chamber pressure shutdown
			45.3		

TABLE I. - Continued. INSERT DESCRIPTION

(6) Insert 6; configuration C; injector 11; characteristic length, 67; no coating

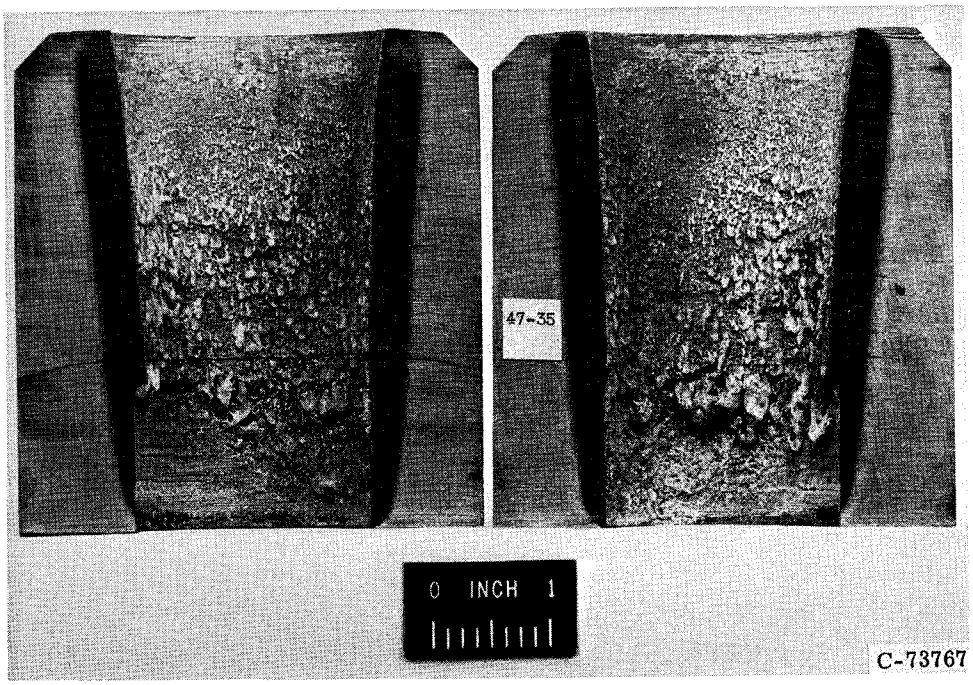

	Material	Form	Manufacturer	Additional layer
Insert	Graphite phenolic with Hf-Si powder additive	Cloth (90^{o} to centerline)	Chance-Vought	None
Envelope	Silica phenolic (MX 2641)	Cloth (90^{o} to centerline)	Fiberite	0.25-in.-thick stainless-steel shell

Run	Chamber pressure, P_c, psia	Oxidant-fuel ratio, O/F	Run time, sec	Total change in effective throat radius, ΔR, in.	Remarks
24	102.0 to 86.6	1.74	60.1	0.0645	Low chamber pressure shutdown
29	105.1 to 89.8	2.51	26.2	.1345	Low chamber pressure shutdown
			86.3		

TABLE I. - Continued. INSERT DESCRIPTION

(7) Insert 7; configuration B; injector 11; characteristic length, 67; no coating

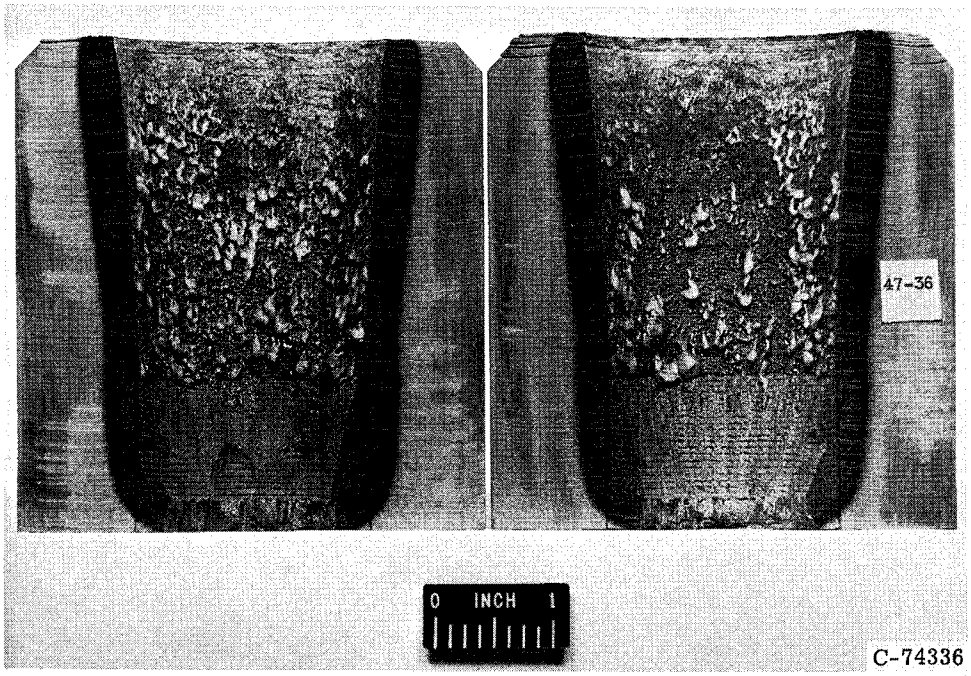

	Material	Form	Manufacturer	Additional layer
Insert	Graphite-phenolic with TaO_2-Si powder additive	Cloth (90° to centerline)	Chance-Vought	None
Envelope	Silica phenolic (MX 2641)	Cloth (90° to centerline)	Fiberite	0.25-in.-thick stainless-steel shell

Run	Chamber pressure, P_c, psia	Oxidant-fuel ratio, O/F	Run time, sec	Total change in effective throat radius, ΔR, in.	Remarks
48	98.4 to 85.0	1.78	53.0	0.0685	Low chamber pressure shutdown

TABLE I. - Continued. INSERT DESCRIPTION

(8) Insert 8; configuration C; injector 11; characteristic length, 67; no coating

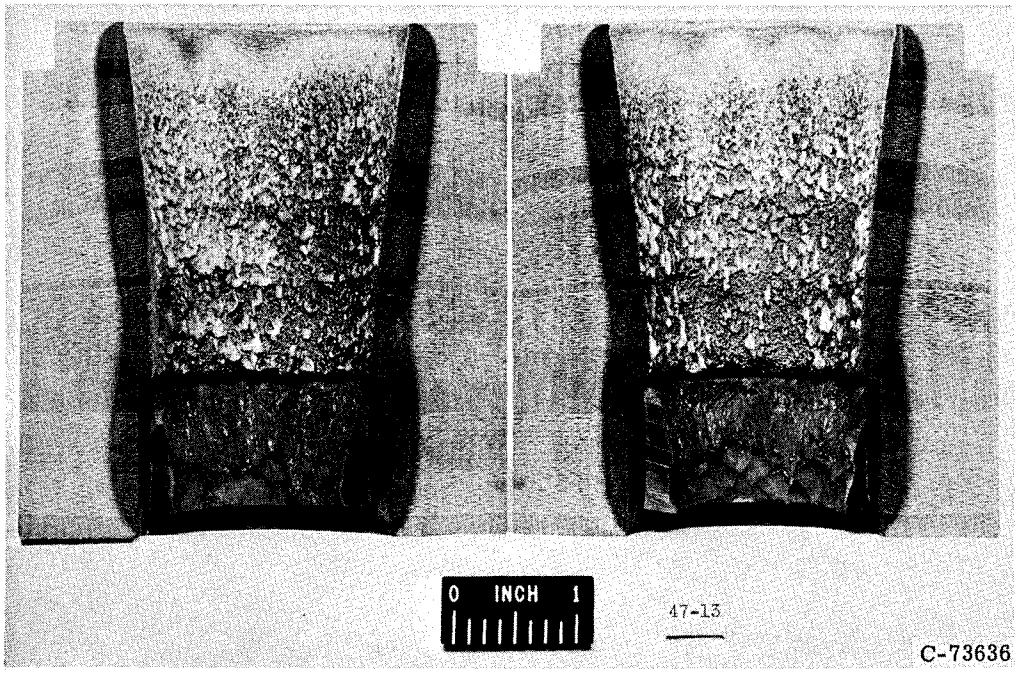

	Material	Form	Manufacturer	Additional layer
Insert	50 WC - 50 Ag	WC powder in Ag matrix	Mallory	0.085-in.-thick Rokide Z on insert outside diameter
Envelope	Silica phenolic (MX 2641)	Cloth (90^{o} to centerline)	Haveg	0.25-in.-thick stainless-steel shell

Run	Chamber pressure, P_c, psia	Oxidant-fuel ratio, O/F	Run time, sec	Total change in effective throat radius, ΔR, in.	Remarks
410	108.5 to 90.0	2.20	39.0	0.0925 (calc)	Insert pitted, Rokide gone

TABLE I. - Continued. INSERT DESCRIPTION

(9) Insert 9; configuration C; injector 11; characteristic length, 67; no coating

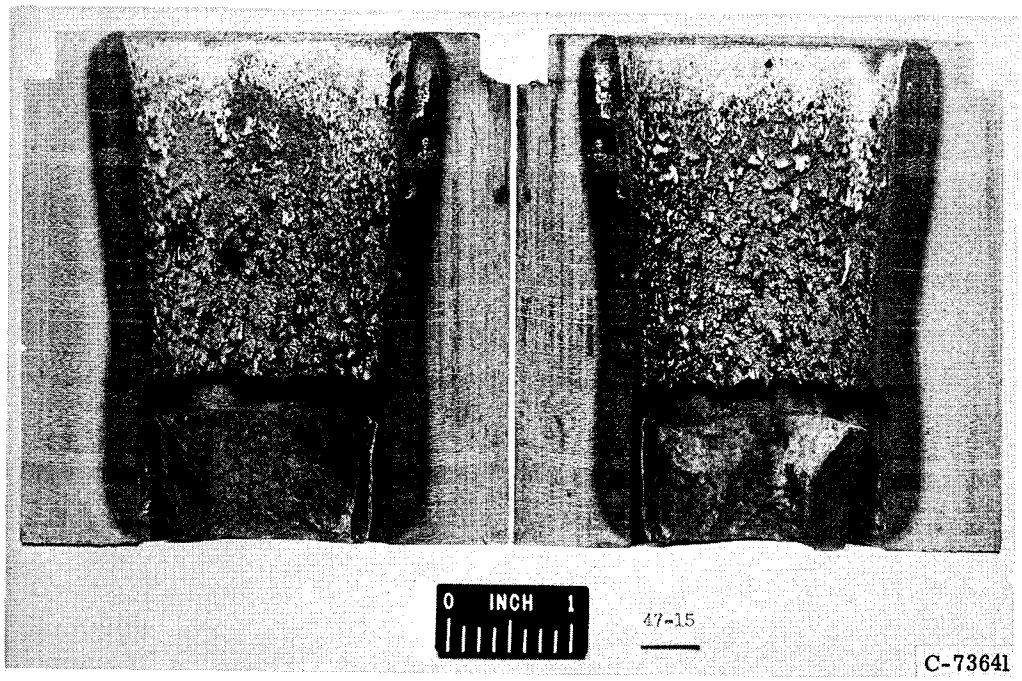

	Material	Form	Manufacturer	Additional layer
Insert	57 WC - 43 Cu	WC powder in Cu matrix	Mallory	0.042-in.-thick Rokide Z
Envelope	Silica phenolic (MX 2641)	Cloth (90^{o} to centerline)	Haveg	0.25-in.-thick stainless-steel shell

Run	Chamber pressure, P_c, psia	Oxidant-fuel ratio, O/F	Run time, sec	Total change in effective throat radius, ΔR, in.	Remarks
8	104.0 to 90.7	1.89	60.0	0.048 (calc)	Melting and cracking

TABLE I. - Continued. INSERT DESCRIPTION

(10) Insert 10; configuration B; injector 11; characteristic length, 67; no coating

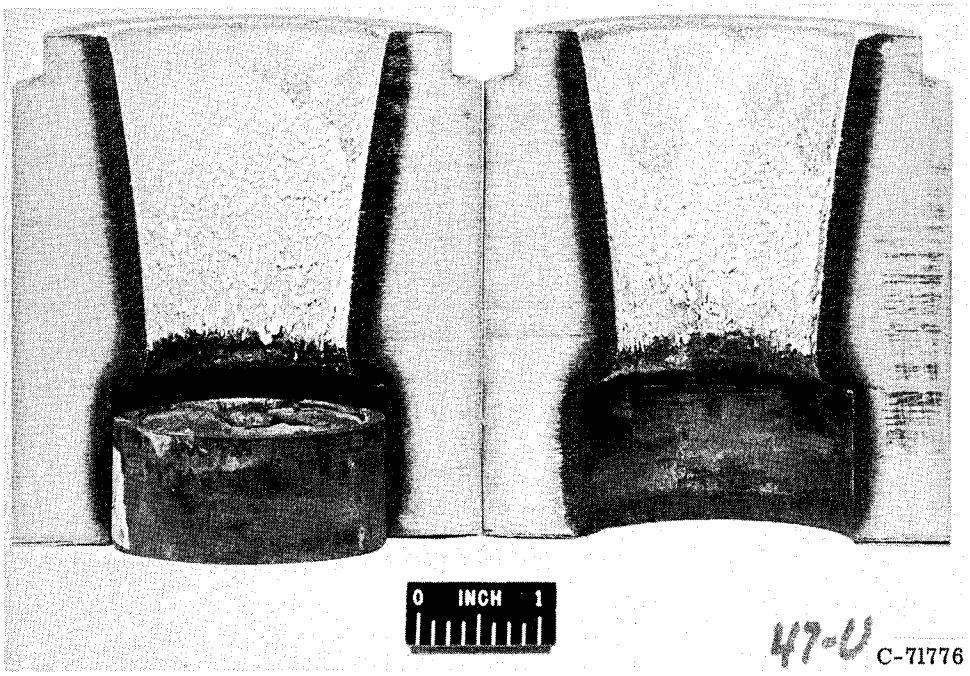

	Material	Form	Manufacturer	Additional layer
Insert	TiB_2 with ZrO_2 filler		Caloboric	0.040-in.-thick Rokide Z, 0.125-in.-thick stainless-steel sleeve with 0.005 interference fit
Envelope	Silica phenolic (MX 2641)	Tape (90° to centerline)	Haveg	0.25-in.-thick stainless-steel shell

Run	Chamber pressure, P_c, psia	Oxidant-fuel ratio, O/F	Run time, sec	Total change in effective throat radius, ΔR, in.	Remarks
341	101 to 93	2.24	21.9	0.0465	Low chamber pressure shutdown
360	101 to 92	2.23	19.2	.1015	Low chamber pressure shutdown
366	97.5 to 92	2.20	13.6	.1345	Low chamber pressure shutdown
			54.7		

TABLE I. - Continued. INSERT DESCRIPTION

(11) Insert 11; configuration D; injector 11; characteristic length, 66; no coating

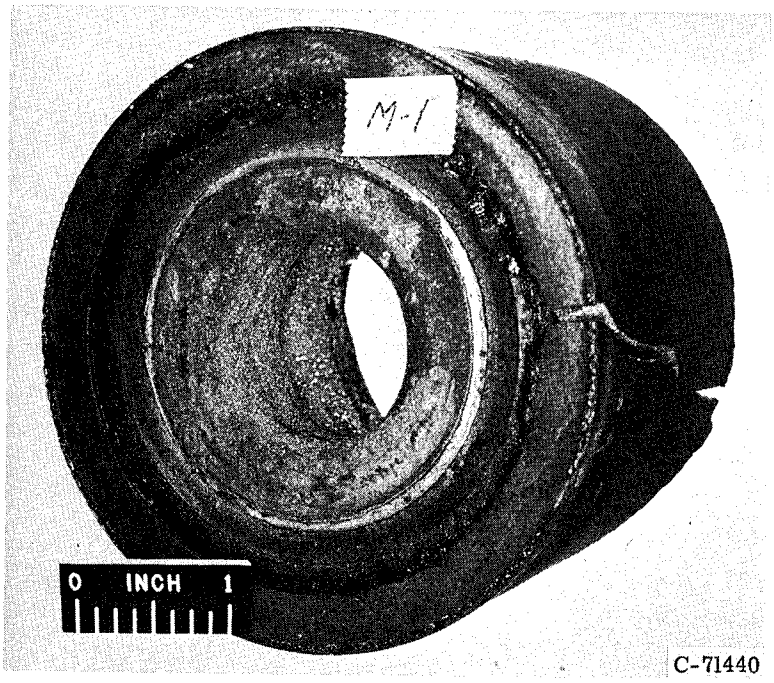

C-71440

	Material	Form	Manufacturer	Additional layer
Insert	ZrC-SiC coated graphite powder with organic resin binder	Pressed and sintered	Magnesium Aerospace	0.125-in.-thick Mo sleeve with 0.005 interference fit
Envelope	Zirconated silica phenolic	Cloth (90^{o} to centerline)	Magnesium Aerospace	0.325-in.-thick nylon sleeve 0.25-in.-thick stainless-steel shell

Run	Chamber pressure, P_c, psia	Oxidant-fuel ratio, O/F	Run time, sec	Total change in effective throat radius, ΔR, in.	Remarks
350	--------	----	3.4	-----	High chamber pressure shutdown
351	105 to 90	2.02	$\frac{23.6}{27.0}$	0.565	Circumferential cracks

TABLE I. - Continued. INSERT DESCRIPTION

(12) Insert 12; configuration D; injector 11; characteristic length, 66: no coating

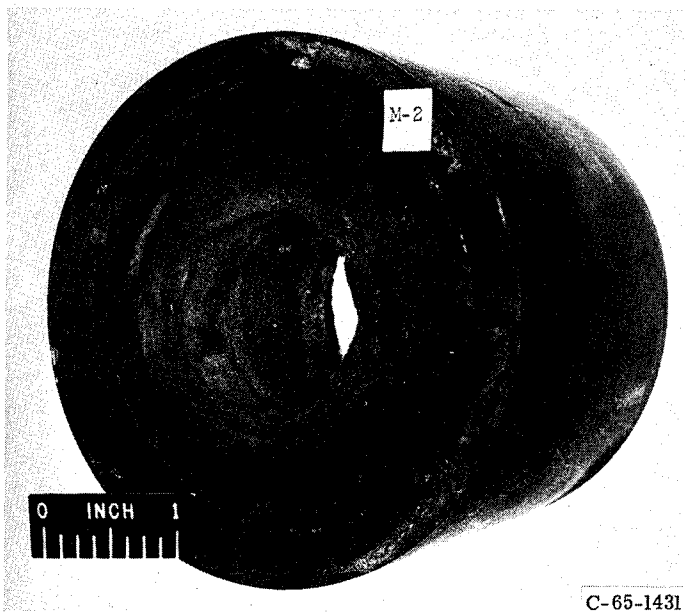

C-65-1431

	Material	Form	Manufacturer	Additional layer
Insert	HfC-SiC coated graphite powder	Pressed and sintered	Magnesium Aerospace	0.125-in. -thick Mo sleeve with 0.005 interference fit
Envelope	Silica phenolic	Cloth (90^{o} to centerline)	Magnesium Aerospace	0.325-in. -thick nylon sleeve, 0.25-in. -thick stainless-steel shell

Run	Chamber pressure, P_c, psia	Oxidant-fuel ratio, O/F	Run time, sec	Total change in effective throat radius, ΔR, in.	Remarks
328	101 to 91	1.68	33.8	0.031	Circumferential crack 1/4 in. from exit plane
352	102.1	1.84	7.1	.0575	Leakage abort
369	----------	----	2.9	------	Low chamber pressure shutdown
370	96.5 to 91.0	2.20	10.8	.1025	Low chamber pressure shutdown, axial cracks
377	96.5 to 91.0	2.18	13.4	.1565	Low chamber pressure shutdown, axial cracks
			68.0		

TABLE I. - Continued. INSERT DESCRIPTION

(13) Insert 13; configuration B; injector 11; characteristic length, 67; no coating

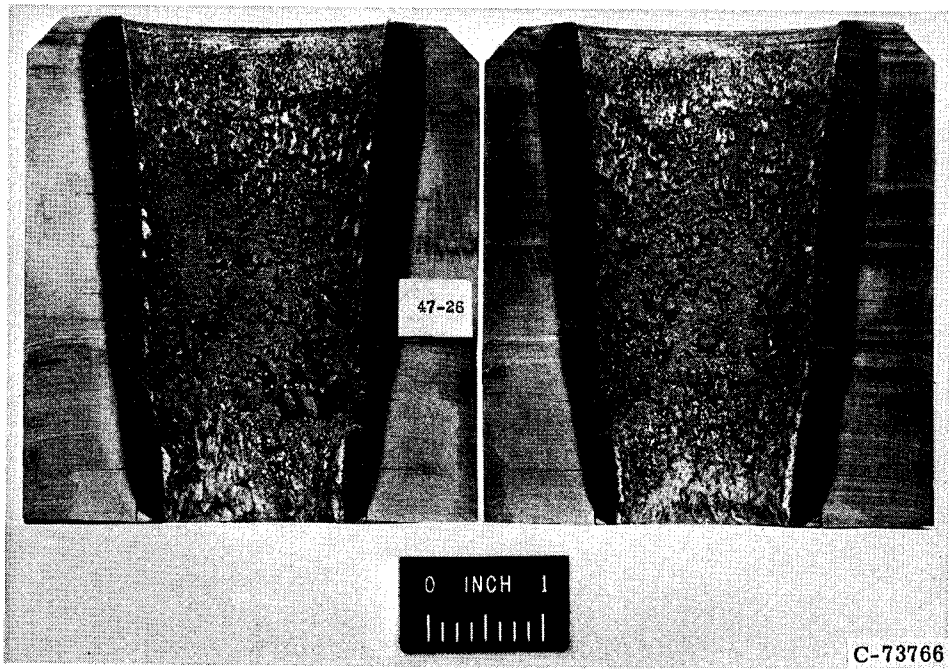

	Material	Form	Manufacturer	Additional layer
Insert	80 SiO_2 - 20 C	Powder sintered and pressed	Avco Corp	None
Envelope	Silica phenolic (MX 2641)	Cloth (90^{o} to centerline)	Haveg	0.25-in.-thick stainless-steel shell

Run	Chamber pressure, P_c, psia	Oxidant-fuel ratio, O/F	Run time, sec	Total change in effective throat radius, ΔR, in.	Remarks
21	102.7 to 89.3	2.40	56.1	0.0395	Low chamber pressure shutdown
30	97.1 to 85.5	2.26	53.1	.112	Low chamber pressure shutdown
			109.2		

TABLE I. - Continued. INSERT DESCRIPTION

(14) Insert 14; configuration B; injector 11; characteristic length, 67; no coating

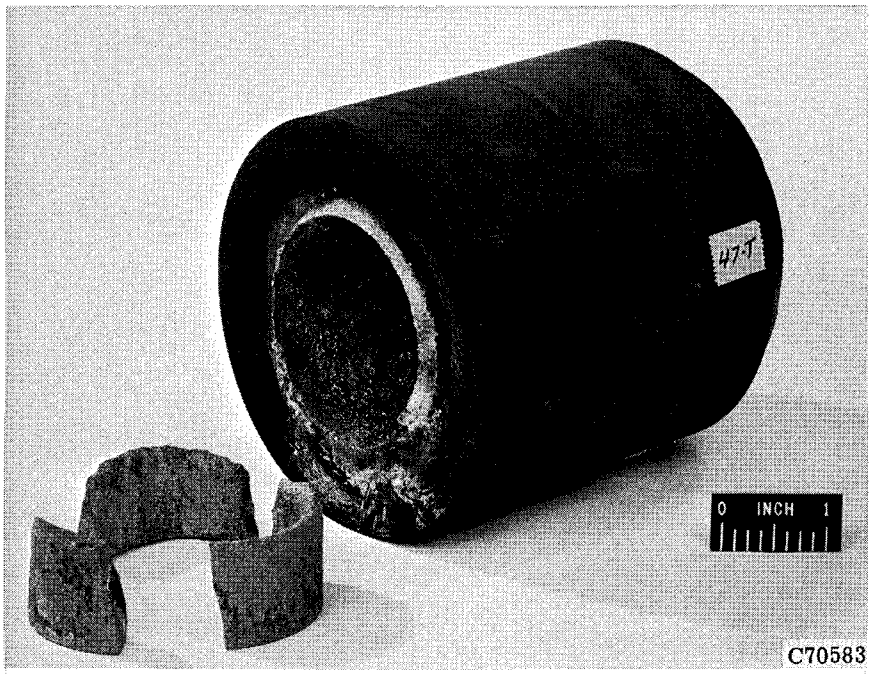

	Material	Form	Manufacturer	Additional layer
Insert	GRB silicon carbide (64 SiC - 33 C - 3 Si)	Composite	Carborundum	0.04-in. -thick Rokide Z on insert outside diameter
Envelope	Silica phenolic (MX 2641)	Tape (90^{o} to centerline)	Haveg	0.25-in. -thick stainless-steel shell

Run	Chamber pressure, P_c, psia	Oxidant-fuel ratio, O/F	Run time, sec	Total change in effective throat radius, ΔR, in.	Remarks
297	105.5 to 103	1.71	60.3	0.0105	Timed shutdown, no apparent cracks
298	100.5 to 95	1.70	75.7 136.0	.037 (calc)	Cracked into three pieces

TABLE I. - Continued. INSERT DESCRIPTION

(15) Insert 15; configuration C; injector 11; characteristic length, 67; no coating

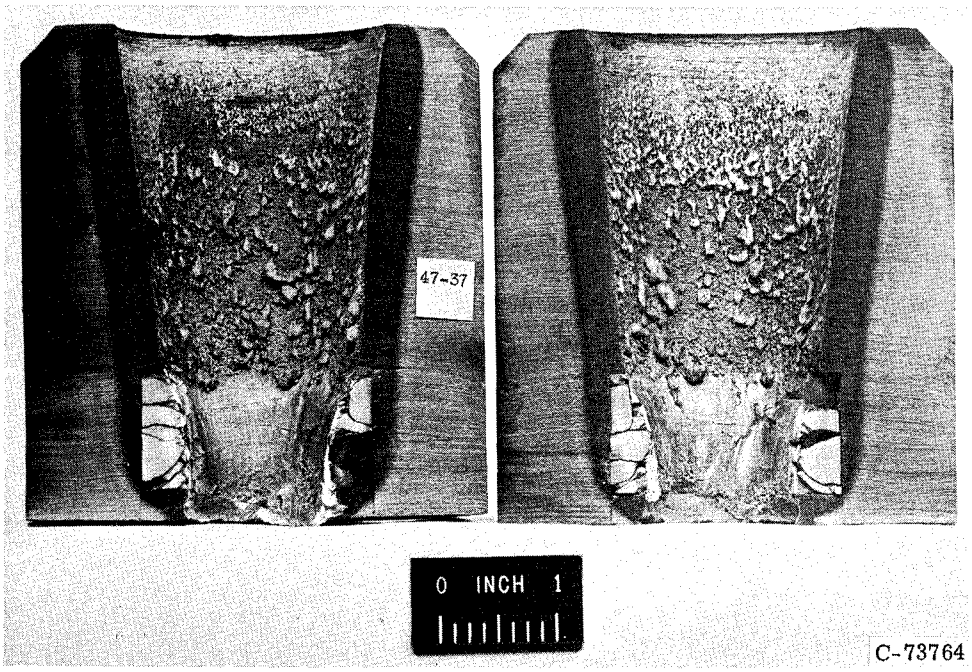

	Material	Form	Manufacturer	Additional layer
Insert	65 ZrO_2 - 35 SiO_2	Hot pressed	Aerospace Corp	None
Envelope	Silica phenolic (MX 2641)	Cloth (90^o to centerline)	Haveg	0.25-in.-thick stainless-steel shell

Run	Chamber pressure, P_c, psia	Oxidant-fuel ratio, O/F	Run time, sec	Total change in effective throat radius, ΔR, in.	Remarks
25	92.8 to 94.1	1.98	60.1	-0.033	Timer shutdown; cracks and local erosion

TABLE I. - Continued. INSERT DESCRIPTION

(16) Insert 16; configuration C; injector 11; characteristic length, 67; no coating

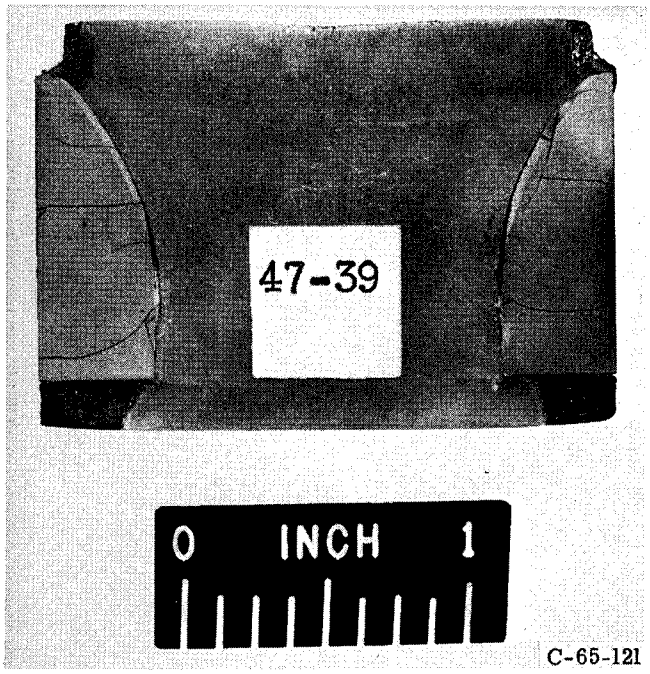

	Material	Form	Manufacturer	Additional layer
Insert	85 BeO - 15 SiC	Hot pressed	Aerospace Corp	None
Envelope	Silica phenolic (MX 2641)	Cloth (90^{o} to centerline)	Haveg	0.25-in.-thick stainless-steel shell

Run	Chamber pressure, P_c, psia	Oxidant-fuel ratio, O/F	Run time, sec	Total change in effective throat radius, ΔR, in.	Remarks
27	101.1 to 97.0	2.14	60.4	-0.0075	Timer shutdown; circumferential and longitudinal cracks

TABLE I. - Continued. INSERT DESCRIPTION

(17) Insert 17; configuration C; injector 12; characteristic length, 50; no coating

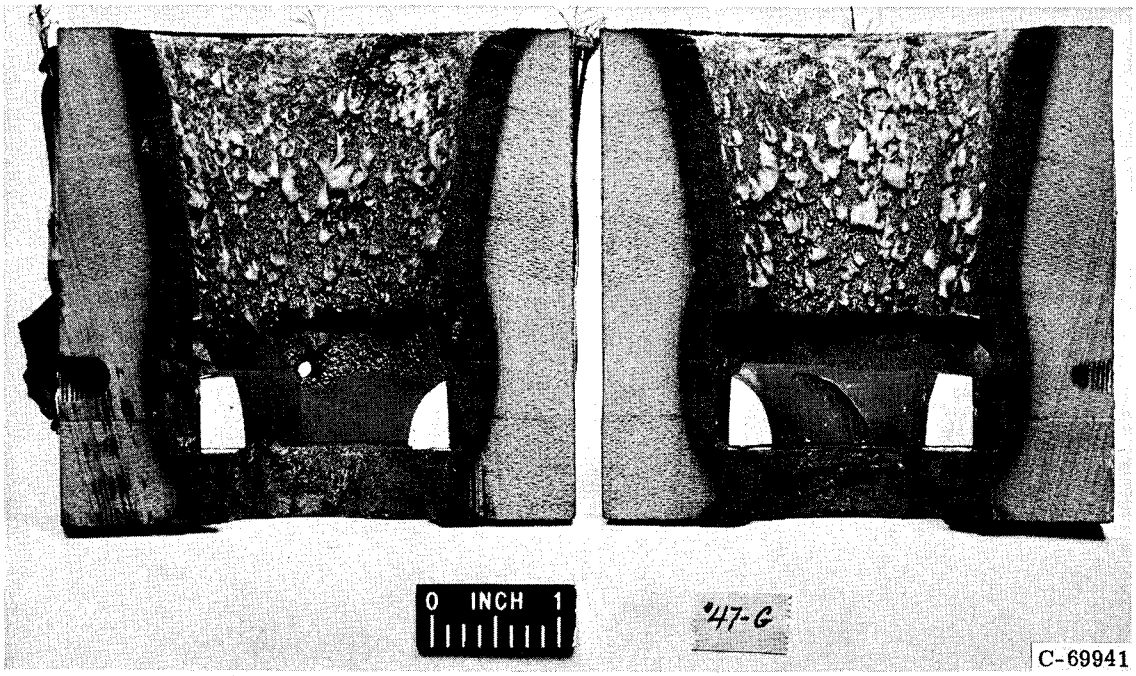

	Material	Form	Manufacturer	Additional layer
Insert	BN		Carborundum	0.125-in.-thick stainless-steel sleeve with 0.005 interference fit
Envelope	Silica phenolic (MX 2641)	Tape (90^{o} to centerline)	Haveg	None

Run	Chamber pressure, P_c, psia	Oxidant-fuel ratio, O/F	Run time, sec	Total change in effective throat radius, ΔR, in.	Remarks
204	107 to 103.5	1.96	26.0	------	Timed shutdown, no cracks
205	102 to 90	2.02	42.6	0.0645	Low chamber pressure shutdown
			68.6		

TABLE I. - Continued. INSERT DESCRIPTION

(18) Insert 15; configuration A; injector 11; characteristic length, 65; no coating

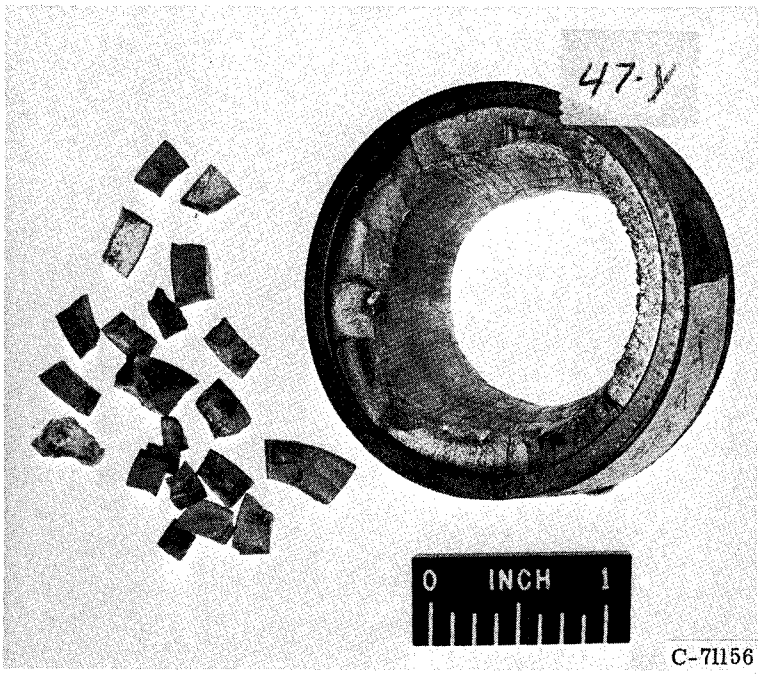

	Material	Form	Manufacturer	Additional layer
Insert	Al_2O_3		General Electric	0.125-in.-thick stainless-steel sleeve with 0.0005 interference fit
Envelope	Silica phenolic (MX 2641)	Tape (90^o to centerline)	Haveg	0.25-in.-thick stainless-steel sleeve

Run	Chamber pressure, P_c, psia	Oxidant-fuel ratio, O/F	Run time, sec	Total change in effective throat radius, ΔR, in.	Remarks
343	104 to 95	2.29	60.3	0.023	Timed shutdown; local erosion and severe cracking

TABLE I. - Continued. INSERT DESCRIPTION

(19) Insert 19; configuration B; injector 11; characteristic length, 67; no coating

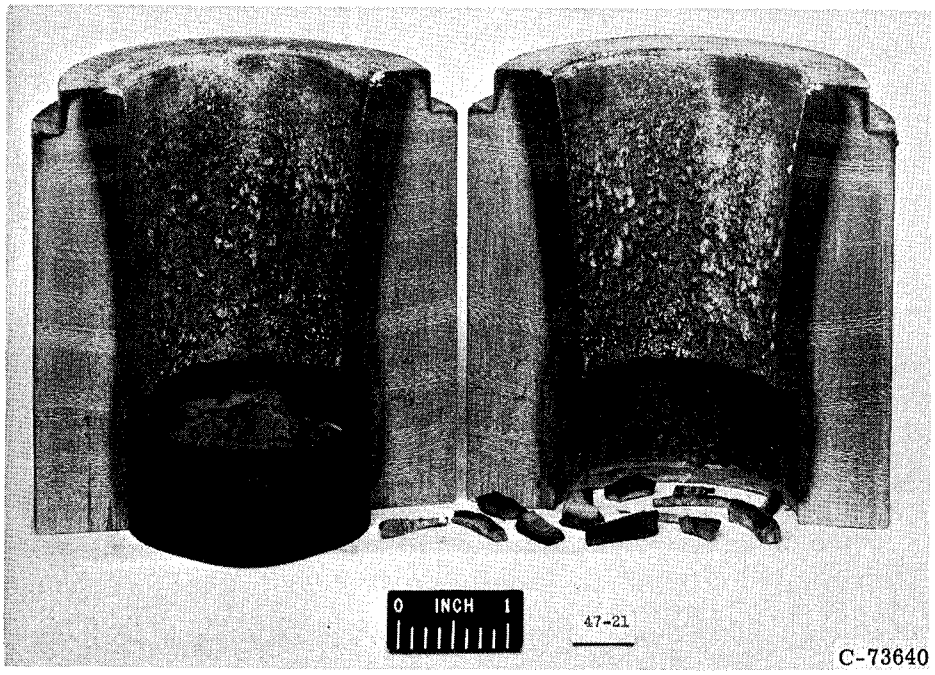

	Material	Form	Manufacturer	Additional layer
Insert	SiN		Haynes-Stellite	0.125-in.-thick stainless-steel sleeve with 0.005 interference fit
Envelope	Silica phenolic (MX 2641)	Cloth (90^{o} to centerline)	Haveg	0.25-in.-thick stainless-steel shell

Run	Chamber pressure, P_c, psia	Oxidant-fuel ratio, O/F	Run time, sec	Total change in effective throat radius, ΔR, in.	Remarks
412	105.5 to 92.0	2.30	54.0	0.1925	Timed shutdown; severe cracking and erosion by oxidation

TABLE I. - Continued. INSERT DESCRIPTION

(20) Insert 20; configuration B; injector 11; characteristic length, 67; no coating

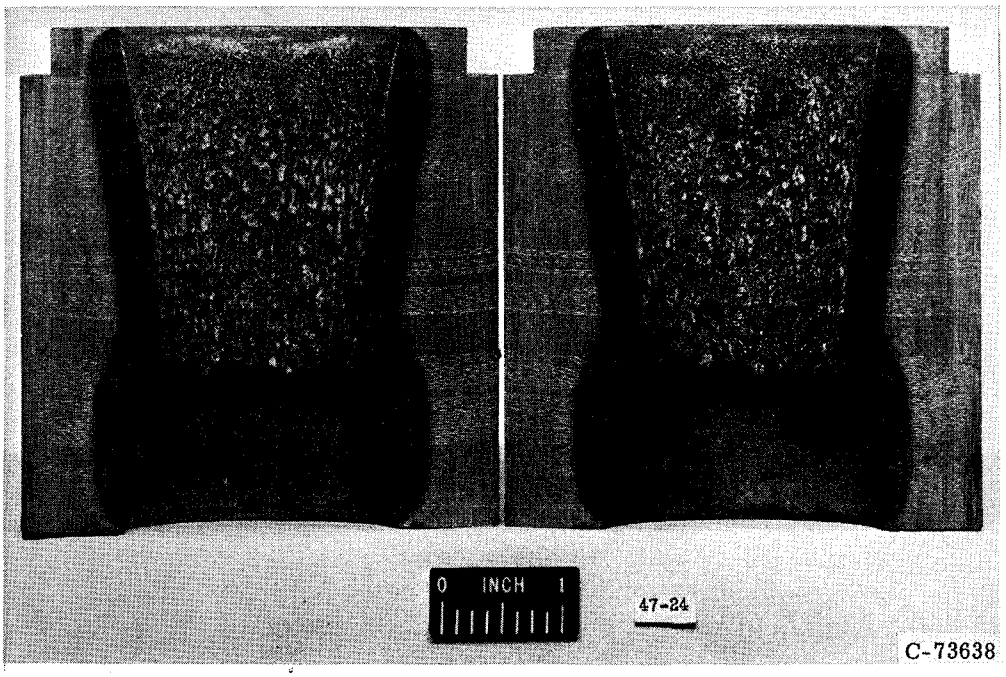

	Material	Form	Manufacturer	Additional layer
Insert	ZrB_2		Norton	0.125-in.-thick stainless-steel sleeve with 0.005 interference fit
Envelope	Silica phenolic (MX 2641)	Cloth (90^o to centerline)	Fiberite	0.25-in.-thick stainless-steel shell

Run	Chamber pressure, P_c, psia	Oxidant-fuel ratio, O/F	Run time, sec	Total change in effective throat radius, ΔR, in.	Remarks
7	98.6 to 91.7	1.99	49.7	0.028 (calc)	Low chamber pressure shutdown; lost insert

TABLE I. - Continued. INSERT DESCRIPTION

(21) Insert 21; configuration C; injector 11; characteristic length, 67; no coating

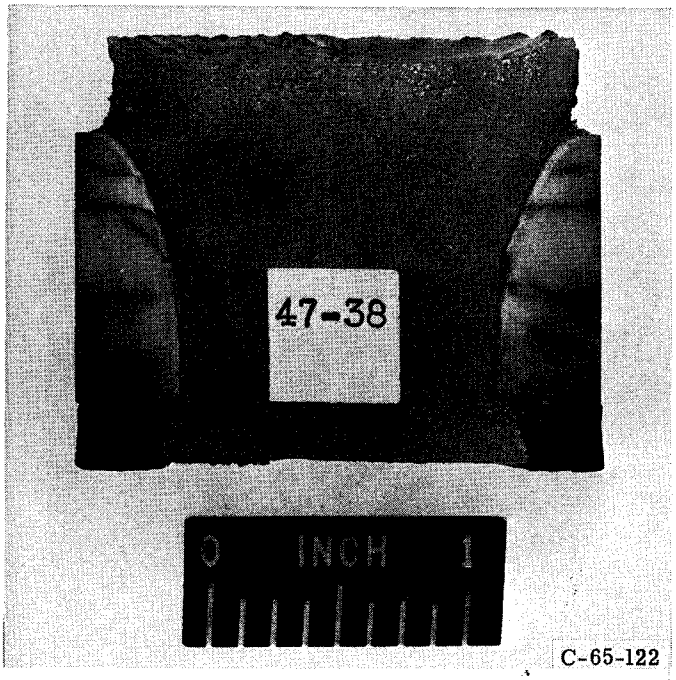

	Material	Form	Manufacturer	Additional layer
Insert	High-density BeO	Hot pressed	Aerospace Corp	None
Envelope	Silica phenolic (MX 2641)	Cloth (90^{o} to centerline)	Haveg	0.25-in.-thick stainless-steel shell

Run	Chamber pressure, P_c, psia	Oxidant-fuel ratio, O/F	Run time, sec	Total change in effective throat radius, ΔR, in.	Remarks
26	100.1 to 95.6	2.08	60.4	-0.006	Timer shutdown; insert cracked

TABLE I. - Continued. INSERT DESCRIPTION

(22) Insert 22; configuration B; injector 11A; characteristic length, 67; no coating

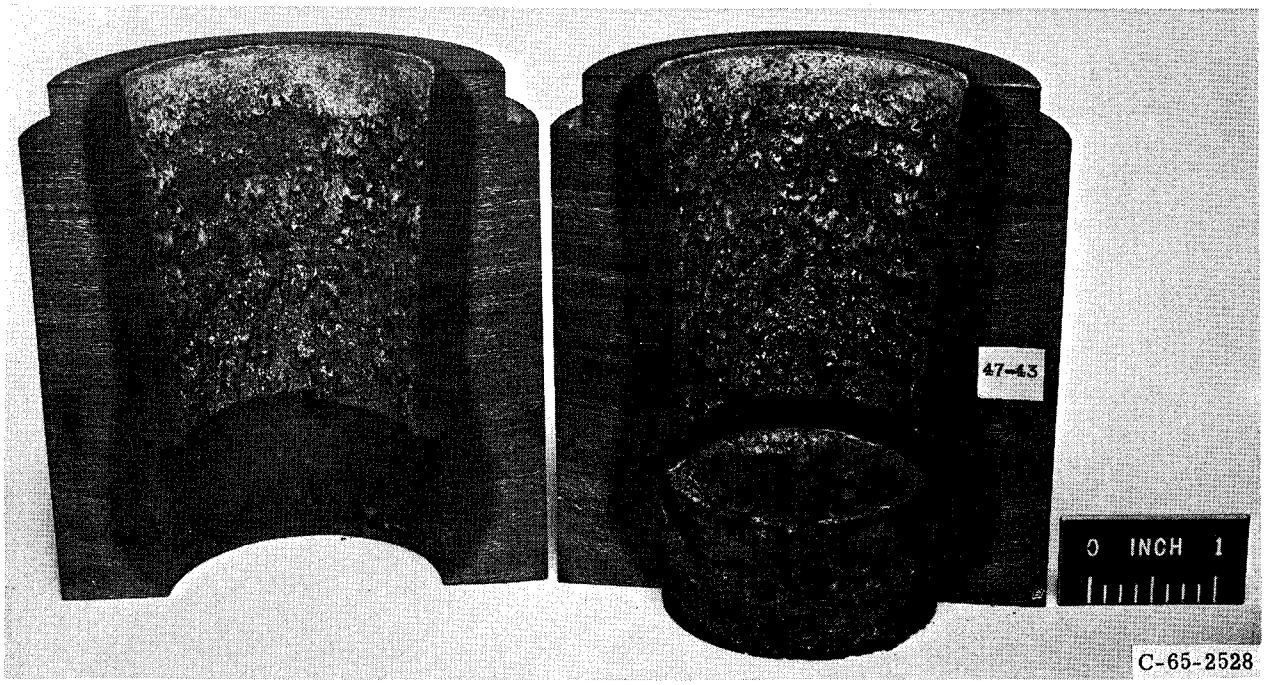

	Material	Form	Manufacturer	Additional layer
Insert	BeO	Pressed and sintered	Brush Beryllium	0.125-in.-thick stainless-steel sleeve with 0.005 interference fit
Envelope	Silica phenolic (MX 2641)	Cloth (90^{o} to centerline)	Haveg	0.25-in.-thick stainless-steel shell

Run	Chamber pressure, P_c, psia	Oxidant-fuel ratio, O/F	Run time, sec	Total change in effective throat radius, ΔR, in.	Remarks
113	101 to 100.5	2.10	58.8	0.003	Timer shutdown; no cracks visible
147	95.9 to 93.7	2.10	54.1	.049	Low chamber pressure shutdown; circumferential cracks
			112.9		

TABLE I. - Continued. INSERT DESCRIPTION

(23) Insert 23; configuration B; injector 12; characteristic length, 50; no coating

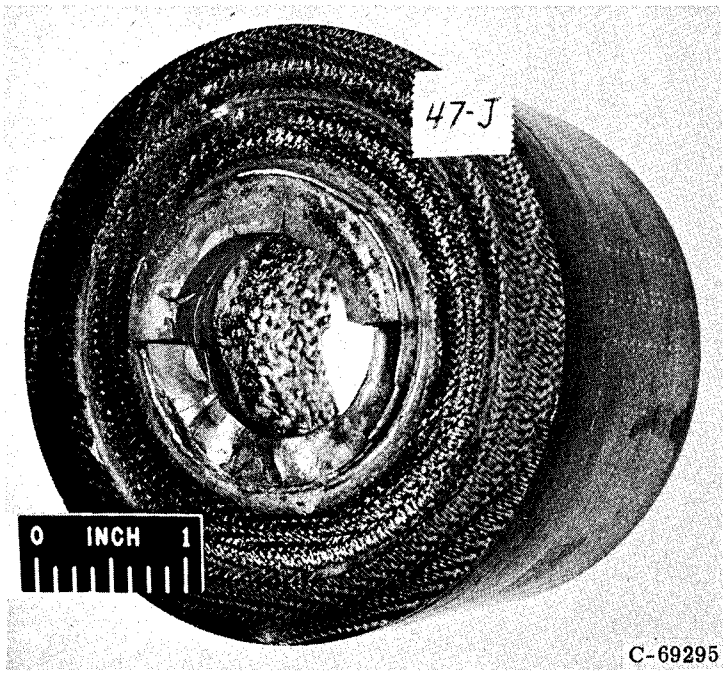

	Material	Form	Manufacturer	Additional layer
Insert	NbC		Kennametal	0.040-in.-thick Rokide Z on insert outside diameter
Envelope	Silica phenolic (MX 2641)	Tape (90^{o} to centerline)	Haveg	0.25-in.-thick stainless-steel shell

Run	Chamber pressure, P_c, psia	Oxidant-fuel ratio, O/F	Run time, sec	Total change in effective throat radius, ΔR, in.	Remarks
215	97 to 93	1.75	56.0	---	Low chamber pressure; shutdown; severe cracking

TABLE I. - Continued. INSERT DESCRIPTION

(24) Insert 24; injector 11; characteristic length, 67; no coating

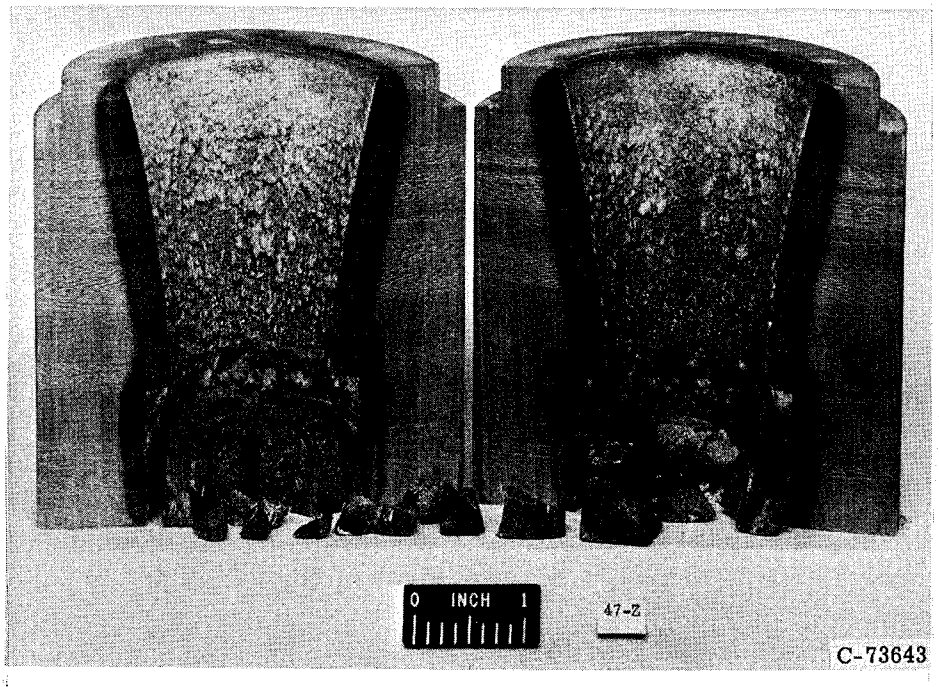

	Material	Form	Manufacturer	Config-uration	Additional layer
Insert	Segmented SiC	KT	Carborundum	B[a]	None
Envelope	Silica phenolic (MX 2641)	Cloth (90° to centerline)	Haveg	B	0.25-in.-thick stainless-steel shell

Run	Chamber pressure, P_c, psia	Oxidant-fuel ratio, O/F	Run time, sec	Total change in effective throat radius, ΔR, in.	Remarks
426	110.0 to 104.0	1.98	52.2	0.0245 (calc)	Insert lost because of ablative failure

[a]Six equal axial segments.

TABLE I. - Continued. INSERT DESCRIPTION

(25) Insert 25; configuration C; injector 11; characteristic length, 67; no coating

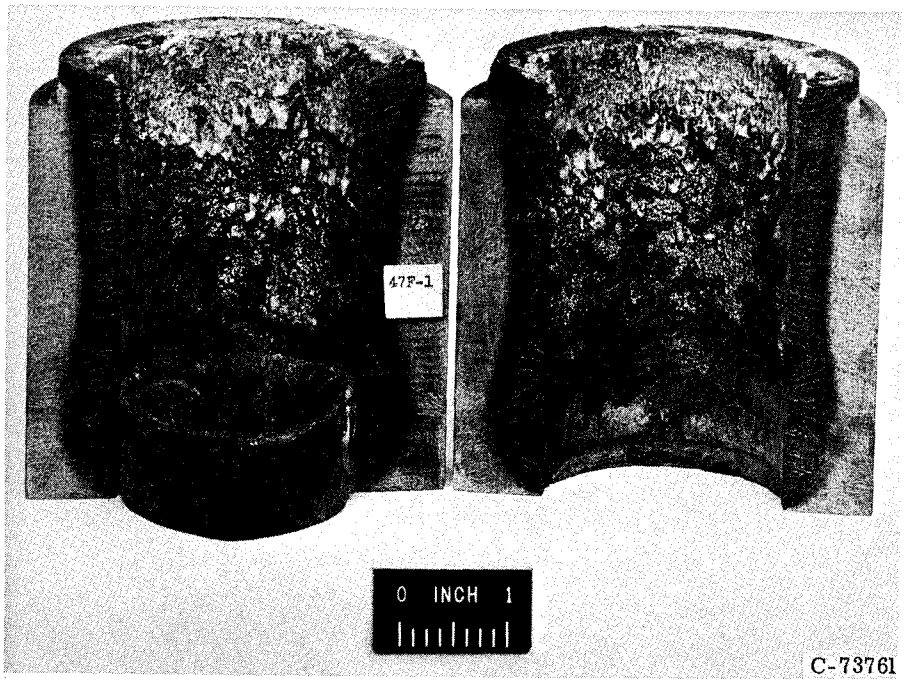

	Material	Form	Manufacturer	Additional layer
Insert	SiC		Avco Corp	0.100-in.-thick Ta sleeve with 0.003 interference fit
Envelope	Silica phenolic (MX 2641)	Cloth (90^{o} to centerline)	Haveg	0.25-in.-thick stainless-steel shell

Run	Chamber pressure, P_c, psia	Oxidant-fuel ratio, O/F	Run time, sec	Total change in effective throat radius, ΔR, in.	Remarks
16	104.4 to 102.4	1.90	60.1	------	Timer shutdown; one circumferential crack
20	99.8 to 89.4	2.05	80.2	0.053	Low chamber pressure shutdown; Ta ring oxidized
				140.3	

TABLE I. - Continued. INSERT DESCRIPTION

(26) Insert 26; configuration C; injector 11; characteristic length, 67; no coating

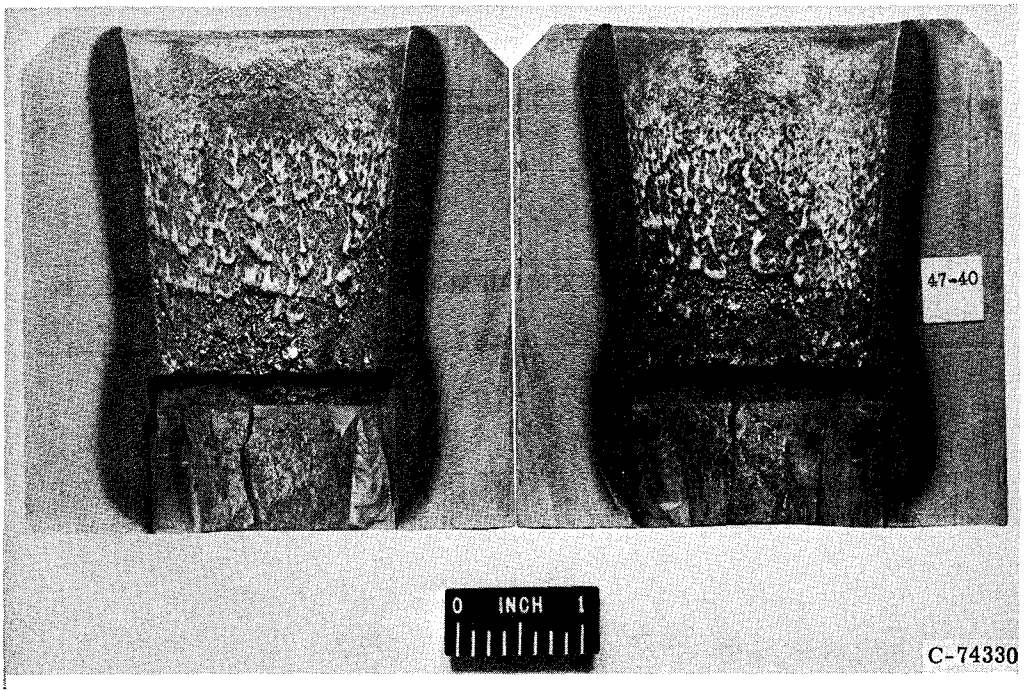

	Material	Form	Manufacturer	Additional layer
Insert	SiC	Hot pressed	Aerospace Corp	None
Envelope	Silica phenolic (MX 2641)	Cloth (90^{o} to centerline)	Haveg	0.25-in.-thick stainless-steel shell

Run	Chamber pressure, P_c, psia	Oxidant-fuel ratio, O/F	Run time, sec	Total change in effective throat radius, ΔR, in.	Remarks
35	101.1 to 96.4	2.09	65.3	0.010	Timer shutdown; axial cracks

TABLE I. - Continued. INSERT DESCRIPTION

(27) Insert 27; configuration B; injector 11; characteristic length, 67; no coating

	Material	Form	Manufacturer	Additional layer
Insert	ZrC		Norton	0.125-in.-thick stainless-steel ring with 0.005 interference fit
Envelope	Silica phenolic (MX 2641)	Cloth (90^{o} to centerline)	Fiberite	0.25-in.-thick stainless-steel shell

Run	Chamber pressure, P_c, psia	Oxidant-fuel ratio, O/F	Run time, sec	Total change in effective throat radius, ΔR, in.	Remarks
425	107.0 to 106.5	2.10	59.2	0.004 (calc)	Timer shutdown; ring melted and insert crack circumferentially

TABLE I. - Continued. INSERT DESCRIPTION

(28) Insert 28; configuration C; characteristic length, 62; no coating

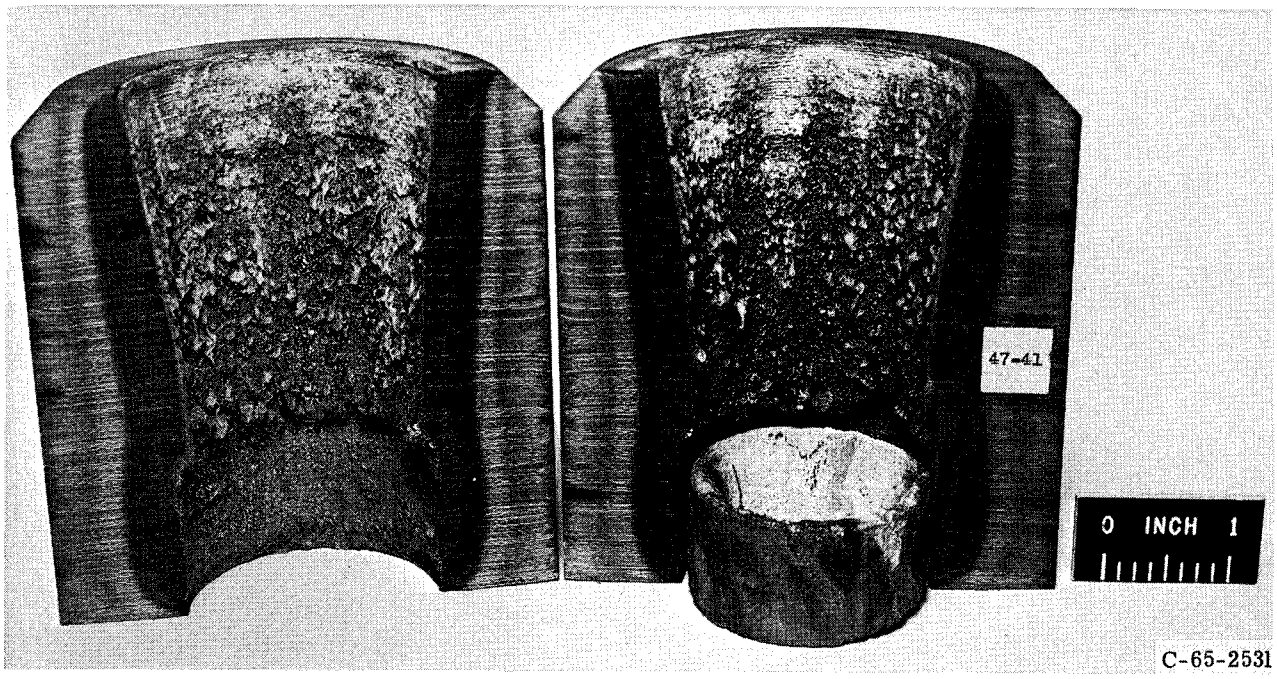

	Material	Form	Manufacturer	Additional layer
Insert	Hypereutectic ZrC (78 Zr - 22 C (2 percent free C))	Cast	Aerospace Corp	None
Envelope	Silica phenolic (MX 2641)	Cloth (90^{o} to centerline)	Haveg	0.25-in.-thick stainless-steel shell

Run	Injector	Chamber pressure, P_c, psia	Oxidant-fuel ratio, O/F	Run time, sec	Total change in effective throat radius, ΔR, in.	Remarks
45	11	104.5 to 90.0	1.95	60.5	0	Timer shutdown; thin ZrO_2 coating
196	11A	99.1 to 99.1	1.93	66.4	0	Timer shutdown; thin ZrO_2 coating
				126.9		

TABLE I. - Continued. INSERT DESCRIPTION

(29) Insert 29; configuration B; injector 11; characteristic length, 67; no coating

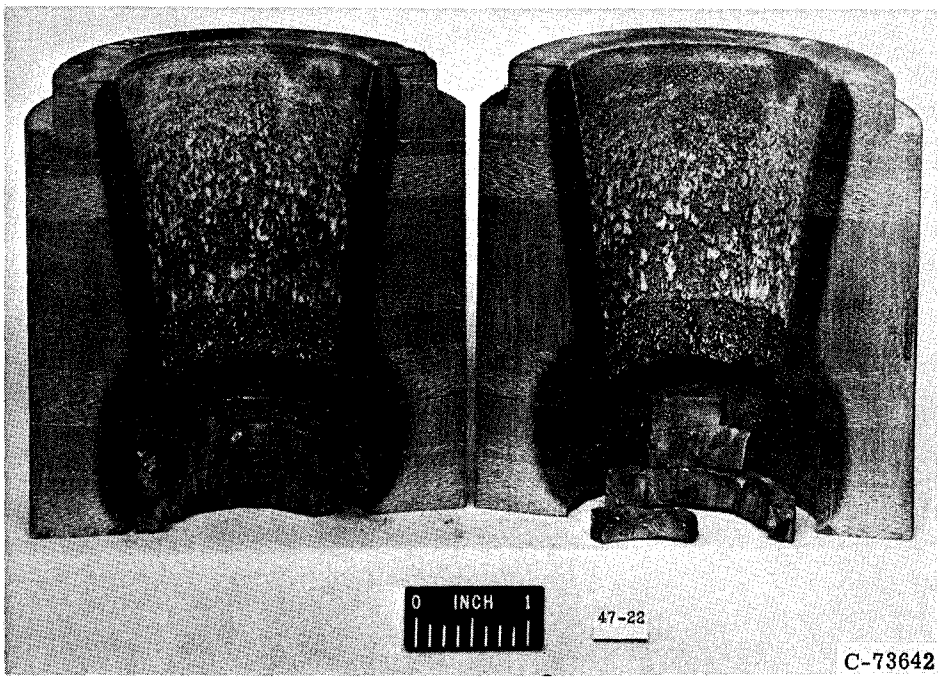

	Material	Form	Manufacturer	Additional layer
Insert	TiB_2		Norton	0.125-in.-thick stainless-steel sleeve with 0.005 interference fit
Envelope	Silica phenolic (MX 2641)	Cloth (90^{o} to centerline)	Haveg	0.25-in.-thick stainless-steel shell

Run	Chamber pressure, P_c, psia	Oxidant-fuel ratio, O/F	Run time, sec	Total change in effective throat radius, ΔR, in.	Remarks
411	110.0 to 91.5	2.05	33.7	---	Low chamber pressure shutdown; severe cracking

TABLE I. - Continued. INSERT DESCRIPTION

(30) Insert 30; configuration B; injector 11; characteristic length, 50; no coating

	Material	Form	Manufacturer	Additional layer
Insert	W	Sintered	General Electric	None
Envelope	Silica phenolic (MX 2641)	Cloth (90^{o} to centerline)	Fiberite	None

Run	Chamber pressure, P_c, psia	Oxidant-fuel ratio, O/F	Run time, sec	Total change in effective throat radius, ΔR, in.	Remarks
171	99.5 to 96.5	2.05	29.5	0	Timer shutdown; no change
172	94 to 88	1.82	51.5	.055	Low chamber pressure shutdown
			81.0		

TABLE I. - Continued. INSERT DESCRIPTION

(31) Insert 31; configuration C; injector 11; characteristic length, 67; no coating

	Material	Form	Manufacturer	Additional layer
Insert	Mo	Sintered	General Electric	0.04-in.-thick Rokide Z on insert outside diameter
Envelope	Silica phenolic (MX 2641)	Cloth (90^{o} to centerline)	Fiberite	0.25-in.-thick stainless-steel shell

Run	Chamber pressure, P_c, psia	Oxidant-fuel ratio, O/F	Run time, sec	Total change in effective throat radius, ΔR, in.	Remarks
301	105.5 to 96.5	1.72	60.6	0.0145	Timed shutdown
315	107 to 89	1.83	35.1	.084	Low chamber pressure shutdown
			95.7		

TABLE I. - Continued. INSERT DESCRIPTION

(32) Insert 32; injector 11; characteristic length, 67; no coating

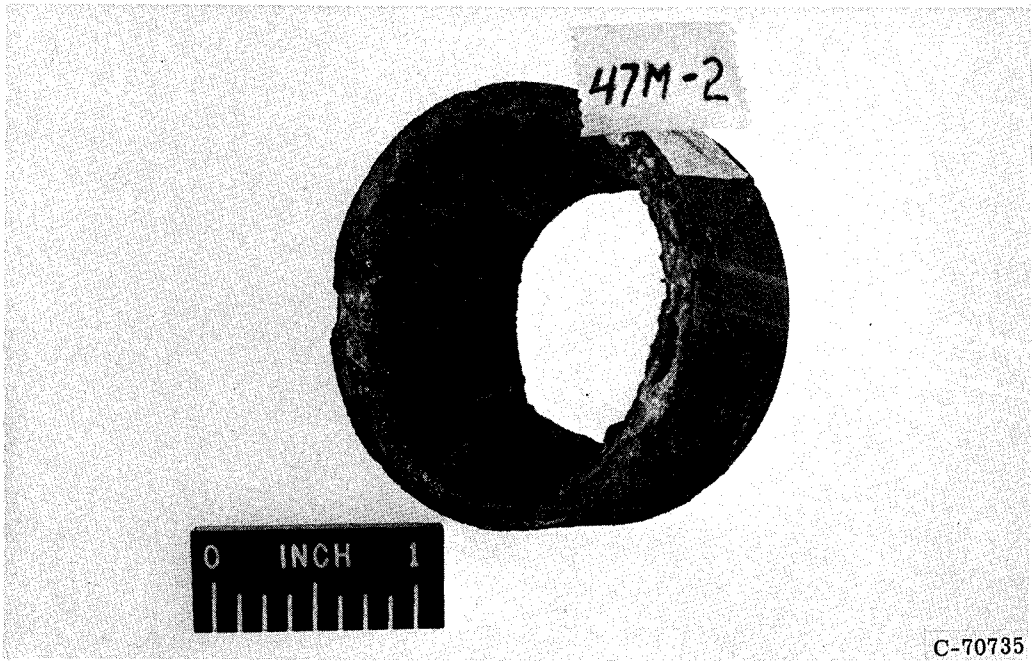

	Material	Form	Manufacturer	Configuration	Additional layer
Insert	Mo	Sintered		C[a]	0.04-in.-thick Rokide Z on outside diameter of insert
Envelope	Silica phenolic (MX 2641)	Cloth (90° to centerline)	Fiberite	C	0.25-in.-thick stainless-steel shell

Run	Chamber pressure, P_c, psia	Oxidant-fuel ratio, O/F	Run time, sec	Total change in effective throat radius, ΔR, in.	Remarks
316	106 to 101	1.86	42.7	0.0075	Failure of insert ablative leading edge

[a]1/8-in.-thick pyrolytic graphite washer (ab radial plane) at insert leading edge.

TABLE I. - Continued. INSERT DESCRIPTION

(33) Insert 33; configuration B; injector 11; characteristic length, 67; no coating

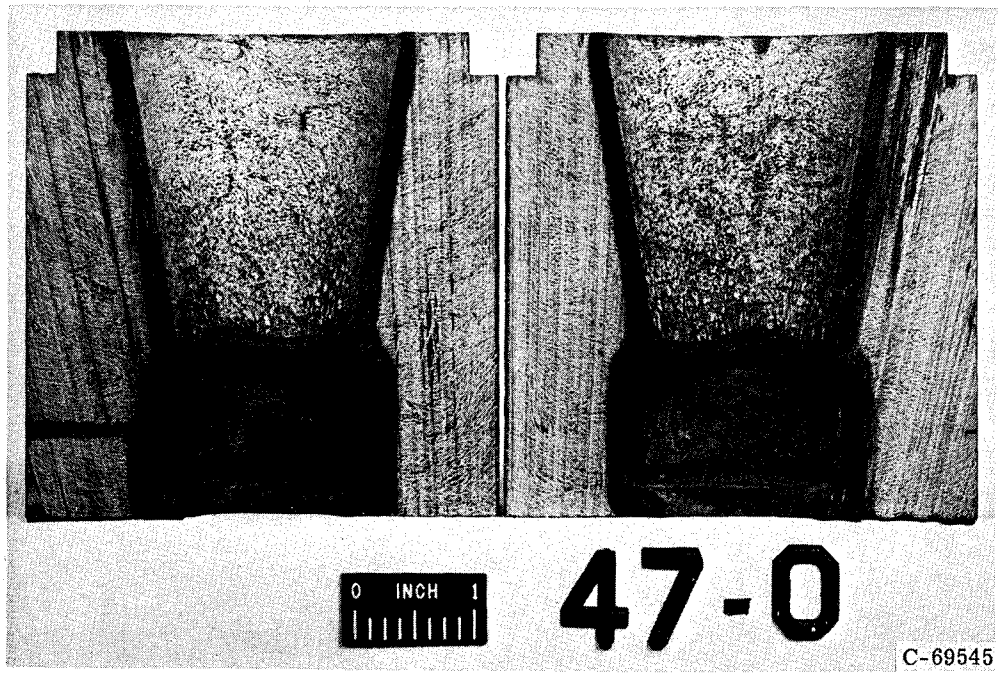

	Material	Form	Manufacturer	Additional layer
Insert	Nb		Wah Chang	0.040-in.-thick Rokide Z on insert outside diameter
Envelope	Silica phenolic (MX 2641)	Chopped squares	Haveg	0.25-in.-thick stainless-steel shell

Run	Chamber pressure, P_c, psia	Oxidant-fuel ratio, O/F	Run time, sec	Total change in effective throat radius, ΔR, in.	Remarks
232	96.5 to 89.5	1.67	17.4	---	Low chamber pressure shutdown; insert completely consumed

TABLE I. - Continued. INSERT DESCRIPTION

(34) Insert 34; configuration B; no coating

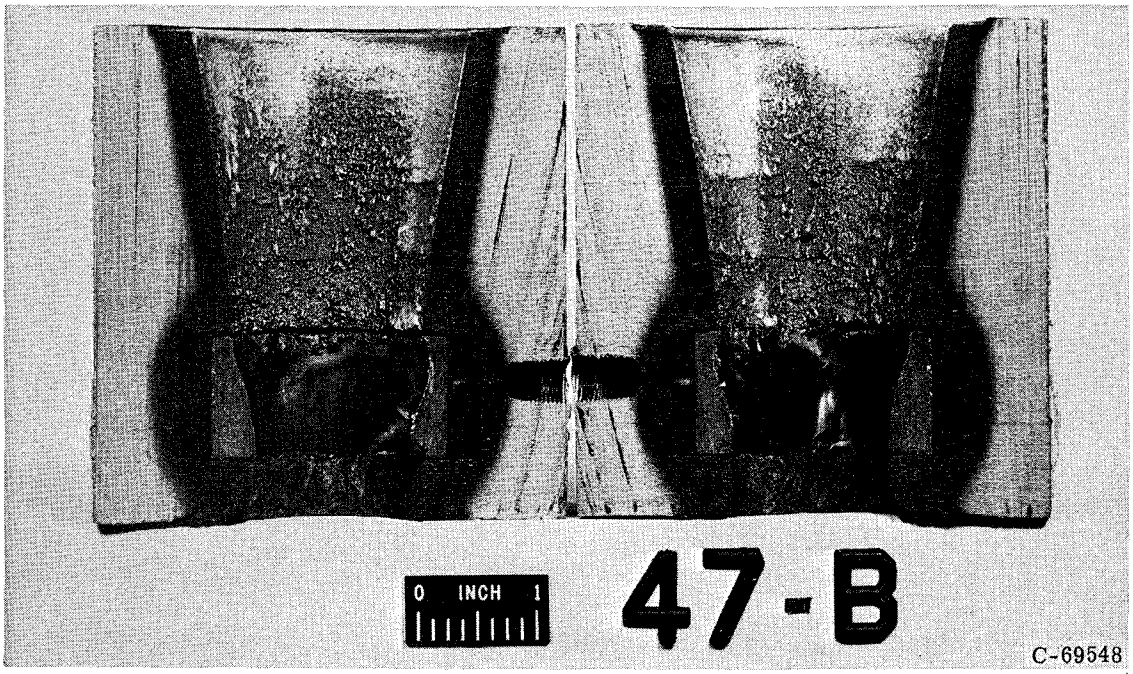

	Material	Form	Manufacturer	Additional layer
Insert	Mo	Arc cast	NASA	1/4-in.-thick graphite cloth sleeve on insert outside diameter
Envelope	Silica phenolic (MX 2641)	Cloth (90^{o} to centerline)	Fiberite	None

Run	Injector	Characteristic length, L^*, in.	Chamber pressure, P_c, psia	Oxidant-fuel ratio, O/F	Run time, sec	Total change in effective throat radius, ΔR, in.	Remarks
223	12	50	100.5	1.68	20.2	----------	Manual abort; lost TC seal
229	11	67	99.5 to 89.5	1.88	39.7	0.045 (calc)	Low chamber pressure shutdown
					59.9		

TABLE I. - Continued. INSERT DESCRIPTION

(35) Insert 35; configuration B; no coating

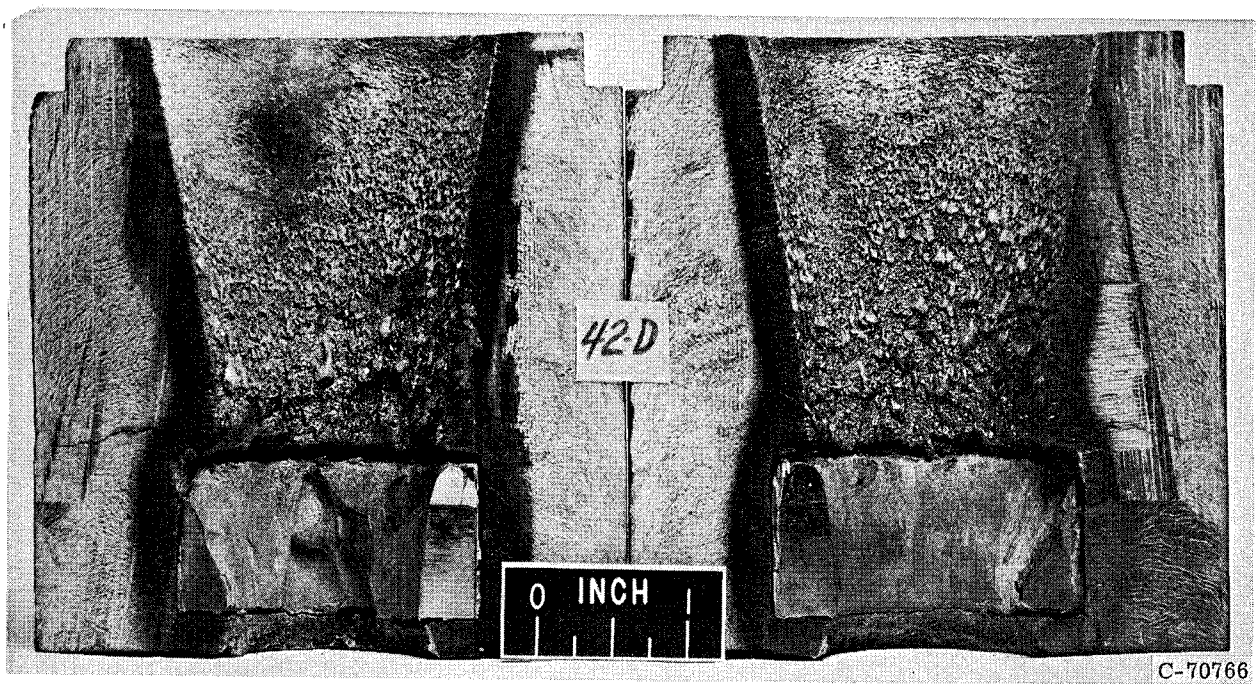

	Material	Form	Manufacturer	Additional layer
Insert	90 Ta - 10 W	Arc cast	NASA	0.030-in.-thick Rokide Z on insert outside diameter
Envelope	Silica phenolic (MX 2641)	Chopped squares	Fiberite	0.25-in.-thick stainless-steel shell

Run	Injector	Characteristic length, L*, in.	Chamber pressure, P_c, psia	Oxidant-fuel ratio, O/F	Run time, sec	Total change in effective throat radius, ΔR, in.	Remarks
206	12	50	106	1.87	11.3	0	Ablative cracked but was replaced
241	11	67	100.7 to 91.2	1.96	31.4	.042	Low chamber pressure shutdown; insert cracked
					42.7		

TABLE I. - Continued. INSERT DESCRIPTION

(36) Insert 36; configuration C; injector 11; characteristic length, 67; no coating

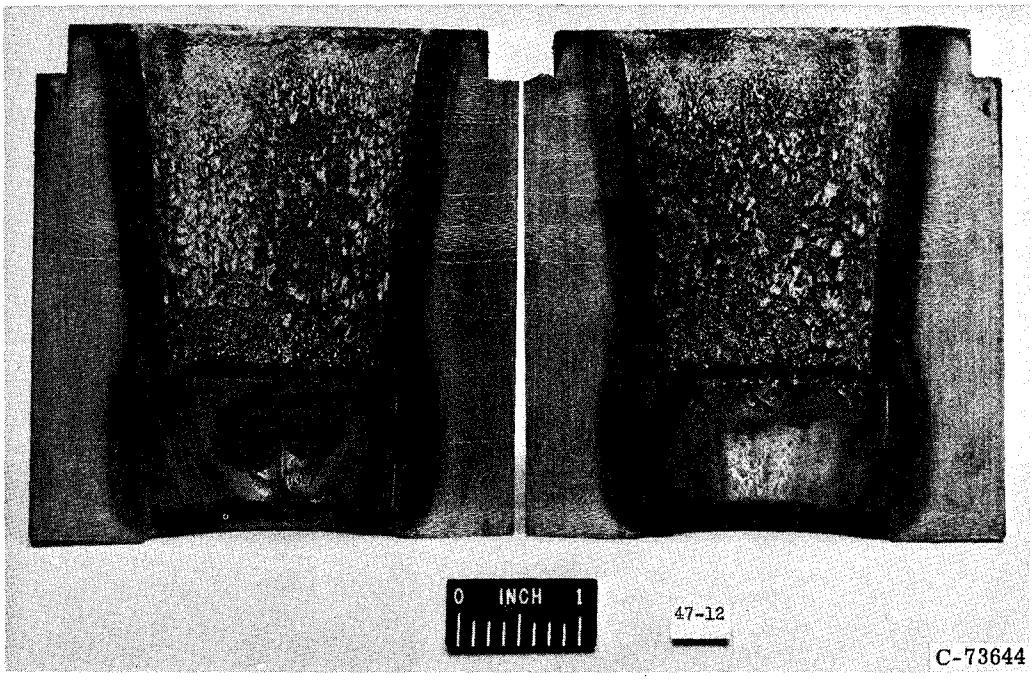

	Material	Form	Manufacturer	Additional layer
Insert	TZM alloy (99 Mo - 0.5 Ti - 0.5 Zr)		Cleveland Tungsten	0.045-in.-thick Rokide Z on insert outside diameter
Envelope	Silica phenolic (MX 2641)	Cloth (90^{o} to centerline)	Haveg	0.25-in.-thick stainless-steel shell

Run	Chamber pressure, P_c, psia	Oxidant-fuel ratio, O/F	Run time, sec	Total change in effective throat radius,	Remarks
413	108.5 to 90.5	2.14	42.6	0.1055	Low chamber pressure shutdown

TABLE I. - Continued. INSERT DESCRIPTION

(37) Insert 37; configuration B; characteristic length, 67; no coating

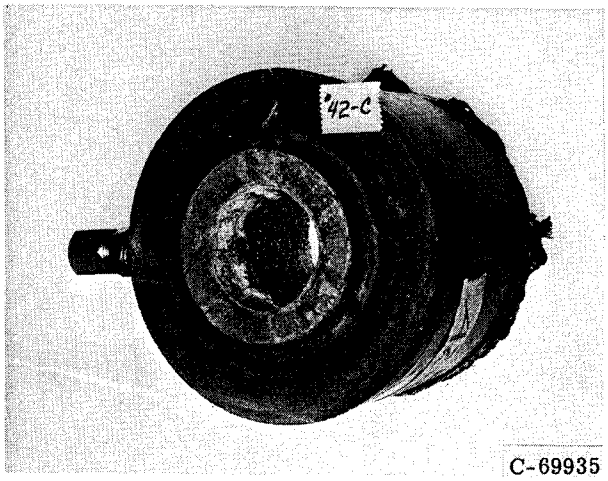

C-69935

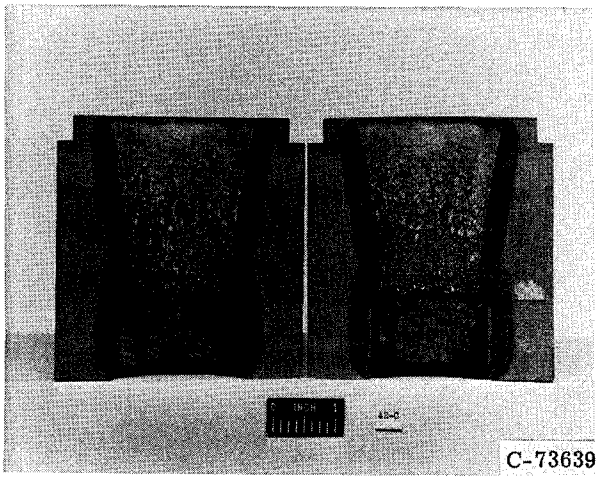
C-73639

	Material	Form	Manufacturer	Additional layer
Insert	80 W - 20 Ag	Sintered and infiltrated	Firth-Sterling	0.030-in. -thick Rokide Z on insert outside diameter
Envelope	Silica phenolic (MX 2641)	Cloth (90^{o} to centerline)	Fiberite	None

Run	Injector	Chamber pressure, P_c, psia	Oxidant-fuel ratio, O/F	Run time, sec	Total change in effective throat radius, ΔR, in.	Remarks
255	10	99.7 to 95.9	2.08	59.8	0.020	Leading edge eroded and ablative cracked
409	11	107.5 to 90.5	2.20	47.8	.0955	Low chamber pressure shutdown
				107.6		

TABLE I. - Continued. INSERT DESCRIPTION

(38) Insert 38; configuration B; injector 12; characteristic length, 50; no coating

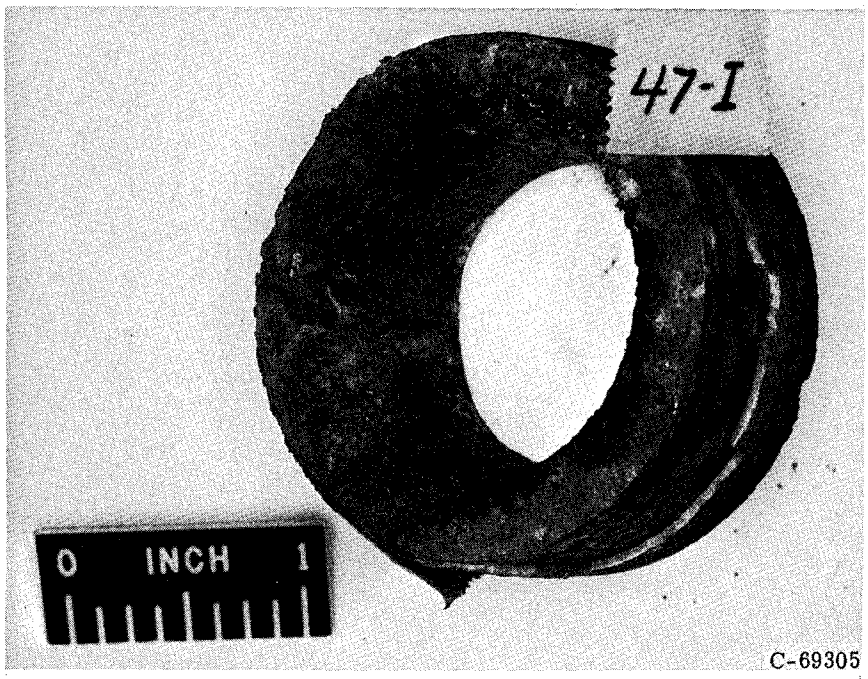

	Material	Form	Manufacturer	Additional layer
Insert	75 W - 25 Ag - Cu eutectic	Flame-sprayed tungsten with Ag-Cu eutectic	Linde-Union Carbide	0.04-in. -thick Rokide Z on insert outside diameter
Envelope	Silica phenolic (MX 2641)	Tape (90^{o} to centerline)	Haveg	0.025-in. -thick stainless-steel shell

Run	Chamber pressure, P_c, psia	Oxidant-fuel ratio, O/F	Run time, sec	Total change in effective throat radius, ΔR, in.	Remarks
220	98.5	1.67	59.3	0	Timed shutdown

TABLE I. - Continued. INSERT DESCRIPTION

(39) Insert 39; configuration C; injector 11; characteristic length, 67; no coating

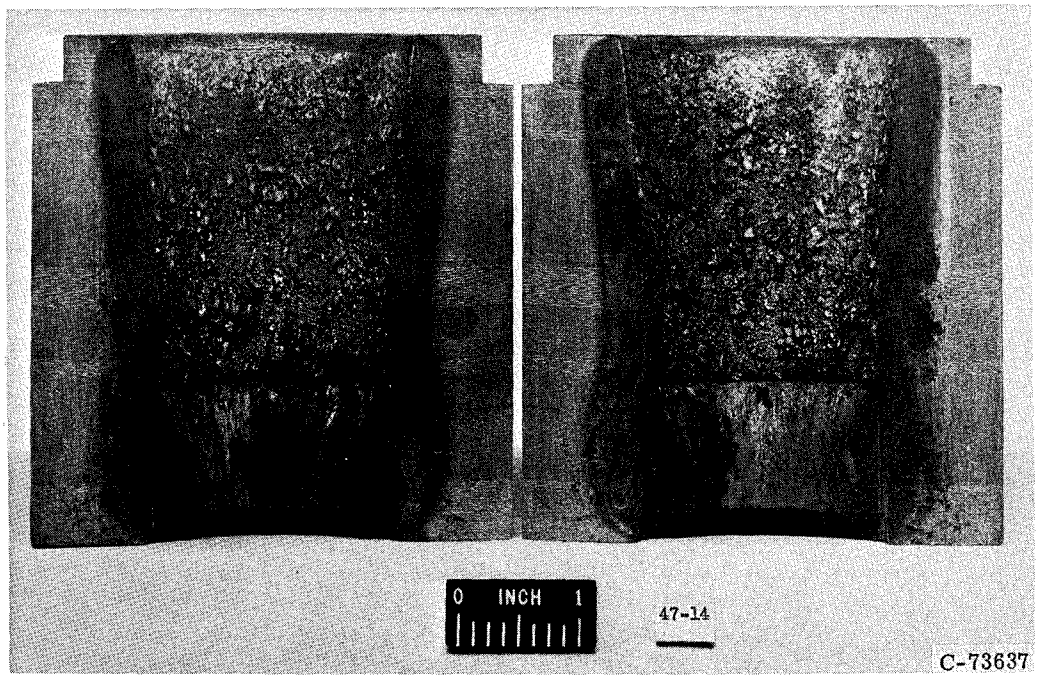

	Material	Form	Manufacturer	Additional layer
Insert	80 W - 20 Cu	Sintered Cu infiltrated	Mallory	0.042-in. -thick Rokide Z on insert outside diameter
Envelope	Silica phenolic (MX 2641)	Cloth (90^{o} to centerline)	Haveg	0.25-in. -thick stainless-steel shell

Run	Chamber pressure, P_c, psia	Oxidant-fuel ratio, O/F	Run time, sec	Total change in effective throat radius, ΔR, in.	Remarks
6	102.0 to 93.1	2.00	59.4	0.0475	Timed shutdown

TABLE I. - Continued. INSERT DESCRIPTION

(40) Insert 40; configuration C; characteristic length, 67; no coating

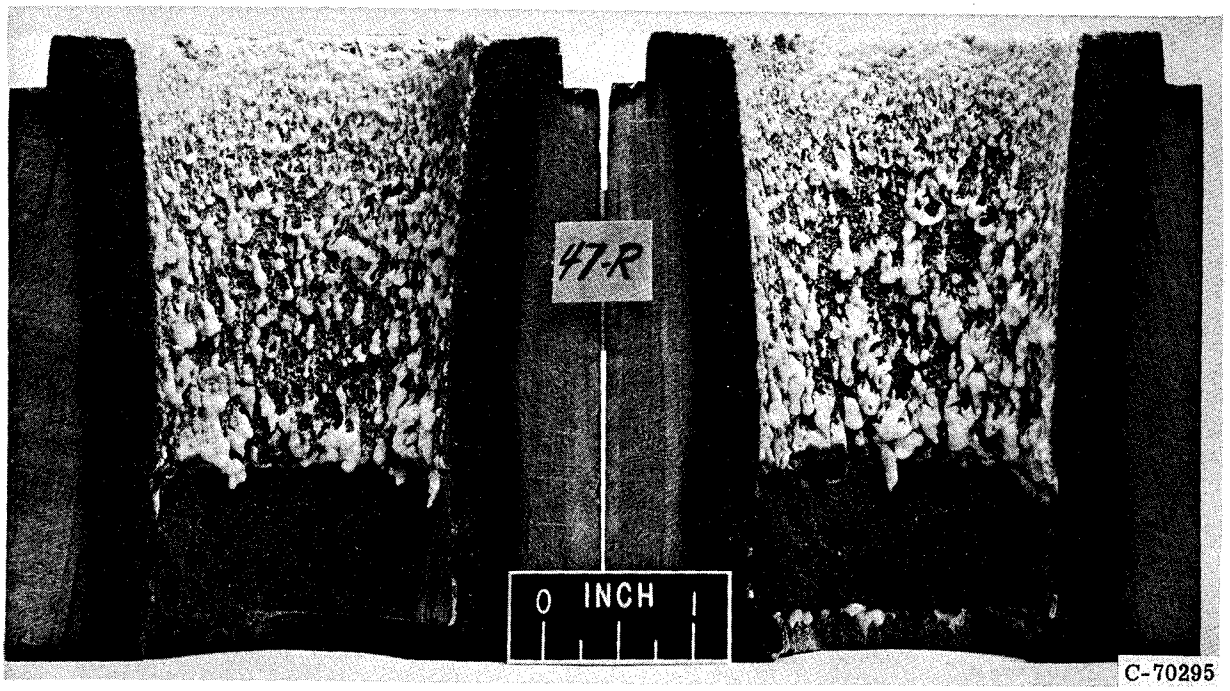

	Material	Form	Manufacturer	Additional layer
Insert	Heat-treated high-density graphite	Molded	American Metal Products	0.04-in. -thick Rokide Z on insert outside diameter
Envelope	Silica phenolic (MX 2641)	Molded squares	Haveg	0.25-in. -thick stainless-steel shell

Run	Injector	Chamber pressure, P_c, psia	Oxidant-fuel ratio, O/F	Run time, sec	Total change in effective throat radius, ΔR, in.	Remarks
266	10	104 to 98	2.10	65.3	0.015	Timed shutdown
271	10	94.5 to 91	2.03	46.1	.040	Low chamber pressure shutdown
277	11	112 to 90.5	2.01	33.4	.1555	Low chamber pressure shutdown
				144.8		

TABLE I. - Continued. INSERT DESCRIPTION

(41) Insert 41; configuration C; characteristic length, 67; no coating

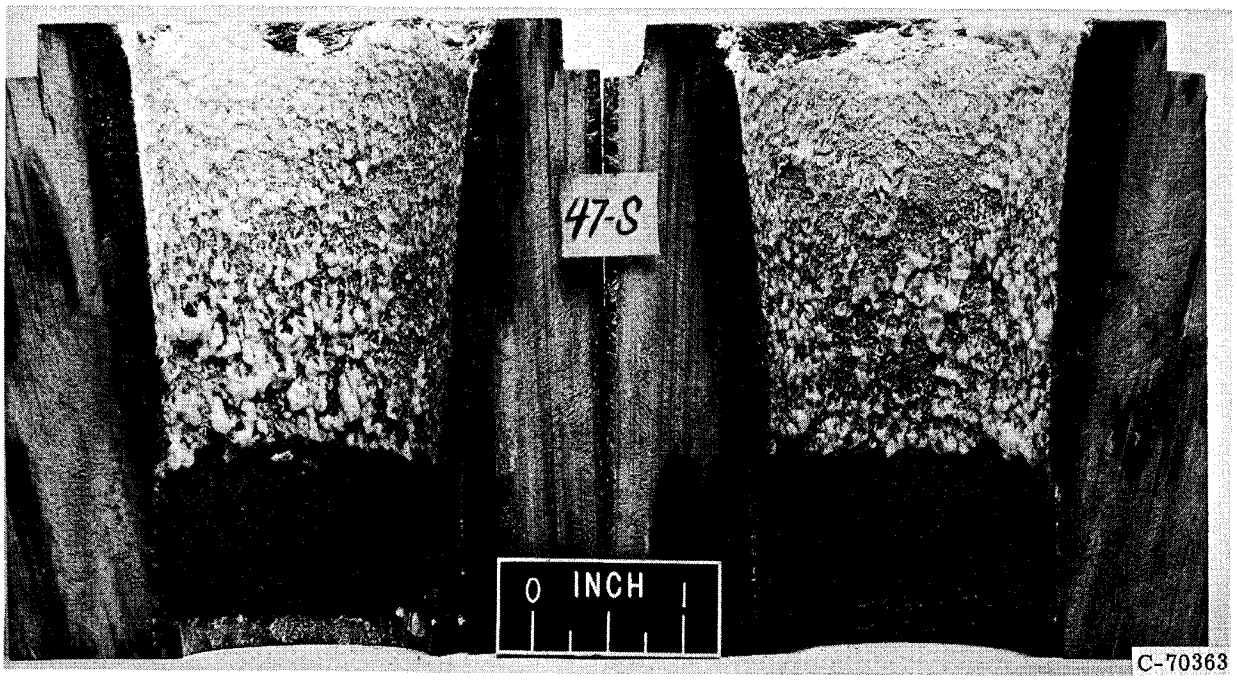

		Material	Form		Manufacturer	Additional layer
Insert		High-density graphite	Molded		American Metal Products	0.040-in.-thick Rokide Z on insert outside diameter
Envelope		Silica phenolic (MX 2641)	Molded squares		Haveg	0.25-in.-thick stainless-steel shell
Run	Injector	Chamber pressure, P_c, psia	Oxidant-fuel ratio, O/F	Run time, sec	Total change in effective throat radius, ΔR, in.	Remarks
267	10	101 to 91.5	2.13	53.7	0.0415	Low chamber pressure shutdown
278	11	103.5 to 90	1.92	26.0	.111	Low chamber pressure shutdown
281	11	96 to 90	2.07	16.1	.150	Low chamber pressure shutdown
				95.8		

TABLE I. - Continued. INSERT DESCRIPTION

(42) Insert 42; configuration A; injector 11; characteristic length, 65; no coating

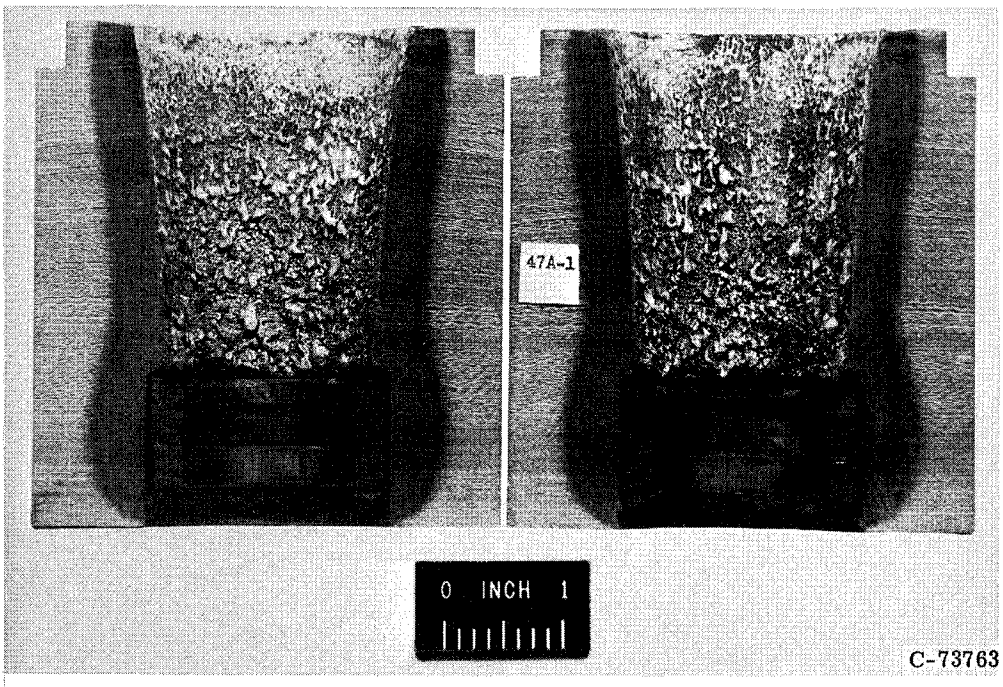

	Material	Form	Manufacturer	Additional layers
Insert	Pyrolytic graphite	Washers with ab radial plane	General Electric	0.040-in. -thick Rokide Z on insert outside diameter
Envelope	Silica phenolic (MX 2641)	Cloth (90^{o} to centerline)	Haveg	0.25-in. -thick stainless-steel shell

Run	Chamber pressure, P_c, psia	Oxidant-fuel ratio, O/F	Run time, sec	Total change in effective throat radius, ΔR, in.	Remarks
15	101.8 to 94.6	2.24	60.0	0.0475	Timed shutdown
19	94.9 to 88.4	2.16	39.0	.092	Low chamber pressure shutdown
			99.0		

TABLE I. - Continued. INSERT DESCRIPTION

(43) Insert 43; configuration B; injector 11; characteristic length, 65; no coating

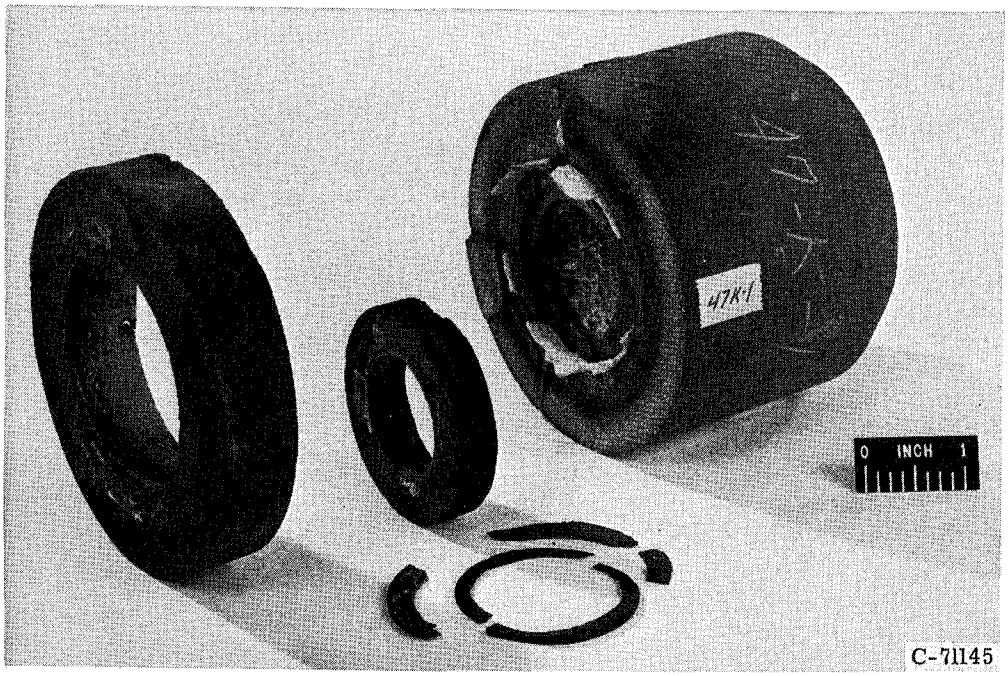

	Material	Form	Manufacturer	Additional layer
Insert	Pyrolytic graphite	Washers with ab radial plane	Space Age Materials	0.040-in. -thick Rokide Z on insert outside diameter
Envelope	Silica phenolic (MX 2641)	Cloth (90^{o} to centerline)	Fiberite	0.25-in. -thick stainless-steel shell

Run	Chamber pressure, P_c, psia	Oxidant-fuel ratio, O/F	Run time, sec	Total change in effective throat radius, ΔR, in.	Remarks
321	105 to 103	1.96	75.3	0.0135	Timed shutdown
340	100 to 99	1.86	95.7	------	Manual shutdown; delamination failure
			171.0		

TABLE I. - Continued. INSERT DESCRIPTION

(44) Insert 44; configuration B; injector 11; characteristic length, 65; no coating

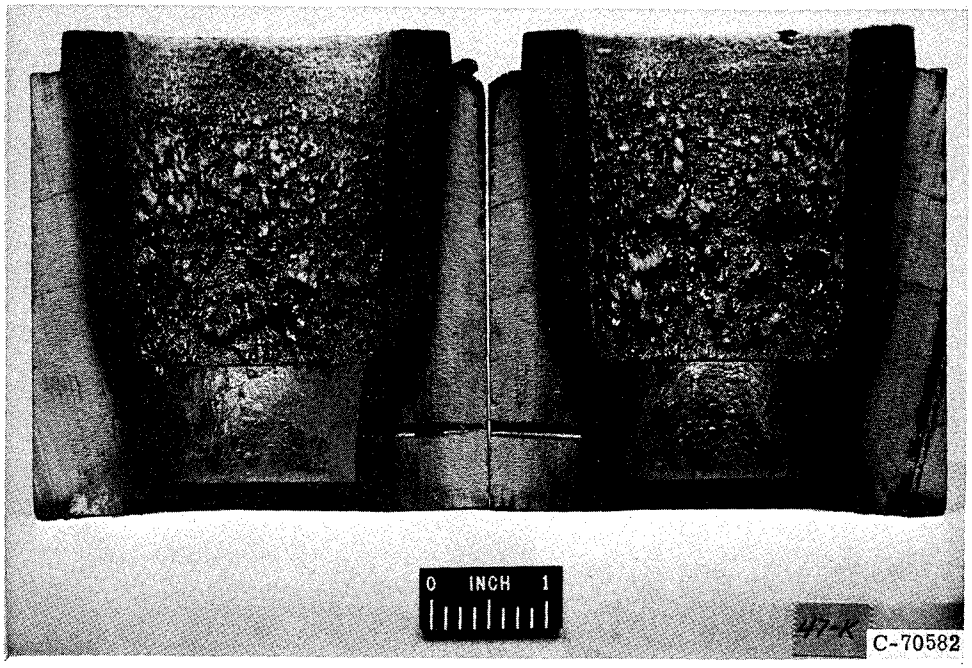

	Material	Form	Manufacturer	Additional layer
Insert	Pyrolytic graphite	Concentric cylinders with ab axial plane	Space Age Materials	0.100-in.-thick asbestos sleeve on insert outside diameter
Envelope	Silica phenolic (MX 2641)	Cloth (90^{o} to centerline)	Haveg	0.25-in.-thick stainless-steel shell

Run	Chamber pressure, P_c, psia	Oxidant-fuel ratio, O/F	Run time, sec	Total change in effective throat radius, ΔR, in.	Remarks
280	103 to 91	1.84	57.6	0.0565	Low chamber pressure shutdown; delamination
296	104 to 96	1.78	53.8	.0945	Low chamber pressure shutdown; delamination
299	102.5 to 94.5	1.73	68.7	.2195	Low chamber pressure shutdown; delamination
			180.1		

TABLE I. - Continued. INSERT DESCRIPTION

(45) Insert 45; configuration E; injector 11; characteristic length, 66; no coating

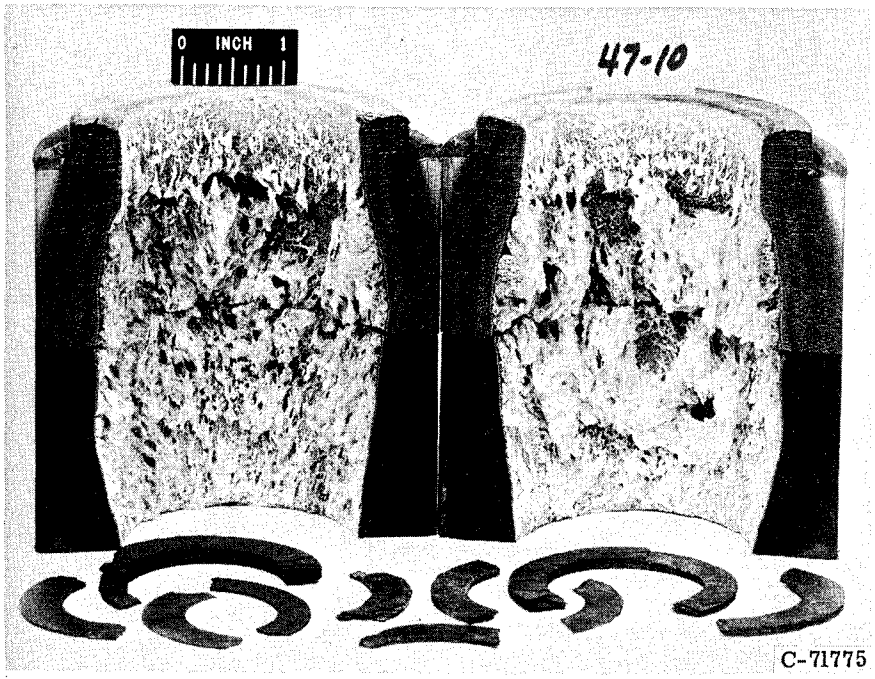

	Material	Form	Manufacturer	Additional layer
Insert	Pyrolytic graphite	Washers with ab radial plane	General Electric	None
Envelope	Silica phenolic (MX 2641)	Cloth (90^{o} to centerline)	Fiberite	0.25-in.-thick stainless-steel shell

Run	Chamber pressure, P_c, psia	Oxidant-fuel ratio, O/F	Run time, sec	Total change in effective throat radius, ΔR, in.	Remarks
342	99 to 100	2.10	60.3	-0.0025	Timed shutdown; washers separated
359	104.5 to 100.5	1.77	120.7	.015	Out of propellant
361	105.5 to 99.5	1.86	125.9	-------	Lost insert
			306.9		

TABLE I. - Continued. INSERT DESCRIPTION

(46) Insert 46; configuration B; injector 12; characteristic length, 50; no precoating; 0.125-inch-thick coating formed during firing

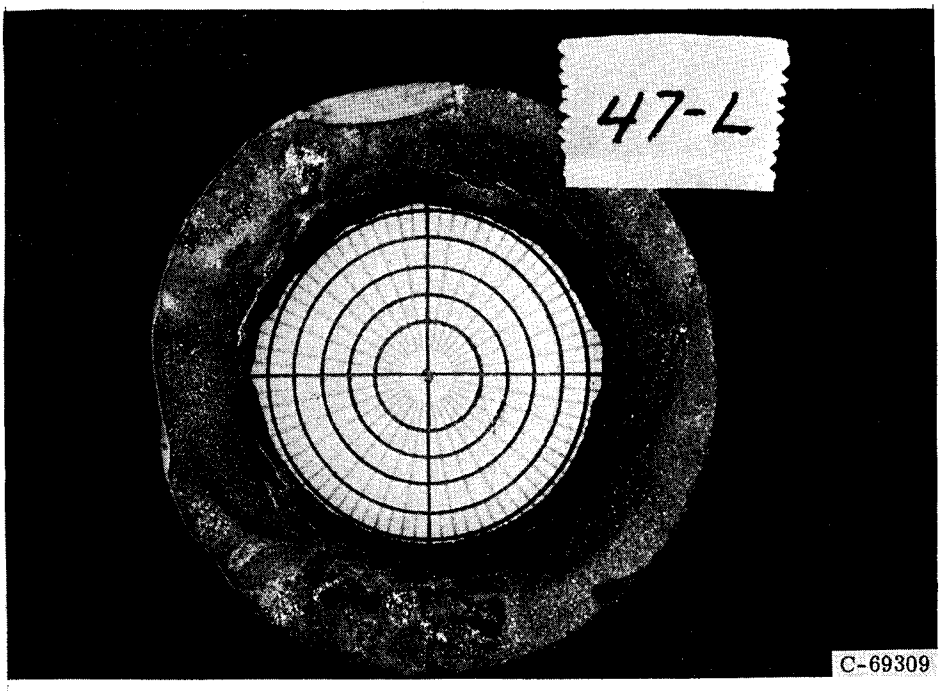

	Material	Form	Manufacturer	Additional layer
Insert	JTA graphite (48 C - 35 Zr - 8 B - 9 Si)	Molding	National Carbon	0.125-in.-thick stainless-steel sleeve at insert outside diameter with 0.005 interference fit
Envelope	Silica phenolic (MX 2641)	Cloth (90^{o} to centerline)	Haveg	0.25-in.-thick stainless-steel shell

Run	Chamber pressure, P_c, psia	Oxidant-fuel ratio, O/F	Run time, sec	Total change in effective throat radius, ΔR, in.	Remarks
212	96 to 90.5	1.60	57.0	---	Circumferential cracks; pieces missing

TABLE I. - Continued. INSERT DESCRIPTION

(47) Insert 47; configuration B; injector 11; characteristic length, 67; no precoating; preoxidized coating partially removed during firing

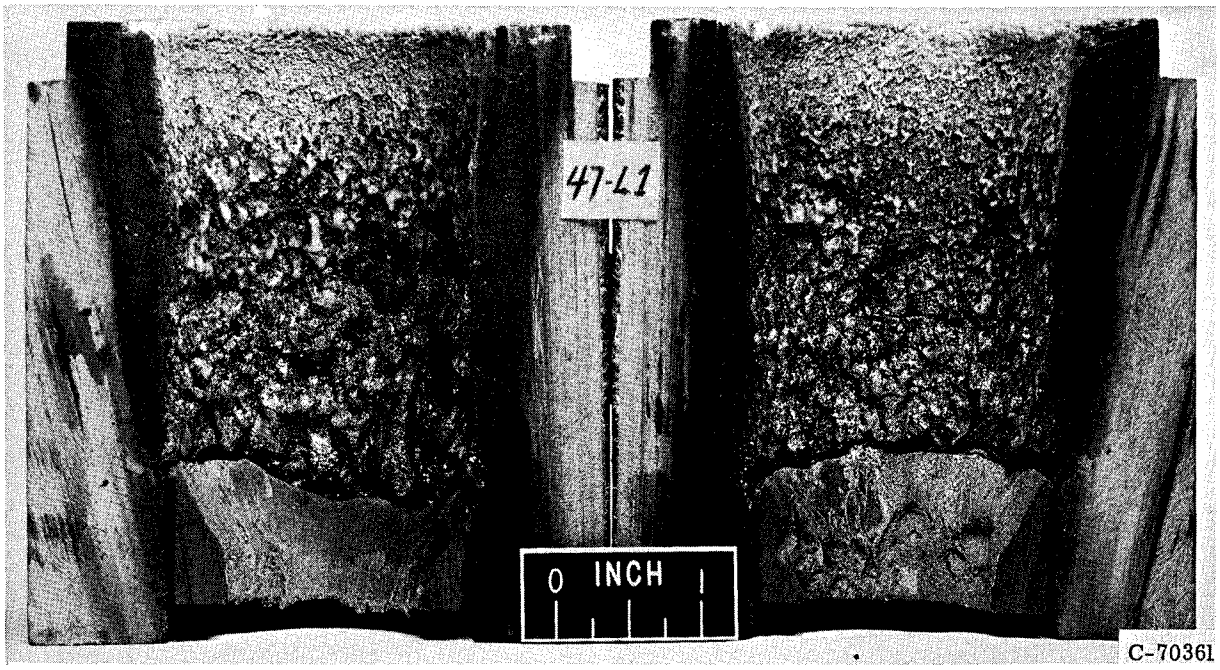

	Material	Form	Manufacturer	Additional layer
Insert	JTA graphite (48 C - 35 Zr - 8 B - 9 Si)	Molding	National Carbon	0.04-in.-thick Rokide Z on insert outside diameter
Envelope	Silica phenolic	Molded squares	Haveg	0.25-in.-thick stainless-steel shell

Run	Chamber pressure, P_c, psia	Oxidant-fuel ratio, O/F	Run time, sec	Total change in effective throat radius, ΔR, in.	Remarks
279	104.5 to 98.5	2.04	60.2	0.007	Timed shutdown
282	100 to 92	1.83	69.3	.042	Low chamber pressure shutdown
			129.5		

TABLE I. - Continued. INSERT DESCRIPTION

(48) Insert 48; configuration D; injector 11; characteristic length, 66; no coating

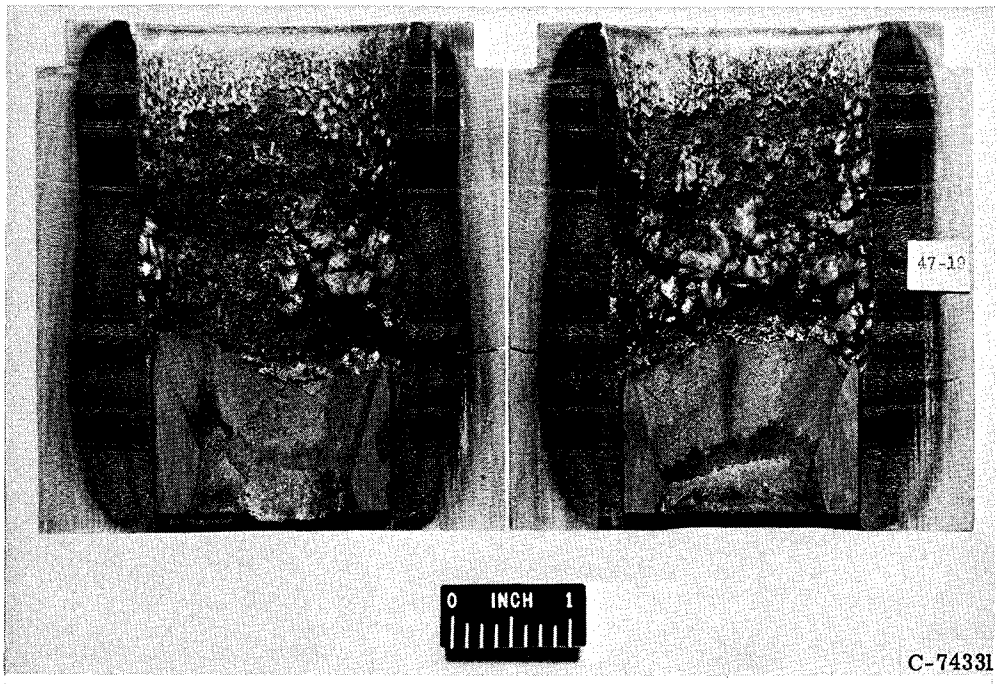

	Material	Form	Manufacturer	Additional layer
Insert	JT 0981 (48 C - 35 Zr - 17 Si)	Molding	National Carbon	None
Envelope	Silica phenolic (MX 2641)	Cloth (90^{o} to centerline)	Haveg	0.25-in.-thick stainless-steel shell

Run	Chamber pressure, P_c, psia	Oxidant-fuel ratio, O/F	Run time, sec	Total change in effective throat radius, ΔR, in.	Remarks
17	104.5 to 89.1	1.81	61.7	0.0065	Timed shutdown; flaky oxide on surface
42	93.3 to 85.7	1.80	139.7	.0325	Low chamber pressure shutdown
			201.4		

TABLE I. - Continued. INSERT DESCRIPTION

(49) Insert 49; configuration D; injector 11; characteristic length, 66; no coating

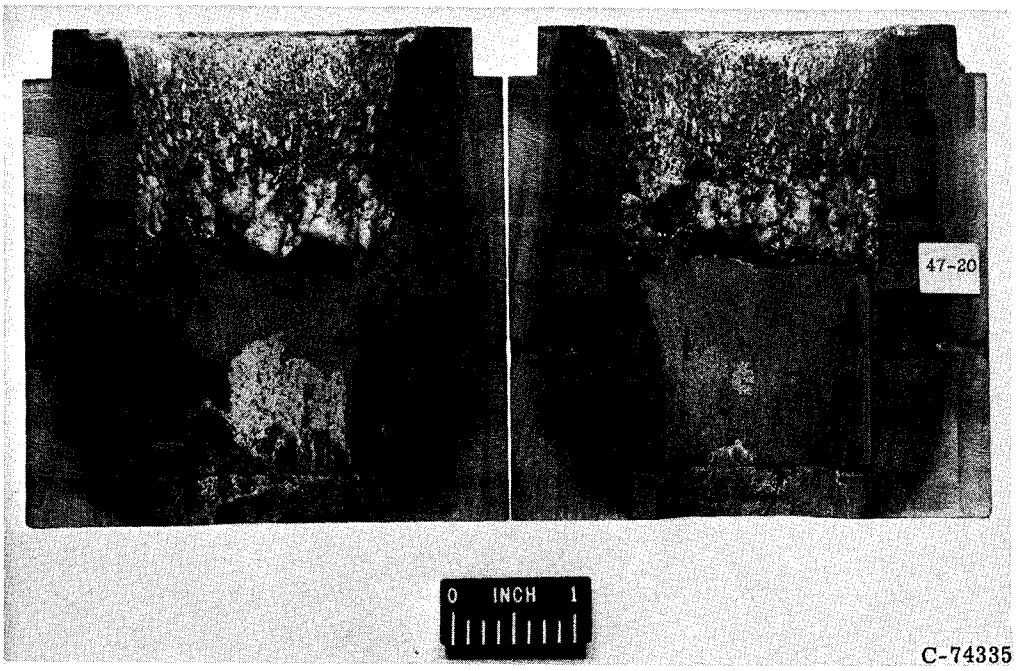

	Material	Form	Manufacturer	Additional layer
Insert	JO 0981 (48 C - 35 Zr - 17 Si)	Molding	National Carbon	None
Envelope	Silica phenolic (MX 2641)	Cloth (90° to centerline)	Haveg	0.25-in.-thick stainless-steel shell

Run	Chamber pressure, P_c, psia	Oxidant-fuel ratio, O/F	Run time, sec	Total change in effective throat radius, ΔR, in.	Remarks
18	99.1 to 97.3	2.19	62.5	0.011	Timed shutdown; flaky oxide formed
43	98.0 to 82.7	2.03	102.5	.070	Low chamber pressure shutdown
			165.0		

TABLE I. - Continued. INSERT DESCRIPTION

(50) Insert 50; configuration F

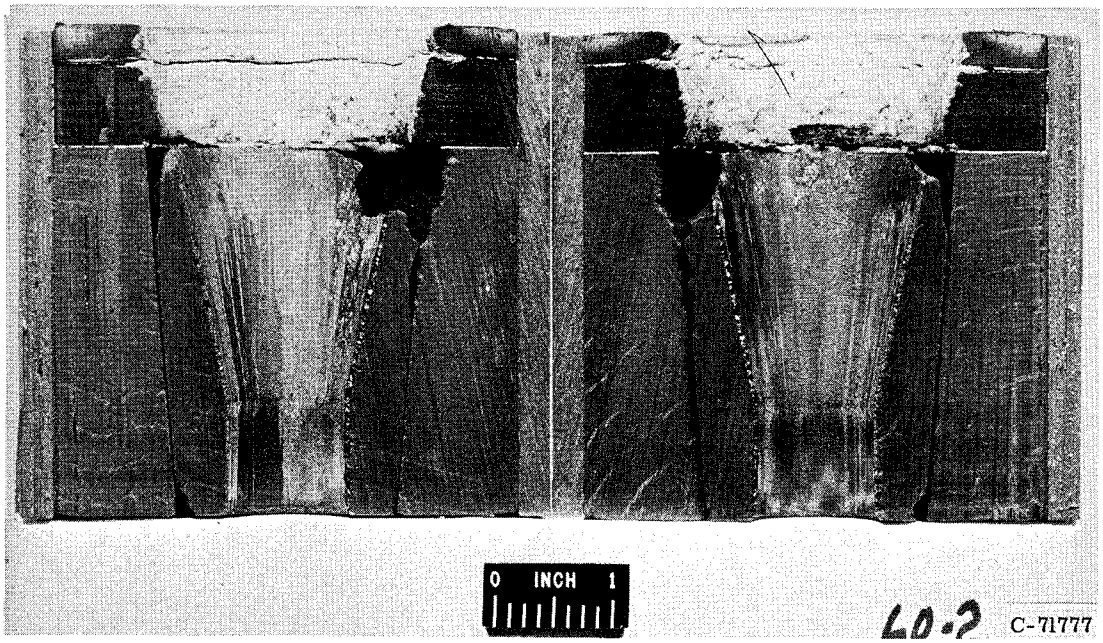

	Material	Form	Manufacturer	Additional layer
Coating	0.040-in.-thick SiC	Pyrolytic		
Insert	Graphite	Molded	Marquardt	None
Envelope	Graphite (MX 2641) upstream	Molding, cloth (90^{o} to centerline)	Marquardt Fiberite	0.3125-in.-thick stainless-steel shell

Run	Injector	Characteristic length, L*, in.	Chamber pressure, P_c, psia	Oxident-fuel ratio, O/F	Run time, sec	Total change in effective throat radius, ΔR, in.	Remarks
221	12	68	100.5 to 98.5	1.46	61.9	0	Timed shutdown
222	12	68	101.5 to 99.5	1.45	121.9		Timed shutdown
235	11	94	96.3 to 93.5	1.54	183.7		Out of propellant
237	11	94	103.5 to 92.5	1.80	252.3		Out of propellant
243	11	94	97.0 to 94.5	2.62	37.0		Manual abort; wrong O/F
244	11	94	96.5 to 94.5	2.06	128.2		Out of propellant
247	10	94	97.5 to 97.0	1.82	129.3		Out of propellant
322	11	94	101.5 to 101.5	1.75	207.3		Out of propellant
323	11	94	103.9 to 103.4	1.56	107.5		Out of propellant
324	11	94	102.5 to 102.5	1.60	177.3		Out of propellant; leading edge failure
					1406.6		

TABLE I. - Continued. INSERT DESCRIPTION

(51) Insert 51; configuration F; injector 11; characteristic length, 94

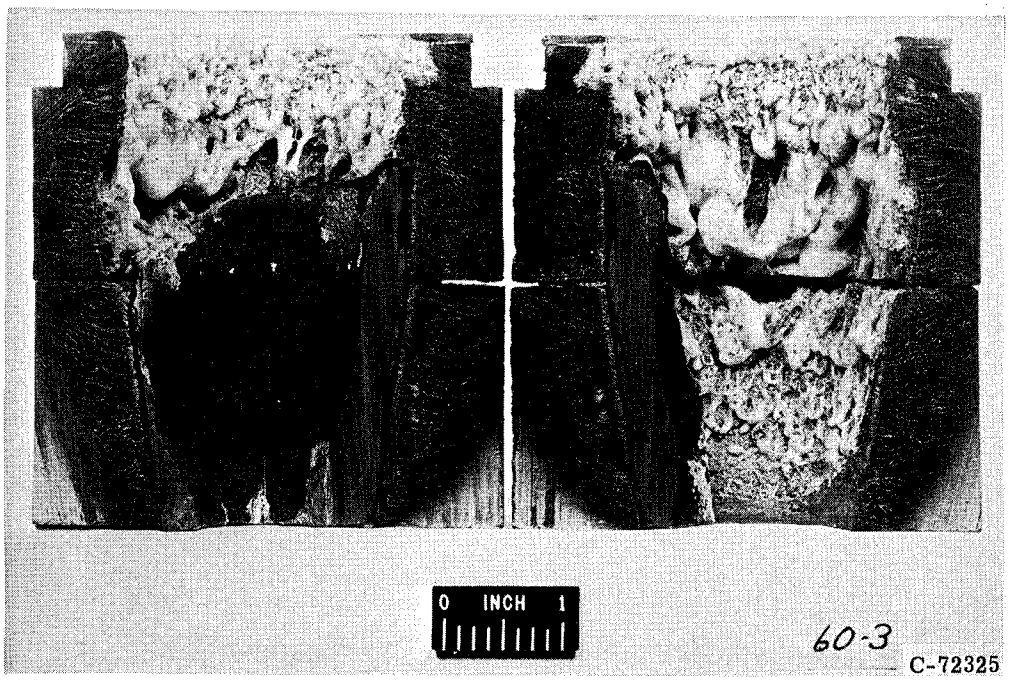

	Material	Form	Manufacturer	Additional layer
Coating	0.040-in. -thick SiC	Pyrolytic		
Insert	Graphite	Molded	Marquardt	None
Envelope	Silica Phenolic (MX 2641)	Cloth (90° to centerline)	Haveg	0.25-in. -thick stainless-steel shell

Run	Chamber pressure, P_c, psia	Oxidant-fuel ratio, O/F	Run time, sec	Total change in effective throat radius, ΔR, in.	Remarks
367	105 to 106	2.30	60.1	0	Timed shutdown
368	99 to 103.5	1.76	248.5	0	Out of propellant
375	101.0	2.16	183.9	0	Out of propellant
376	122.0 to 96.0	2.21	258.5	.1185	Manual abort; erosion began 230 sec after start of firing
			751.0		

TABLE I. - Continued. INSERT DESCRIPTION

(52) Insert 52; configuration B; injector 12; characteristic length, 50

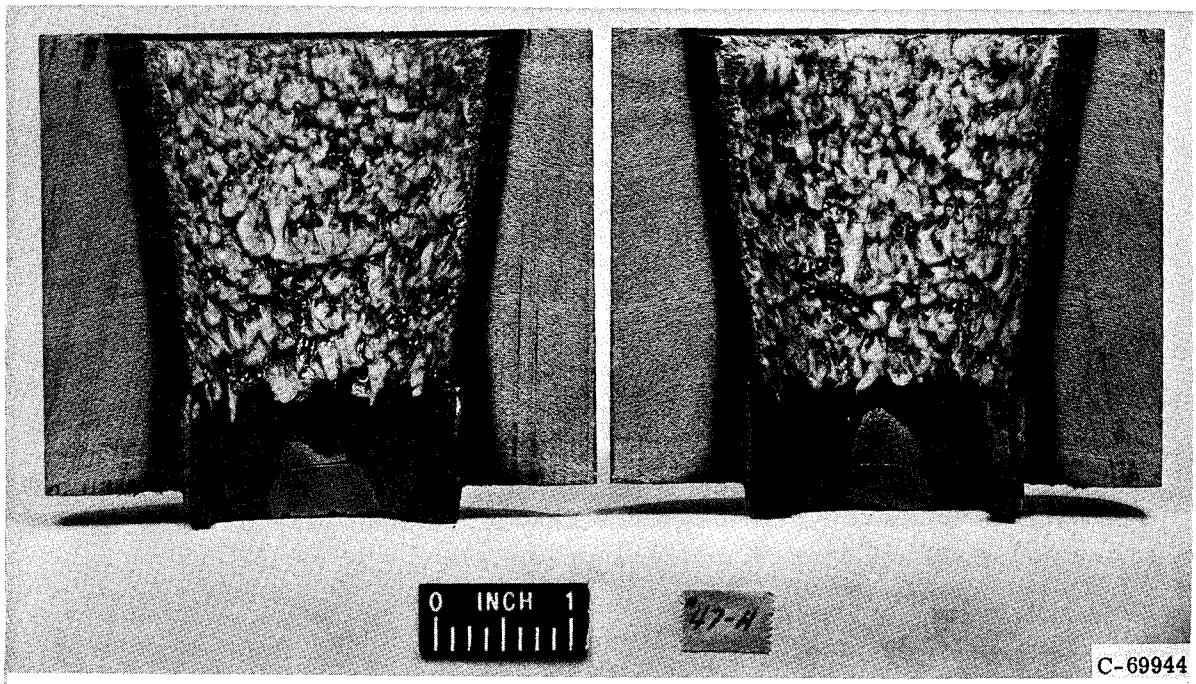

	Material	Form	Manufacturer	Additional layer
Coating	0.020-in.-thick pyrolytic graphite	Pyrolytic graphite with ab axial plane		
Insert	Graphite	Pyrolyzed cloth	American Metal Products	0.040-in.-thick Rokide Z on insert outside diameter
Envelope	Silica phenolic (MX 2641)	Cloth (90^{o} to centerline)	Haveg	0.025-in.-thick stainless-steel shell

Run	Chamber pressure, P_c, psia	Oxidant-fuel ratio, O/F	Run time, sec	Total change in effective throat radius, ΔR, in.	Remarks
213	100.5 to 102	1.82	60.0	0	Timed shutdown; coating intact
214	100.5 to 91	1.88	26.0	Not measured	Low chamber pressure shutdown; most of coating gone
			86.0		

TABLE I. - Continued. INSERT DESCRIPTION

(53) Insert 53; configuration C; injector 10; characteristic length, 67

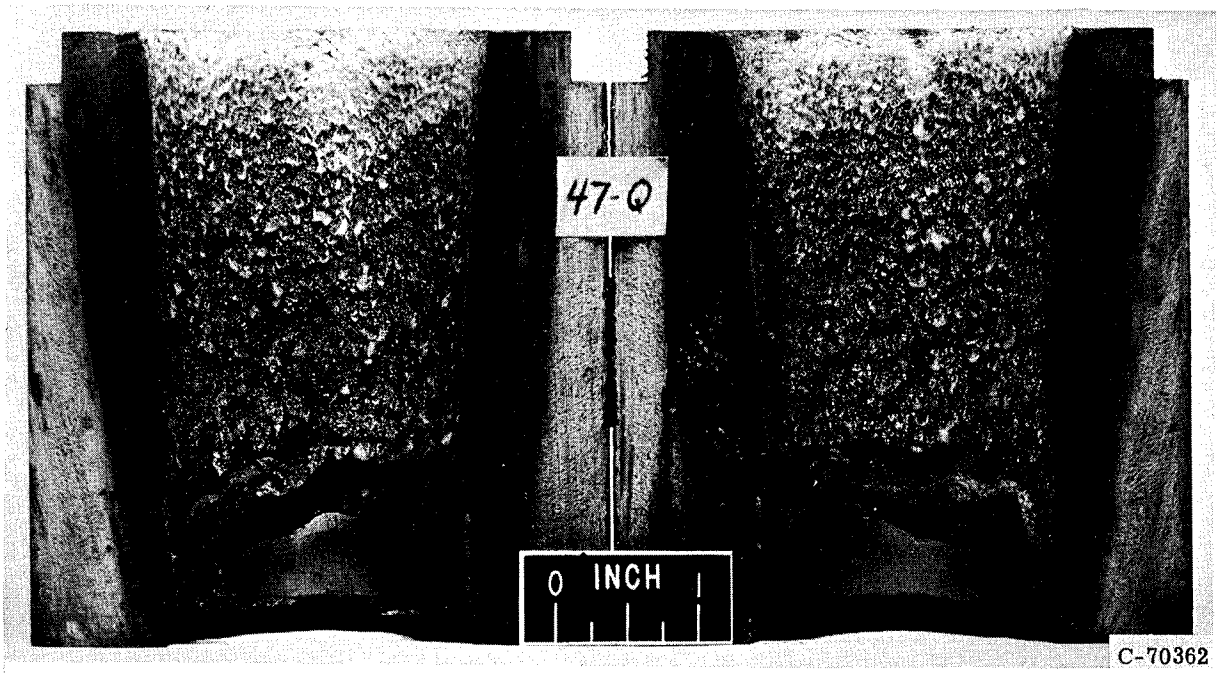

	Material	Form	Manufacturer	Additional layer
Coating	0.060-in.-thick pyrolytic graphite	Pyrolytic graphite with ab axial plane		
Insert	Graphite	Pyrolyzed cloth	American Metal Products	0.040-in.-thick Rokide Z on insert outside diameter
Envelope	Silica phenolic (MX 2641)	Cloth (90^{o} to centerline)	Haveg	0.25-in.-thick stainless-steel shell

Run	Chamber pressure, P_c, psia	Oxidant-fuel ratio, O/F	Run time, sec	Total change in effective throat radius, ΔR, in.	Remarks
262	96.5 to 95.0	2.03	59.8	0	Timed shutdown; no change
272	95.5 to 93.5	2.12	130.2	.127	Manual abort; leading edge failure
			190.0		

TABLE I. - Continued. INSERT DESCRIPTION

(54) Insert 54; configuration B; injector 11; characteristic length, 67

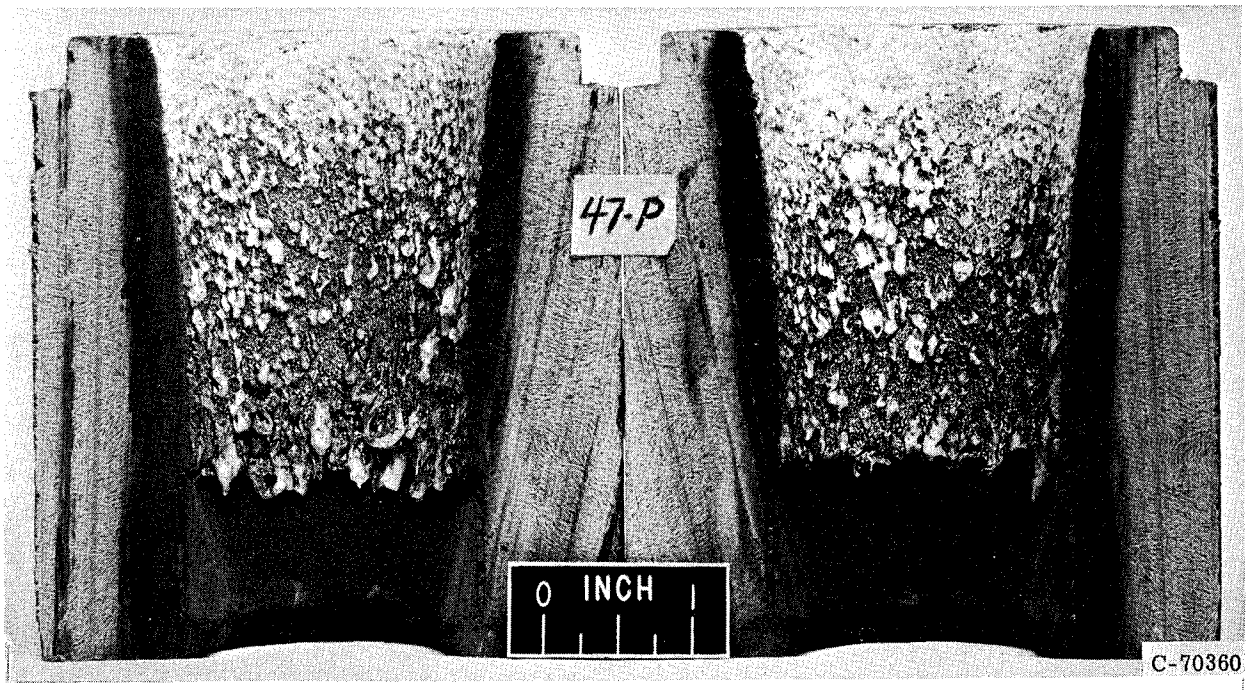

	Material	Form	Manufacturer	Additional layer
Coating	0.020-in.-thick BN	Vapor deposited		
Insert	ATJ graphite	Molded	High temperature materials	0.040-in.-thick Rokide Z on insert outside diameter
Envelope	Silica phenolic (MX 2641)	Molded squares	Haveg	0.25-in.-thick stainless-steel shell

Run	Chamber pressure, P_c, psia	Oxidant-fuel ratio, O/F	Run time, sec	Total change in effective throat radius, ΔR, in.	Remarks
233	100.5 to 88	1.80	55.5	0.051	Low chamber pressure shutdown; coating completely gone
276	100.5 to 89.5	1.91	29.2	.1065	Low chamber pressure shutdown
283	97.5 to 91.0	1.85	27.6	.148	Low chamber pressure shutdown
			112.3		

TABLE I. - Continued. INSERT DESCRIPTION

(55) Insert 55; configuration C; injector 11; characteristic length, 67

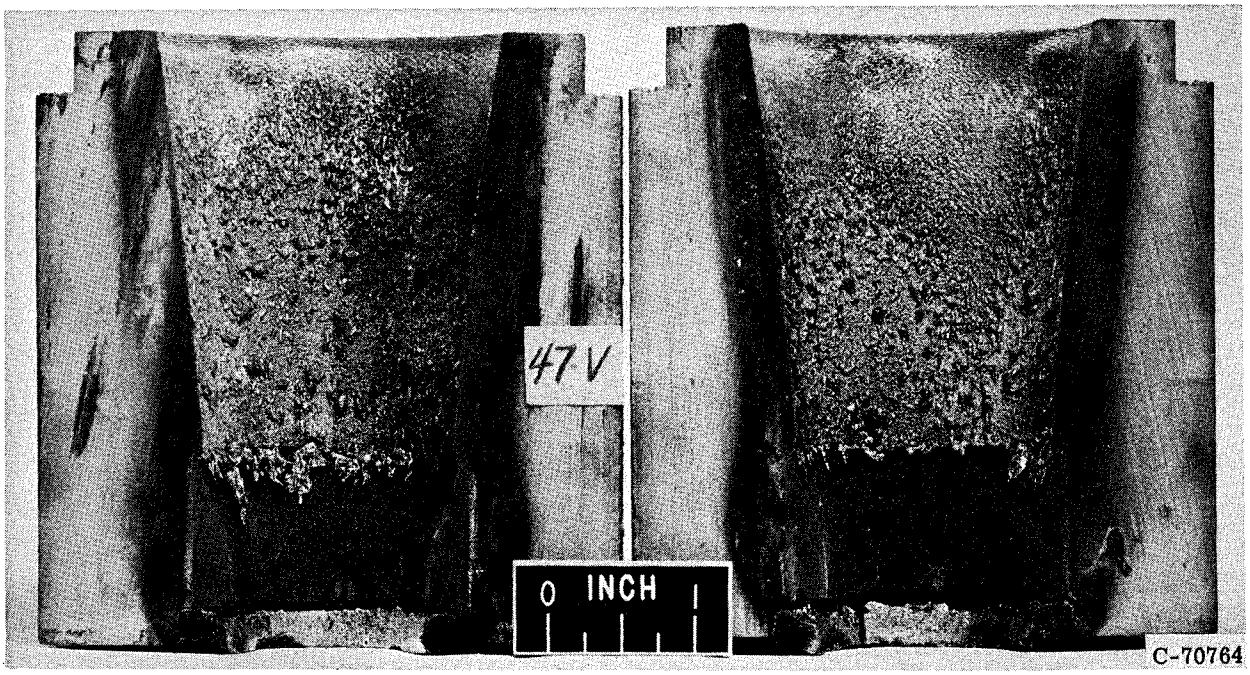

	Material	Form	Manufacturer	Additional layer
Coating	0.010 in. -thick TaC	Vapor deposited		
Insert	ATJ graphite	Molded	High temperature materials	0.100-in. -thick Rokide Z on insert outside diameter
Envelope	Silica phenolic (MX 2641)	Cloth (90^{o} to centerline)	Fiberite	0.25-in. -thick stainless-steel sleeve

Run	Chamber pressure, P_c, psia	Oxidant-fuel ratio, O/F	Run time, sec	Total change in effective throat radius, ΔR, in.	Remarks
303	104.5 to 90.5	1.82	56.1	0.0725	Low chamber pressure shutdown; coating completely gone

TABLE I. - Continued. INSERT DESCRIPTION

(56) Insert 56; configuration C; injector 11; characteristic length, 67

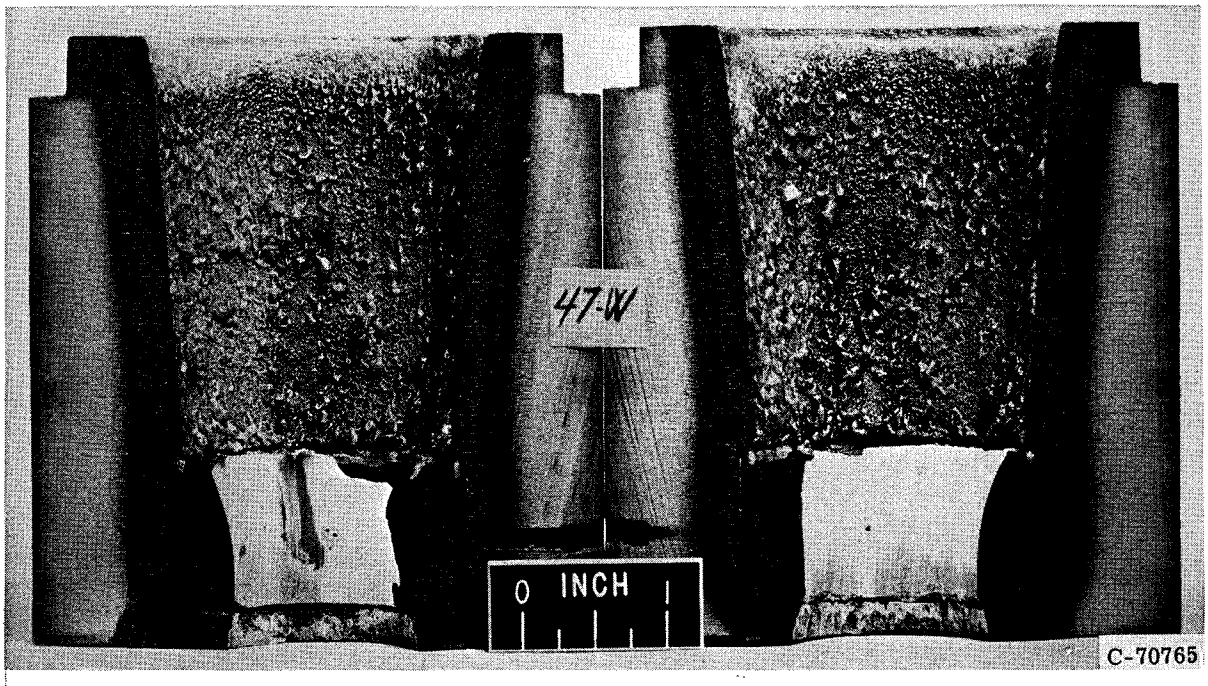

	Material	Form	Manufacturer	Additional layer
Coating	0.010-in.-thick ZrC	Vapor deposited		
Insert	ATJ graphite	Molded	High temperature materials	0.100-in.-thick Rokide Z on insert outside diameter
Envelope	Silica phenolic (MX 2641)	Cloth (90^{o} to centerline)	Haveg	0.25-in.-thick stainless-steel shell

Run	Chamber pressure, P_c, psia	Oxidant-fuel ratio, O/F	Run time, sec	Total change in effective throat radius, ΔR, in.	Remarks
300	104 to 101	1.74	60.6	0	Timed shutdown; coating oxidized and leading edge of coating gone

TABLE I. - Concluded. INSERT DESCRIPTION

(57) Insert 57; configuration C; injector 11; characteristic length, 67

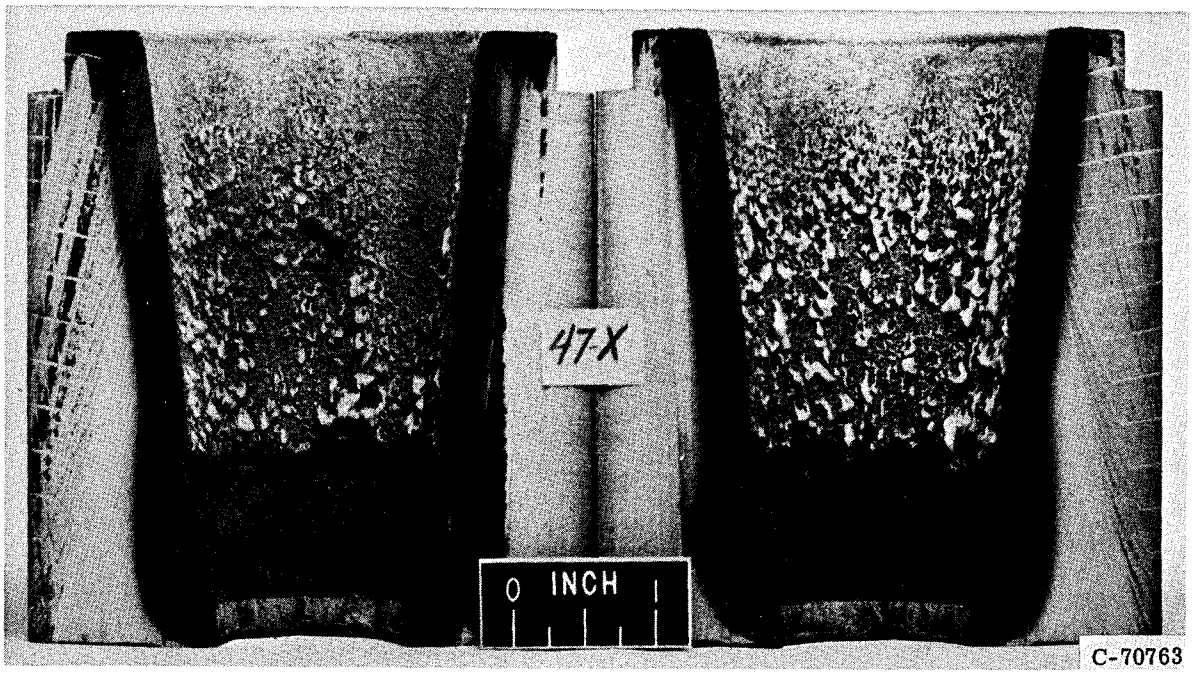

	Material	Form	Manufacturer	Additional layer
Coating	0.010-in.-thick NbC	Vapor deposited		
Insert	ATJ graphite	Molded	High temperature materials	0.10-in.-thick Rokide Z on insert outside diameter
Envelope	Silica-phenolic (MX 2641)	Cloth (90^{o} to centerline)	Fiberite	0.250-in.-thick stainless-steel shell

Run	Chamber pressure, P_c, psia	Oxidant-fuel ratio, O/F	Run time, sec	Total change in effective throat radius, ΔR, in.	Remarks
302	101.5 to 89.5	1.78	46.4	0.0615	Low chamber pressure shutdown; coating all gone

TABLE II. - MEASURED VARIABLES

Measured variable	Full-scale range	Standard deviation
Chamber pressure, P_c	150 psig	±2.2 psig
Oxidant flow differential pressure, ΔP_O	100 psi	±1.5 psi
Oxidant flow (turbinemeter), $W_{O,t}$	0.48 lb H_2O/sec	±0.0071 lb H_2O/sec
Oxidant temperature	10^o to 120^o F	±1.5^o F
Fuel flow differential pressure, ΔP_F	100 psi	±1.5 psi
Fuel flow (turbinemeter), $W_{F,t}$	0.504 lb H_2O/sec	±0.0074 lb H_2O/sec
Fuel temperature	20^o to 160^o F	±1.5^o F
Measured throat area, A_t	----------	±0.015 in.^{2}
Density, ρ	lb/ft^3	----------
Gravitational constant, g	32.174 ft/sec	----------
Run time, sec	Clock timer	±0.7 sec

TABLE III. - INSERT MATERIALS

Insert	Lewis designation	Description	Total run time, sec	Number of runs	Configuration (fig. 6)	Located in table -
		Ablative-reinforced plastic materials				
1	47-28	Pyrolized graphite phenolic with SiC-C additive	138	3	A	I(1)
2	47-30	Prechar silica epoxy (cloth 90° to centerline)	130	2	B	I(2)
3	47-32	Prechar silica epoxy (cloth 60° to centerline)	83	2	B	I(3)
4	47-33	Graphite phenolic with ZrC-SiC additive	57	1	B	I(4)
5	47-34	Graphite phenolic with Hf-Si additive	45	2	B	I(5)
6	47-35	Graphite phenolic with Hf-Si additive	86	2	C	I(6)
7	47-36	Graphite phenolic with TaO_2-Si additive	53	1	B	I(7)
		Composite materials				
8	47-13	50 WC - 50 Ag	39	1	C	I(8)
9	47-15	57 WC - 43 Cu	60	1	C	I(9)
10	47 U	TiB_2 with ZrO_2 filler	55	3	B	I(10)
11	M-1	ZrC-SiC coated graphite powder with organic resin binder	27	2	D	I(11)
12	M-2	HfC-SiC powder with organic resin binder	68	5	D	I(12)
13	47-26	80 SiO_2 - 20 C	109	5	D	I(13)
14	47 T	GRB (64 SiC - 33 C - 3 Si)	136	2	B	I(14)
		Refractory compounds				
15	47-37	65 ZrO_2 - 35 SiO_2	60	1	C	I(15)
16	47-39	85 BeO - 15 SiC	60	1	C	I(16)
17	47 G	BN (stainless-steel sleeve)	69	2	C	I(17)
18	47 Y	Al_2O_3 (stainless-steel sleeve)	60	1	A	I(18)
19	47-21	SiN	54	1	B	I(19)
20	47-24	ZrB_2 (stainless-steel sleeve)	50	1	B	I(20)
21	47-38	BeO	60	1	C	I(21)
22	47-43	BeO (stainless-steel sleeve)	113	2	B	I(22)
23	47 J	NbC	56	1	B	I(23)
24	47 Z	Axially segmented SiC (kT)	52	1	B	I(24)
25	47 F-1	SiC (Ta sleeve)	140	2	C	I(25)
26	47-40	SiC	65	1	C	I(26)
27	47-23	ZrC (stainless-steel sleeve)	59	1	B	I(27)
28	47-41	Hypereutectic ZrC	127	2	C	I(28)
29	47-22	TiB_2 (stainless-steel sleeve)	33	1	B	I(29)

TABLE III. - Concluded. INSERT MATERIALS

Insert	Lewis designation	Description	Total run time, sec	Number of runs	Configuration (fig. 6)	Located in table -
		Refractory metals and alloys				
30	47 C	Sintered W	81	2	B	I(30)
31	47 M-1	Sintered Mo	96	2	C	I(31)
32	47 M-2	Sintered Mo	43	1	C	I(32)
33	47 O	Nb	17	1	B	I(33)
34	47 B	Arc-cast Mo	60	2	B	I(34)
35	42 D	90 Ta - 10 W	43	2	B	I(35)
36	47-12	TZM alloy	43	1	C	I(36)
		Infiltrated refractory metals				
37	42 C	80 W - 20 Ag	108	2	B	I(37)
38	47 I	75 W - 25 Ag-Cu eutectic	59	1	B	I(38)
39	47-14	80 W - 20 Cu	59	1	C	I(39)
		Graphite materials				
40	47 R	Heat-treated high-density graphite	145	3	C	I(40)
41	47 S	High-density graphite	96	3	C	I(41)
42	47 A-1	Pyrolytic graphite (washers with ab plane radial)	99	2	A	I(42)
43	47 K-1	Pyrolytic graphite (washers with ab plane radial)	171	2	B	I(43)
44	47 K	Pyrolytic graphite (concentric cylinders with ab plane axial)	180	3	B	I(44)
45	47-10	Pyrolytic graphite (washers with ab plane radial)	307	3	E	I(45)
46	47 L	JTA graphite (stainless-steel sleeve)	57	1	B	I(46)
47	47 L-1	JTA graphite	129	2	B	I(47)
48	47-19	JT 0981 graphite	201	2	D	I(48)
49	47-20	JT 0981 graphite	165	2	D	I(49)
		Coated materials				
50	60-2	0.040-in.-thick SiC coating on graphite in graphite	1407	10	F	I(50)
51	60-3	0.040-in.-thick SiC coating on graphite in ablative material	751	4	F	I(51)
52	47 H	0.020-in.-thick pyrolytic graphite coating on graphite cloth	86	2	B	I(52)
53	47 Q	0.060-in.-thick pyrolytic graphite on graphite cloth	190	2	C	I(53)
54	47 P	0.020-in.-thick BN on ATJ graphite	112	3	B	I(54)
55	47 V	0.010-in.-thick TaC on ATJ graphite	56	1	C	I(55)
56	47 W	0.010-in.-thick ZrC on ATJ graphite	61	1	C	I(56)
57	47 X	0.010-in.-thick NbC on ATJ graphite	46	1	C	I(57)

TABLE IV. - CALCULATIONS

Parameter	Equation	Standard deviation
Oxidant flow:		
Venturi meter	$W_{O,v} = 0.00951\sqrt{\Delta P_O \rho_O}$	±0.010 lb/sec
Turbine meter	$W_{O,t} = \rho_O/\rho_{H_2O}$	±0.015 lb/sec
Average	$W_O = (W_{O,v} + W_{O,t})/2$	±0.018 lb/sec
Fuel flow:		
Venturi meter	$W_{F,v} = 0.00589\sqrt{\rho_F \Delta P_F}$	±0.007 lb/sec
Turbine meter	$W_{F,t} = \rho_O/\rho_{H_2O}$	±0.010 lb/sec
Average	$W_F = (W_{F,v} + W_{F,t})/2$	±0.012 lb/sec
Total propellant flow	$W_{Total} = W_F + W_O$	±0.021 lb/sec
Oxidant-to-fuel ratio	$O/F = W_O/W_F$	±0.049
Experimental characteristic exhaust velocity	$C^*_{exp} = P_c A_t g/W_T$	±117 ft/sec
Efficiency of characteristic exhaust velocity	$\eta_{C^*} = C^*_{exp}/C^*_{theor\ equilibrium}$	±2.2 percent
Change in effective throat radius:		
Planimeter	ΔR_{plan} = Effective radius after firing minus initial radius	±0.009 in.
Calculated	ΔR_{calc} = Calculated radius at end of firing minus initial radius, or $\sqrt{\frac{C^* W_{total(end)}}{\pi P_c(end) g}}$ - Initial radius	±0.015 in.
Overall throat erosion rate	$OER = \frac{\Delta R_{total} \times 10^3}{\text{Total firing time}}$	±0.018 mils/sec
Characteristic chamber length	$L^* = \frac{\text{Chamber volume}}{\text{Throat area}}$	±0.5 in.

TABLE V. - THROAT INSERT TEST DATA

Insert	Lewis designation	Description	Total time, sec	Number of runs	Overall erosion rate, mils/sec	Primary failure mechanism	Located in table -
(a) Ablative-reinforced plastic materials							
1	47-28	Pyrolyzed graphite phenolic with SiC-Si additive	138	3	1.50	Erosion by oxidation	I(1)
2	47-30	Precharred silica epoxy (reinforcement, 90^{o} to centerline)	130	2	1.16	Erosion by oxidation	I(2)
3	47-32	Precharred silica epoxy (reinforcement, 60^{o} to centerline)	83	2	2.08	Erosion by oxidation	I(3)
4	47-33	Graphite phenolic with ZrC-Si additive	57	1	2.57	Erosion by oxidation	I(4)
5	47-34	Graphite phenolic with Hf-Si additive	45	2	1.77	Erosion by oxidation	I(5)
6	47-35	Graphite phenolic with Hf-Si additive	86	2	1.56	Erosion by oxidation (insert completely gone)	I(6)
7	47-36	Graphite phenolic with TaO_2-Si	53	1	1.29	Erosion by oxidation	I(7)
(b) Composite materials							
8	47-13	50 WC - 50 Ag	39	1	2.37	Erosion by oxidation (lost Rokide on outside diameter)	I(8)
9	47-15	57 WC - 43 Cu	60	1	.80	Cracked and melted	I(9)
10	47 U	TiB_2 with ZrO_2 filler (stainless-steel sleeve)	55	3	2.46	Erosion by oxidation	I(10)
11	M-1	Coating of ZrC-SiC on graphite powder with organic resin binder (molybdenum sleeve)	27	2	2.09	High erosion and cracking	I(11)
12	M-2	Coating of HfC-SiC on graphite powder with organic resin binder (molybdenum sleeve)	68	5	2.30	High degree of erosion and cracking	I(12)
13	47-26	80 SiO_2 - 20 C	109	2	1.03	High degree of erosion	I(13)
14	47 T	GRB (64 SiC - 33 C - 3 Si)	136	2	.27(calc)	Insert cracked into three pieces	I(14)

TABLE V. - Continued. THROAT INSERT TEST DATA

Insert	Lewis designation	Description	Total time, sec	Number of runs	Overall erosion rate, mils/sec	Primary failure mechanism	Located in table -
(c) Refractory compounds							
15	47-37	ZrO_2-SiO_2	60	1	None	Severe longitudinal and circumferential cracks and local erosion	I(15)
16	47-39	85 BeO - 15 SiC	60	1	None	Longitudinal and circumferential cracks	I(16)
17	47 G	BN (stainless-steel sleeve)	69	2	.93	Sleeve melted at leading edge and high degree of oxidation	I(17)
18	47 Y	Al_2O_3 (stainless-steel sleeve)	60	1	.38	Severe cracking and local erosion	I(18)
19	47-21	SiN	54	1	3.57	Erosion by oxidation and cracks formed	I(19)
20	47-24	ZrB_2 (stainless-steel sleeve)	50	1	.56(calc)	Insert and ring disappeared; insert retention failure	I(20)
21	47-38	BeO	60	1	None	Longitudinal and circumferential cracks	I(21)
22	47-34	BeO (stainless-steel sleeve)	113	2	.43	Crack (circumferential sleeve melted)	I(22)
23	47 J	NbC	56	1	Not measured	Severe cracking (pieces missing)	I(23)
24	47 Z	Axially segmented SiC (KT)	52	1	.56(calc)	Insert retention failure	I(24)
25	47 F-1	SiC; in Ta sleeve	140	2	.38	Circumferential crack and Ta at leading edge oxidized	I(25)
26	47-40	SiC	65	1	.15	Five axial cracks	I(26)
27	47-23	ZrC; in stainless-steel sleeve	59	1	None	One circumferential and three axial cracks (sleeve melted)	I(27)
28	47-41	Hypereutectic ZrC	61	1	None	Thin oxide (no cracks)	I(28)
29	47-22	TiB_2 (stainless-steel sleeve)	33	1	Not measured	Sleeve gone and insert cracked (pieces missing)	I(29)

TABLE V. - Continued. THROAT INSERT TEST DATA

Insert	Lewis designation	Description	Total time, sec	Number or runs	Overall erosion rate, mils/sec	Primary failure mechanism	Located in table -
(d) Refractory metals and alloys							
30	47 C	Sintered W	81	2	0.68	Severe oxidation	I(30)
31	47 M-1	Sintered Mo	96	2	.88	Severe oxidation	I(31)
32	47 M-2	Sintered Mo	43	1	.18	Upstream oxidation	I(32)
33	47 O	Nb	17	1	Not measured	Insert completely oxidized	I(33)
34	47 B	Arc-cast Mo	60	2	.75(calc)	Severe oxidation	I(34)
35	42 D	90 Ta - 10 W	43	2	.98	Insert cracked and oxidized	I(35)
36	47-12	TZM alloy	43	1	2.48	Insert oxidized 75 percent	I(36)
(e) Infiltrated refractory metals							
37	42 C	80 W - 20 Ag	108	2	1.07	Oxidation	I(37)
38	47 I	75 W - 25 Ag-Cu eutectic	59	1	None	Oxidation upstream of throat	I(38)
39	47-14	80 W - 20 Cu	59	1	.70	Oxidation (copper depleted on inside diameter)	I(39)
(f) Graphite materials							
40	47 R	Heat-treated high-density graphite	145	3	1.07	High erosion	I(40)
41	47 S	High-density graphite	96	3	1.57	High erosion	I(41)
42	47 A-1	Pyrolytic graphite ab radial plane	99	2	.93	Leading-edge failure and high degree of erosion	I(42)
43	47 K-1	Pyrolytic graphite ab radial plane	171	2	Not measured	Separation between planes	I(43)
44	47 K	Pyrolytic graphite ab axial plane	180	3	1.22	High degree of erosion due to delamination	I(44)
45	47-10	Pyrolytic graphite ab radial plane	307	3	.12	Erosion and flow behind insert; insert was lost	I(45)
46	47 L	JTA graphite (stainless-steel ring)	57	1	Not measured	Ring melted and insert cracked and oxidized	I(46)
47	47 L-1	JTA graphite	129	2	.33	Leading-edge erosion	I(47)
48	47-19	JT 0981 graphite	199	2	.16	Upstream erosion	I(48)
49	47-20	JT 0981 graphite	165	2	.42	High degree of erosion	I(49)

TABLE V. - Concluded. THROAT INSERT TEST DATA

Insert	Lewis designation	Description	Total time, sec	Number of runs	Overall erosion rate, mils/sec	Primary failure mechanism	Located in table -
		(g) Coated materials					
50	60-2	0.040-in.-thick RM 005 SiC on graphite in graphite	1407	10	0	Leading-edge failure; graphite gave large heat sink and high outside diameter temperature	I(50)
51	60-3	0.040-in.-thick RM 005 SiC on graphite in ablative material	751	4	0	Leading-edge failure and ablative char-through	I(51)
52	47 H	0.020-in.-thick pyrolytic graphite on graphite cloth	86	2	Not measured	Coating largely consumed and leading-edge failure	I(52)
53	47 Q	0.060-in.-thick pyrolytic graphite on graphite cloth	190	2	.67	Coating largely consumed and leading-edge failure	I(53)
54	47 P	0.020-in.-thick boralloy on ATJ graphite	112	3	1.32	Coating completely consumed	I(54)
55	47 V	0.010-in.-thick TaC on ATJ graphite	56	1	1.29	Coating completely consumed	I(55)
56	47 W	0.010-in.-thick ZrC on ATJ graphite	61	1	0	Coating partially consumed and oxidized to zirconium dioxide	I(56)
57	47 X	0.010-in.-thick NbC on ATJ graphite	46	1	1.33	Coating completely consumed	I(57)

TABLE VI. - THERMAL SHOCK INDEX

Material	Insert	Lewis designation	Degree of thermal stress	Thermal shock index, R', Btu/(ft)(hr)
W	20	47 C	None	89 000
Arc-cast Mo	34	47 B	None	50 000
BeO (100 percent dense aerospace)	21	47-38	Minor	28 000
JTA graphite	47	47 L-1	None	16 200
GRB-SiC	14	47 T	Minor	15 000
85 BeO - 15 SiC	16	47-39	Minor	8 680
BeO (90 percent dense aerospace)	(Not tested, free standing)	(Not tested, free standing)	Moderate	7 600
SiC "KT"	26	47-40	Moderate	7 450
SiN	19	47-21	Moderate	4 850
TiB_2	29	47-22	Severe	2 640
NbC	23	47 J	↓	2 200
Al_2O_3	18	47 Y		2 000
BN	17	47 G		2 000
ZrC	27	47-23		950
Zircon (ZrO_2-SiO_2)	15	47-37		658

TABLE VII. - INSERT STRESS ANALYSIS

Insert	Composition	Calculated maximum temperature difference, ΔT, ^{o}F	Time of maximum ΔT, sec	Maximum strength, psi		Calculated tangential stress, psi		Calculated axial stress, psi		Conclusions from analysis
				Tension	Compression	Inside	Outside	Inside	Outside	
30	Sintered W	512	9.2	175 000 to 200 000	200 000	98 000 (compression)	67 000 (tension)	87 000 (compression)	41 300 (tension)	No failure
34	Sintered Mo	510	----	35 000 to 65 000	70 000	65 158 (compression)	48 162 (tension)	79 846 (compression)	32 020 (tension)	No failure
15	Zircon (ZrO_2-SiO_2)	4508	9.7	8 700	Unknown	411 412 (compression)	510 923 (compression)	260 706 (tension)	143 057 (tension)	Will fail in all modes
18	Al_2O_3 prestressed 1/8-in. stainless-steel band, 0.055 interference	2970	8.4	35 000	300 000 to 400 000	759 000 (compression)	366 000 (tension)	783 000 (tension)	297 000 (tension)	Will fail in all modes
(a)	KT SiC prestressed 1/8-in. stainless-steel band, 0.005 interference	883	10.5	15 000	200 000	4 024 (compression)	739 (compression)	3 315 (compression)	859 (compression)	No failure
25	AVCO SiC prestressed 1/8-in. Ta band, 0.005 interference	910	11.2	10 000	120 000	5 070 (compression)	876 (compression)	3 800 (compression)	910 (compression)	No failure

[a]Insert was not tested.

"The aeronautical and space activities of the United States shall be conducted so as to contribute . . . to the expansion of human knowledge of phenomena in the atmosphere and space. The Administration shall provide for the widest practicable and appropriate dissemination of information concerning its activities and the results thereof."

—NATIONAL AERONAUTICS AND SPACE ACT OF 1958

NASA SCIENTIFIC AND TECHNICAL PUBLICATIONS

TECHNICAL REPORTS: Scientific and technical information considered important, complete, and a lasting contribution to existing knowledge.

TECHNICAL NOTES: Information less broad in scope but nevertheless of importance as a contribution to existing knowledge.

TECHNICAL MEMORANDUMS: Information receiving limited distribution because of preliminary data, security classification, or other reasons.

CONTRACTOR REPORTS: Technical information generated in connection with a NASA contract or grant and released under NASA auspices.

TECHNICAL TRANSLATIONS: Information published in a foreign language considered to merit NASA distribution in English.

TECHNICAL REPRINTS: Information derived from NASA activities and initially published in the form of journal articles.

SPECIAL PUBLICATIONS: Information derived from or of value to NASA activities but not necessarily reporting the results of individual NASA-programmed scientific efforts. Publications include conference proceedings, monographs, data compilations, handbooks, sourcebooks, and special bibliographies.

Details on the availability of these publications may be obtained from:

SCIENTIFIC AND TECHNICAL INFORMATION DIVISION

NATIONAL AERONAUTICS AND SPACE ADMINISTRATION

Washington, D.C. 20546